The Seismic Analysis of a Typical South African Unreinforced Masonry Structure

by
Thomas van der Kolf

Thesis presented in fulfilment of the requirements for the degree of Masters in the Faculty of Civil Engineering at Stellenbosch University

Supervisor: Dr. Trevor Neville Haas

April 2014

The financial assistance of the National Research Foundation (NRF) towards this research is hereby acknowledged. Opinions expressed and conclusions arrived at, are those of the author and are not necessarily to be attributed to the NRF.

Declaration

By submitting this thesis electronically, I declare that the entirety of the work contained therein is my own, original work, that I am the owner of the copyright thereof, (unless to the extent explicitly otherwise stated) that reproduction and publication thereof by Stellenbosch University will not infringe any third party rights and that I have not previously in its entirety or in part submitted it for obtaining any qualification.

April 2014

Abstract

South Africa has some regions which are susceptible to moderate seismic activity. A peak ground acceleration of between 0.1g and 0.15g can be expected in the southern parts of the Western Cape. Unreinforced Masonry (URM) is commonly used as a construction material for 2 to 4 storey buildings in underprivileged areas in and around Cape Town. URM is typically regarded as the material most vulnerable to damage when subjected to earthquake excitation. In this study, a three-storey URM building was analysed by applying seven earthquake time-histories, that can be expected to occur in South Africa, to a finite element model. Experimental data was used to calibrate the in- and out-of-plane stiffness of the URM. A linear modal dynamic analysis and non-linear implicit dynamic analysis were performed. The results indicated that tensile cracking of the in-plane piers was the dominant failure mode. The building relied on the post-cracking capacity to resist the 0.15g magnitude earthquake. It is concluded that URM buildings of this type are at risk of failure especially if sufficient ductility is not provided. The results also showed that connection failure must be investigated further. Construction and material quality will have a large effect on the ability of typical URM buildings to withstand moderate magnitude earthquakes in South Africa.

Opsomming

Sekere gebiede in Suid-Afrika het 'n risiko van matige seismiese aktiwiteit. Aardbewings met maksimum grondversnellings van tussen 0.1g en 0.15g kan in die suidelike gedeeltes van die Wes-Kaap voorkom. Twee- tot vier-verdieping onbewapende messelwerkgeboue kom algemeen voor in die lae sosio-ekonomiese gebiede van Kaapstad. Oor die algemeen word onbewapende messelwerkgeboue as die gebou-tipe beskou wat die maklikste skade opdoen tydens aardbewings. In hierdie studie is sewe aardbewings, wat tipies in Kaapstad verwag kan word, identifiseer en gebruik om 'n tipiese drie-verdieping onbewapende messelwerkgebou te analiseer. Eksperimentele data is gebruik om die materiaaleienskappe in die in-vlak asook uit-vlak rigtings te kalibreer. Beide 'n liniêre modale en nie-liniêre implisiete dinamiese analises is uitgevoer. Die resultate dui daarop dat die dominante falingsmode die kraak van in-vlak messelwerk-tussenkolomme is. Die gebou moes sy plastiese kapasiteit benut om die 0.15g aardbewing te kan weerstaan. Die gevolgtrekking is dat dié tipe onbewapende messelwerkgeboue 'n risiko inhou om mee te gee, veral as genoegsame vervormbaarheid nie verskaf word nie. Die resultate toon ook dat konneksie-faling verder ondersoek moet word. Kwaliteit van vakmanskap en van materiaal het 'n groot invoed op die vermoë van onbewapende messelwerkgeboue om aardbewings van matige intensiteit in Suid-Afrika te weerstaan.

Acknowledgements

I would like to thank my study leader, Dr. Trevor Haas, for the support over the two years and time spent reviewing my work, especially the time over the festive season.

To all my colleagues and friends, thank you for the advice, help and fun times in the office. Jacques, Franel, Van Zyl, Francois and Ron, your help is appreciated, both during office hours, and late nights at Aandklas. Thank you for the motivation, good humour and sound advice during all hours of the day.

Finally I would like to thank my parents for all the support during my many years of studies; from my first year to the proof reading of my thesis at the very end. Also Gideon and Alex for your much appreciated help.

Chapter 1

Introduction

Many destructive natural disasters occur annually. Hurricanes, fires and floods cause large scale damage to buildings and other infrastructure and are a common occurrence. Few disasters have such a sudden, often unexpected and disastrous effect as earthquakes. For years structural engineers have adapted their designs and developed new design techniques to enhance infrastructure against the effect of seismic events. This is especially the case in countries situated in regions of high seismicity. With sound structural design, structures can resist the effects of earthquakes with large Richter magnitudes.

South Africa is a country with regions of low to moderate seismicity. Earthquakes are rare and therefore not perceived as a major threat by the general public. If an earthquake were to occur in densely populated areas, the damage to buildings not designed for seismic events can be significant. The current South African loading code, SANS 10160 (2009), has a section dealing with seismic design. This is a new code that replaces SABS 0160 (1989). SANS 10160-4, greatly expanded on the scope and content of SABS 0160 regarding seismic design.

Many different building types are used worldwide in seismic active regions. Modern reinforced concrete and steel structures are common and generally perform well in areas of moderate seismicity due to the ductile nature of the materials. Masonry structures are also common and include both reinforced and unreinforced masonry (URM) systems. Since reinforcing adds additional ductility to a structure by increasing the tensile strength of structural elements, reinforced masonry buildings are able to perform well during seismic excitation. The same can not be said for URM, which has shown poor performance in past earthquakes and is considered the construction material most vulnerable to seismic excitation (Bruneau, 1994).

URM is widely used in South Africa including the seismically active regions within the Western Cape. Advantages including low cost, good thermal insulation, durability and good compressive strength make URM a popular building material in residential areas. Two to four storey URM buildings are common in Cape Town and the surrounding areas, including the Cape Flats. These buildings were constructed prior to the implementation of SABS 0160. There is great uncertainty whether these structures were designed for seismic action, whether they meet the current design provisions and whether these structures are able to resist moderate intensity earthquakes that

can be expected to occur in Cape Town and its surrounding regions.

In this study, a typical three storey residential URM building from Cape Town and its surrounding areas will be analysed to determine whether it can resist a moderate intensity earthquake that could be expected to occur in Cape Town.

1.1 Background to the Problem

Earthquakes are a very common and destructive phenomenon. They occur globally, from very remote locations, to some of the busiest city centres. According to the United States Geological Survey (USGS, 2012) several million earthquakes occur worldwide, annually. Most of these earthquakes are however minor earthquakes and many of them occur in remote locations and go unnoticed by the public. The National Earthquake Information Centre (NEIC) identifies more than 20 000 earthquakes annually with a Richter magnitude larger than 4.5. Magnitude 4.5 earthquakes are minor quakes that are felt as a tremor by humans in a close proximity to the origin. As the intensity of earthquakes increases above 5 on the Richter scale, damage to property occurs. It is these earthquakes that concern structural engineers. There have been many destructive earthquakes across the world that have claimed numerous lives. The USGS lists more than twenty earthquakes which resulted in a death toll exceeding 50 000.

Some regions of the Western Cape are seismically active. Earthquakes with a magnitude between 6.0–6.5 can be expected in the southern part of the Western Cape when a return period of 475 years is considered. This is the return period used for the design of residential structures in South Africa. In 1969, a 6.3 Richter magnitude earthquake occurred in Tulbagh in the Western Cape. It is the most destructive earthquake to occur in South African history causing an estimated $24 million (at 2002 currency rates) in property damage and 9 fatalities (Kijko, Retief, & Graham, 2002). Damage would have been significantly more if the earthquake occurred within the Cape Town Central Business District. During the time period 1620-1971, a total of seven earthquakes occurred with a Richter magnitude in the range 5.9–6.5. Davies and Kijko (2003) suggest that 80% of all buildings in Cape Town could experience light damage when an earthquake return period of 40 years is considered. The amount of structures that could experience high levels of damage leading to collapse has not yet been determined. It is necessary to design structures that are located in these seismic active areas to resist low to moderate intensity earthquakes in order to prevent catastrophic damage.

URM is widely used to construct 2 to 4 storey residential buildings in the seismically active regions of Cape Town and its surrounding areas. URM is a brittle material with low tensile strength. This causes URM buildings to typically perform poorly under lateral excitation. URM is therefore considered to be the most vulnerable type of structure when subjected to earthquake excitation (Bruneau, 1994; Tomaževič, 1999). Bruneau (1994) reports that URM buildings suffer considerable damage in low to moderate seismic events. This can be attributed to the low tensile and shear strength of masonry as well as the large reduction in strength once cracking has initiated. Due to the poor performance of URM structures, they are no longer constructed

in areas with high intensity seismic activity. Reinforced masonry buildings are however used as alternative due to the increased ductility that the reinforcement provides. In South Africa, URM is commonly used in seismic active areas. However, research shows that URM can withstand moderate seismic events if proper design procedures are followed (Tomaževič, 1999).

South African structural design codes make provisions for the use of URM in seismic regions by including mandatory design requirements in the seismic loading code, SANS 10160-4 (2009). The code is a revision of SABS 0160 (1989) that provided design loads for seismic actions. Wium and van Zijl (2005) explain that engineers in the Western Cape were aware of the seismic provisions in SABS 0160, but did not apply them since they regarded the requirements to be too conservative. During the revision process, the scope and design concepts of the code was expanded to better reflect content of other international loading codes such as Eurocode 8 EN 1998-1 (2004). Many URM structures in Cape Town were built prior to the implementation of both the new SANS and older SABS loading codes. It is unclear to what extent seismic design was accounted for during the design process of these URM low income apartments on the Cape Flats.

URM consists of bricks joined together with mortar. Clay brick masonry is widely used in Cape Town. Due to the different material properties of bricks and mortar and the complex material interactions, masonry exhibits a non-uniform behaviour. Tests show that the properties of the masonry material will not simply be a straight forward combination of material properties of the clay bricks and mortar (McNary & Abrams, 1985). Different mortar strengths and brick strengths as well as construction quality and material workability will cause masonry to have a large degree of uncertainty with regard to material properties. The uncertainty of the material characteristics and high degree of variation between properties obtained for different structures makes the evaluation of the seismic performance of an URM structure difficult. This is further complicated by the uncertainties of South African seismic risk and the random nature of seismic events. SANS 10160-4 expanded on the conceptual design requirements of SABS 0160. Tomaževič (1999) confirms that URM requires a sound conceptual design to account for the many uncertainties associated with URM and seismic loads.

When analysing an URM building, there are many ways to account for the non-homogeneous material. The material can be analysed on a micro or a macro level. Micro material models include the bricks and mortar as separate materials, each with their own material characteristics along with a suitable model to represent interactions between the materials. These models are time consuming and computer resource intensive and therefore impractical for modelling an entire building. The micro material focus is limited to a very specific masonry problem with detailed experimental input required to provide accurate results. It has the advantage that it can account for various failure modes of URM structural elements. Macro material models represent the masonry as a single material. The material properties are obtained from empirical data or specific experimental tests and applied to a model so that the behaviour of masonry elements in different directions can be represented. This is more suited for modelling a complete URM structure. Various models can be applied to the material to model the plastic behaviour and cracking initiation. Each method has various advantages and drawbacks. Macro material models

do not provide detailed information on failure of masonry elements at the basic brick-mortar unit level. There are however methods to determine whether failure of the masonry will occur.

To determine whether a typical South African URM structure will be able to resist the seismic events that can be expected to occur in the Western Cape, it is necessary to perform an analysis of a typical URM structure. This must be performed by taking the uncertainties relating to the material and seismic excitation into account while remaining sufficiently accurate and relevant to predict building performance. Minimal research has been performed on the performance of buildings for South African conditions and further research is therefore required.

1.2 Problem Statement

Certain regions of the Western Cape are seismically active. This requires that structures located in Cape Town and its surrounding areas are designed for moderate seismic action. URM residential buildings of two to four storeys are common in the low socio-economic areas surrounding Cape Town, such as the Cape Flats. Many of these buildings were constructed prior to the implementation of the South African seismic loading codes, SABS 0160 and SANS 10160-4. There is great uncertainty whether the seismic requirements were considered during the design of these structures. It is unclear how these buildings will behave during a moderate magnitude earthquake that can be expected to occur in the seismic active regions of the Western Cape. These buildings are nevertheless common in densely populated areas. If an earthquake occurs in these areas, the damage and possible loss of lives, could be large.

1.3 Objectives

A typical three-storey clay brick URM building, representing a large portion of low cost residential buildings found in the Cape Flats area, will be analysed to asses the behaviour of the structure when subjected to an earthquake that is likely to occur in the seismically active areas of Cape Town and its surrounding areas.

Many URM residential buildings located in these seismic areas were designed before the seismic loading codes, SABS 0160 and SANS 10160-4 came into effect. South African loading codes will be examined to asses whether the structure meets the conceptual seismic requirements of the current design code, SANS 10160-4.

With each of the analyses performed on the structure, an attempt will be made to analyse and explain the behaviour of the building to shed light on the performance of URM structures in South Africa and determine whether the current state of older structures leave them at risk of failure.

1.4 Methodology

In order to meet the objectives presented in Section 1.3, it is necessary to conduct a literature review to explore the different concepts relevant to the current project.

Literature regarding the seismic history of South Africa will be presented. The seismic hazard of the Cape Town and its surrounding areas will be investigated. To evaluate the seismic design requirements for South Africa, both the older SABS 0160 and new SANS 10160-4 seismic design codes will be examined. Important factors influencing seismic design will be identified.

URM material characteristics will be researched as well as the use of URM as construction material in South Africa. The seismic performance of URM will also be discussed.

Analysis methods will be examined in order to choose a method suitable to the current project.

A review of the literature will provide the necessary theory to conduct a suitable analysis.

A relevant material model will be chosen to account for the typical material properties used in South Africa. The model must account for the non-homogeneous nature of masonry and provide accurate results relating to URM seismic performance. The material model will be calibrated using experimental data from other authors to ensure the validity of the model.

A building will be selected that represents typical URM residential buildings located on the Cape Flats. The building will be analysed with regard to the conceptual design requirements of SANS 10160-4. A finite element model of the building will be created in ABAQUS. During the modelling process, assumptions and simplifications will be made.

Several earthquakes will be selected to represent a range of different earthquakes that can be expected to occur in the seismic active regions of the Western Cape. The earthquakes will be selected to analyse the response of the building to a range of different excitation parameters.

The dynamic characteristics of the structure will be determined after which a range of dynamic time-history analyses will be performed to determine the behaviour of the building to the selected earthquakes. The results will be analysed with regard to typical failure modes observed for past earthquakes. Possible points of failure will be identified and the reasons for the behaviour explained.

Results from the different analysis types will be compared to evaluate the validity of results. When applicable, discrepancies in the results obtained by different analyses will be explained.

The effect that certain parameters have on the results will be examined to justify specific choices of parameter values and to extend the applicability of results to a broader range of buildings.

1.5 Delimitations

URM has many uncertainties relating to the material and construction practices. Minimal research data is available on the use of URM in South African conditions. This paper will

therefore select a building that is considered typical of a large portion of URM buildings in the Western Cape, rather than considering a specific structure. International research will be used to assign certain material properties since research on the seismic behaviour of URM in South Africa is scarce.

Although the building will be analysed with regard to the conceptual requirements of SANS 10160-4, whether the practical design requirements were adhered to during construction will require a large scale examination of existing structures in the Western Cape, and falls outside the scope of the project.

The magnitude of forces that is to be transferred by connections will be determined. Detailed modelling of connections and evaluation of connection capacity will however not be included since it can differ widely from structure to structure and will depend on the design of a specific building.

Issues relating to the difference in strength of in-situ materials at different sites, the effect of age and construction quality will not be quantified since further research is required.

Soil-foundation interactions is complex and should be studied for specific sites. This will not be attempted since the current project aims to study a typical building, rather than a specific structure. The effect that ground type has on the seismic response of the building will however be considerd through the choice of ground type.

1.6 Thesis Layout

The Literature will be presented in Chapter 2 to give a background to the matter covered in the project. Information regarding the occurrence of earthquakes in South Africa will be presented including the seismic risk of the Western Cape region and past earthquakes that occurred. A broad overview of the seismic design code SANS 10160-4 will be included along with important factors that affect seismic design. The use of URM in South Africa as well as the material properties and behaviour will be discussed. Thereafter the seismic performance and common failure modes will be addressed. Finally literature regarding design and analysis methods of URM will be discussed to shed light on the procedures used in later chapters.

A masonry material model will be calibrated using experimental data described in Chapter 3. Important aspects regarding the non-homogeneous nature of the material will be addressed by performing different calibrations for the in- and out-of-plane directions. In addition, a non-linear material will be selected along with relevant dynamic properties such as damping.

In Chapter 4, the modelling process will be discussed. Initially the building choice and layout will be presented. The building will be assessed with regard to the basic conceptual seismic design requirements presented in SANS 10160-4 to evaluate the building resistance when regarding basic design and layout. This highlights whether the building will have sufficient capacity to resist seismic actions outside the scope of the original design and intended use. The simplifications and assumptions made during the modelling process will be presented along with the finite

element model that will be used for analysis. To verify the validity of the finite element model, an elastic static analysis will be performed under vertical and horizontal loads. This will ensure that irregularities can be eliminated before analysis commences.

Several earthquakes will be selected to represent possible earthquakes that could occur in South Africa. The acceleration time histories and earthquake properties will be discussed in Chapter 5. A modal analysis will be performed to determine the natural frequencies and corresponding modes of vibration of the structure. This will allow a modal time history analysis to be performed after which the results will be discussed.

The analysis performed in Chapter 5 is linear and does therefore not take non-linear material data into account. The model will be simplified as a MDOF mass-spring model and analysed in Chapter 6. The results of the mass-spring analysis will be used to validate the results of the modal dynamic analysis performed in Chapter 5. A sensitivity analysis will be performed to determine the effects of variable parameters on the model response. Finally an implicit non-linear analysis will be performed to determine the post cracking response of the structure. The mass-spring analysis, sensitivity analysis and implicit dynamic analysis along with results are discussed in Chapter 6.

Lastly, a conclusion is made regarding the performance of the structure. This is presented in Chapter 7 along with recommendations for future studies.

1.7 Summary

The basic introduction to the project was presented in this chapter. Background information was included along with the problem statement. In Chapter 2, a literature review will be presented to provide an understanding of the seismic history and design in South Africa along with information on the properties behaviour and analysis of URM. This information will be used in Chapters 3 to 6 to analyse an URM structure.

Chapter 2

Literature Review

2.1 Introduction

The purpose of this Literature Review is to discuss the relevant literature that will be used during this thesis. Various articles are consulted and comparisons are then drawn. Initially, the cause of earthquakes will be broadly discussed in Section 2.2 including the rate of occurrence and global distribution. Two major scales used to define the magnitude and intensity of a particular seismic event, the Richter magnitude scale and Modified Mercalli intensity scale are also explained along with a comparison between the two scales. The frequency and distribution of earthquakes in South Africa are addressed in Section 2.3 with examples of past seismic events including damage and seismic properties. South Africa has earthquakes of both natural and mining origin. The areas affected by the earthquake types and regions where seismic design must be implemented, are also presented. South Africa uses SANS 10160-4 (2009) as structural loading code. SANS 10160-4 supersedes SABS 0160 (1989). Issues regarding the revision of SABS 0160 are discussed in Section 2.4. Thereafter, important concepts of SANS 10160-4 relating to seismic design are examined in Sections 2.4.1 to 2.4.7. This includes the peak ground acceleration, redundancy factor, response spectrum, ground types, behaviour factor, natural period of vibration and basic design and detailing principles. For each of the topics, an explanation is provided and comparison made to the treatment of the concept in SANS 10160-4 and SABS 0160.

The material properties of unreinforced masonry are discussed in 2.5. Elastic material properties, including elastic modulus, Poisson ratio, compressive strength, tensile strength and shear strength are specified in Sections 2.5.2 to 2.5.5. Material data from different authors are summarised. This data can be used to define the elastic behaviour of masonry until cracking occurs. After cracking has initiated, the material will respond in the plastic range as discussed in Section 2.5.6. The use of masonry in South Africa and application of masonry during construction are considered in Sections 2.5.7 and 2.5.8 respectively.

After the behaviour and properties of masonry are considered at the material level, the seismic behaviour of masonry buildings and structural elements is discussed in Section 2.6. First, the structural system of typical unreinforced masonry buildings is examined. Seismic failure modes,

in- and out-of-plane seismic resistance and behaviour of floor diaphragms are then explained.

In Section 2.7, two commonly used design methods are presented. The two methods are the static lateral force method implemented by SANS 10160-4, as well as the displacement based design method.

Finally, different modelling and analysis methods are discussed in Section 2.8. The methods are generally categorized as linear or non-linear methods. Information regarding the use of 2D or 3D analysis techniques are also outlined in Section 2.8.3. This chapter should provide sufficient information so that an analysis of a typical unreinforced masonry structure in the Cape Town area can be performed.

2.2 The Cause of Earthquakes

Earthquakes are a very common and destructive phenomenon. They occur globally, from very remote locations, to some of the busiest city centres. According to the United States Geological Survey (USGS, 2012) several million earthquakes occur worldwide annually. Most of these earthquakes are however minor tremors and many of them occur in remote locations and go unnoticed by the public. The National Earthquake Information Centre (NEIC) identifies more than 20 000 earthquakes annually with a Richter magnitude larger than 4.5. Magnitude 4.5 earthquakes are minor quakes that are felt as a tremor by humans in a close proximity to the origin. As the intensity of earthquakes increase above 5 on the Richter scale, damage to property will start to occur. It is these earthquakes that concern structural engineers.

There have been many destructive earthquakes across the world that have claimed numerous lives. The USGS lists more than twenty earthquakes which resulted in a death toll exceeding 50 000. To understand why earthquakes are as widespread, one must investigate their cause.

The Earth has a solid outer layer, called the Lithosphere. Under the Lithosphere lies the soft Asthenosphere. According to the commonly accepted plate tectonics theory (Tarbuck & Lutgens, 2008), the Lithosphere is divided into several plates that are able to move on the softer Asthenosphere. At the boundaries between the plates, weaker rock exists, which are called faults. Plate movement takes place along the fault lines. As a plate moves, large stresses develop at the fault zones as the solid rock resists movement. Strain energy develops at the fault zones, until slippage occurs, when the rock is no longer able to resist plate movement. All strain energy is suddenly released as the rock in the fault zones breaks apart and movement occurs. The movement will cause the ground to shake horizontally and vertically as shock waves are released. This is what we observe as an earthquake. The exact underground location where the initial energy is released is termed the *focus* or *hypocentre*. The *epicentre* is the location on the surface, above the focus. Figure 2.1 shows the locations of the major plate boundaries (lines indicated in yellow) across the world. Previously recorded earthquakes have been indicated on the map, showing the locations of the most active faults.

Only earthquakes with a Richter magnitude equal or greater than 6 are shown on the map. Red circles indicate earthquakes where accurate information of the location and depth of the

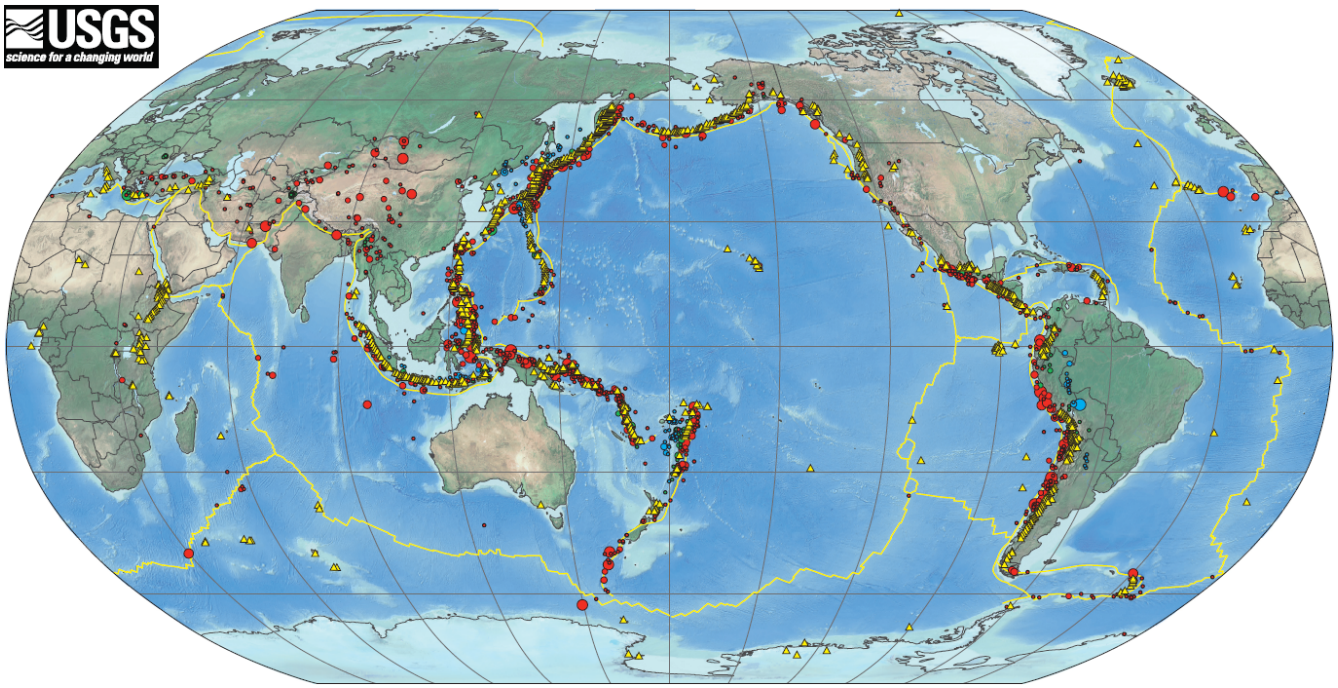

Figure 2.1: A USGS map of the world indicating major recorded earthquakes with a Richter magnitude equal or greater than 6 and the primary plate boundaries (USGS, 2012).

earthquake is known. This is commonly only the case for earthquakes that were recorded after the implementation of the World-Wide Standardized Seismograph Network in 1964. Earthquakes that are indicated with a yellow triangle are events recorded before 1964. Many of these events have poor location data and had to be relocated using modern wave property algorithms and empirical data of surrounding areas. The largest shapes indicate earthquakes with a Richter magnitude larger than 8.

Earthquake size can be represented using different scales. The commonly used Richter scale is a method of representing the energy contained in an earthquake. The value is calculated by taking the logarithm of the amplitude of waves measured by a seismograph with adjustments made to account for distance from the epicentre. The intensity of an earthquake is normally measured using the Modified Mercalli intensity (MMI) scale. It measures the effects of an earthquake on a scale of I to XII. The intensity is a measure of the impact an earthquake has on people, structures and the natural environment. Table 2.1 shows a comparison between earthquake magnitude and the corresponding expected intensity (Saradj, 2007).

2.3 Earthquakes in South Africa

South Africa is not considered an earthquake prone country by the general public. They are however unaware that South Africa has certain areas that are at risk of low to moderate sized earthquakes. Earthquakes with Richter magnitudes between 6 and 7 have been recorded in certain parts of South Africa. A prime example is the destructive Tulbagh earthquake that occurred on 26 September 1969. The Tulbagh earthquake, with a Richter magnitude of 6.3, is

Table 2.1: A comparison between Richter magnitude and corresponding Mercalli intensity for the range of earthquakes expected in South Africa (Saradj, 2007).

Richter Magnitude	**MMI**	**Description**
4.0 – 4.9	IV – V	**IV.** Felt indoors by many, outdoors by few during the day. At night, some awakened. Dishes, windows, doors disturbed; walls make cracking sound. Sensation like heavy truck striking building. Standing motor cars rock noticeably.
		V. Felt by nearly everyone; many awakened. Some dishes, windows broken. Unstable objects overturned. Pendulum clocks may stop.
5.0 – 5.9	VI – VII	**VI.** Felt by all, many frightened. Some heavy furniture moved; a few instances of fallen plaster. Damage slight.
		VII. Damage negligible in buildings of good design and construction; slight to moderate in well-built ordinary structures; considerable damage in poorly built or badly designed structures; some chimneys broken.
6.0 – 6.9	VIII – IX	**VIII.** Damage slight in specially designed structures; considerable damage in ordinary substantial buildings with partial collapse. Damage great in poorly built structures. Fall of chimneys, factory stacks, columns, monuments, walls. Heavy furniture overturned.
		IX. Damage considerable in specially designed structures; well-designed frame structures thrown out of plumb. Damage great in substantial buildings, with partial collapse. Buildings shifted off foundations.

one of seven earthquakes with a magnitude in the range 5.1–6.5 to occur in the period 1620–1971. The Tulbagh earthquake is the most destructive earthquake in South African history. Damage included an estimated $24 million (at 2002 currency rates) in property damage and 9 fatalities (Kijko et al., 2002).

Although major earthquakes are normally produced as a result of tectonic plate movement, moderate sized earthquakes can also be caused by mining activity. During the process of mining, large amounts of rock is removed. This causes the settlement of surrounding rock which is under extreme pressure. The settlement of the rock causes tremors that are observed at the surface as earthquakes. The majority of earthquakes in the central and northern parts of the country occur as a result of mining activities.

The South African Council for Geosciences (2013) compiled a list of the most notable earthquakes that occurred in South Africa in the 20th Century. The location, intensity/magnitude and description of these earthquakes (including the Tulbagh earthquake) are given in Table 2.2.

Table 2.2: Earthquakes of note which occurred in the 20th Century in South Africa (South African Council for Geosciences, 2013).

Date	**Region**	**Intensity/ Magnitude**
20/02/1912	Near Koffiefontein	VIII / 6
Remarks: Felt all over South Africa. Many Farm buildings completely destroyed.		
31/12/1932	Off Cape St. Lucia	VIII / 6.0–6.5
Remarks: Poorly constructed buildings badly damaged, one or two collapsed, cracks and fissures in ground reported.		
29/09/1969	Ceres Tulbagh Wolseley	VIII–IX / 6.3
Remarks: Serious damage to certain buildings in the area, damage varied from almost total destruction of both old and poorly constructed buildings, to large cracks in better built ones. 12 people were killed and many more injured.		
08/12/1976	Welkom	VII / 5.2
Remarks: Extensive damage to many buildings and breaking of windows. The most dramatic event was the collapse of a six storey block of flats. The building collapsed 75 minutes after the seismic event (see Figure 2.2).		
07/03/1992	Carletonville	VII / 4.7
Remarks: Unusual amount of damage recorded, due to the high population density around the epicentral area. Houses were damaged as far as Pretoria, 100km away.		

Table 2.2 lists earthquakes that are both natural and mining induced. Damage from the earthquakes ranges from cracks and broken windows to complete building collapse.

Figure 2.2 shows a 6 storey unreinforced masonry (URM) building that collapsed during the 5.2 magnitude mining induced earthquake that occurred in Welkom in 1976. Figure 2.3 shows damage to several buildings after an earthquake in Stilfontein in 2005. The Stilfontein earthquake, with a magnitude of 5.3, is the largest mining induced earthquake in South African history. Several buildings were damaged, 58 people were injured and two mineworkers were killed during the incident (Linzer et al., 2007).

Figure 2.2: The 6 storey building that collapsed during the 1976 earthquake in Welkom. (South African Council for Geosciences)

Figure 2.3: Two damaged buildings after the Stilfontein earthquake (Linzer et al., 2007).

Davies and Kijko (2003) performed an assessment of the possible impact that seismic activity could have on the South African insurance industry. This involves the estimation of damage using probabilistic methods for different building types across various locations in South Africa. It was determined that the expected annual damage from earthquakes for Cape Town is 1.08% of building replacement costs. If an earthquake with a return period of 40 years is considered, 80% of all buildings could experience light damage. For earthquakes where return periods of 475 years are considered for design, the damage to under designed buildings will be significantly greater. When a 6.9 Richter magnitude earthquake (the maximum magnitude considered by Davies and Kijko (2003)) occurs close to Cape Town, it is expected that between 30% and 61% of all URM buildings will be damaged. There is a high uncertainty regarding the expected damage to URM buildings due to the varying performance of URM buildings in past earthquakes. From a monetary point of view, the impact that earthquakes could have on the South African economy if proper design procedures are not adhered to, can not be ignored. This has already caught the attention of the South African insurance industry leading to the study performed by Davies and Kijko (2003).

From Figure 2.1 it is clear that there are no major plate boundaries close to South Africa. Apart from plate boundaries, there are many smaller faults around the world not indicated on the map. The closest active fault to Cape Town is the Milnerton fault which is located approximately 8 kilometres off the west coast and runs through Milnerton. Even though this is not a major fault, it is active and capable of producing moderate sized earthquakes. A fault can be considered to be active if an earthquake occurred within the last 10 000 years. This is applicable to normal design situations where earthquakes with a return period of 475 years are considered. This criteria will be different depending on the importance of the buildings to be designed. A nuclear power station such as Koeberg should be designed for seismic action if seismic events have occurred in the area within the last 350 000 years (Tomaževič, 1999), proving that the Milnerton fault is indeed very active. Little information is available on the precise location of faults and seismological risk of South Africa (Singh, Kijko, & Durrheim, 2009). An important step in determining the seismic risk is to determine a seismotectonic model of the country. This has not yet been done. Current hazard profiles were based on the analysis of the main tectonic structures and present day seismicity correlations. Distinguishing between natural and mining induced earthquakes is also difficult. It is necessary to consult the history of mining activity in a particular area in order to possibly assess the cause of earthquakes in areas where mining occurs (Singh et al., 2009).

Figure 2.4 displays the locations of earthquakes along with their magnitudes that occurred in and around South Africa from 1620 to 1970. The map clearly shows the seismic active area surrounding Cape Town, as well as concentrations in the central part of the country, among others. The map has been overlain with the seismic hazard zones of South Africa, taken from SANS 10160-4 (2009). Natural earthquakes are denoted as *zone I* and mining induced earthquakes are denoted as *zone II*.

The seismic map has been developed from recorded earthquakes as well as historical documented cases where monitoring equipment were not available. This is the case for earthquakes that

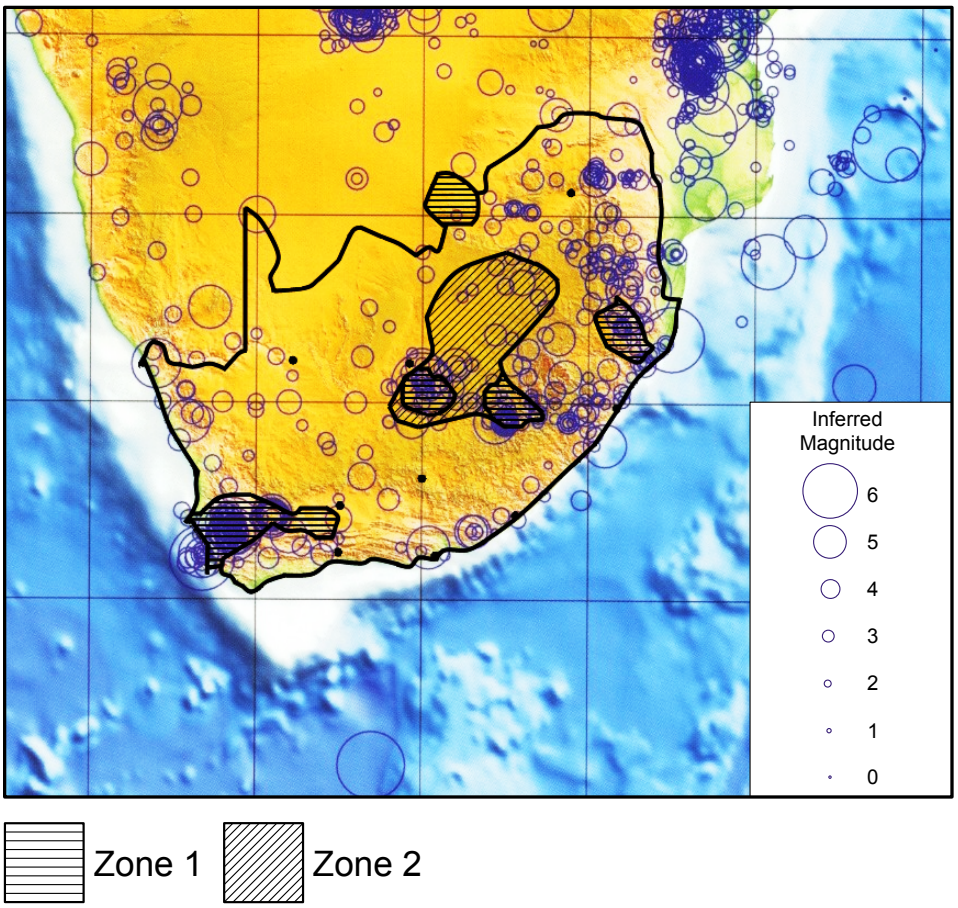

Figure 2.4: Map of magnitudes, inferred from the maximum Modified Mercalli scale intensities of known earthquakes from 1620 to 1970. Map obtained from Geosciences and overlain with seismic hazard zones as illustrated in SANS 10160-4 (2009).

occurred prior to 1900. Written accounts of seismic events were assigned a value on the Mercalli intensity scale which was then converted to Richter magnitude. This is a rather inaccurate way of determining the size of seismic events but is nevertheless the only way that historical events, without sufficient information can be quantified. Amongst the earthquakes identified using this method were earthquakes that occurred in 1809 and 1811 with estimated intensities of VI–VIII (magnitude 6.1) and VII (magnitude 5.5–6) respectively.

2.4 South African Design Codes

The current structural loading code in South Africa is SANS 10160 (2009). The code consists of 8 parts. Part 4 addresses seismic actions. It is a new code that, until recently, was in draft form. The purpose of the design code is to provide rules, strategies and limitations for the design of structures in order to prevent major catastrophic structural failures in the event of an earthquake and therefore preventing loss of life. The main focus of the code is not to prevent damage to buildings but rather to limit and control damage so that structural collapse does not occur.

SANS 10160-4 supersedes SABS 0160 (1989) (hereafter simply referred to as SANS and SABS respectively) that was first published in 1989 and revised in 1993. The sections dealing with seismic actions were considered inadequate (Dunaiski, Retief, & Goliger, 2007). Wium and van Zijl (2005) report of a meeting held in 2003 where many designers in the Western Cape area admitted to knowing of the seismic requirements of SABS but not applying it as they believed it to be unrealistic. They believed the code requirements were too stringent and could not be economically justified. The code also applied only to small regions in the country. The problem was made worse due to the fact that South Africa's earthquake history was not in the public domain and was poorly documented. The decision to revise SABS was already made in 1998 at the South African National Conference on Loading. The first step was made in 2004 through the establishment of a local committee in the Western Cape. The committee decided that the code had to be revised in order to ensure the provisions were realistic and to assure the industry that the seismic code is relevant (Wium & van Zijl, 2005). During the revision process, the knowledge and awareness in the industry about principles of seismic design was to be improved. At the same time, the trust of local engineers in the seismic code had to be built.

Eurocode 8 EN 1998-1 (2004) was used together with UBC (1997) as basis for the revision of SABS. Dunaiski et al. (2007) lists various advantages that led to the use of Eurocode 8 as basis for the revision. Eurocode 8 includes up to date information on seismic design. Insufficient resources are available for a complete rewrite of the South African code. In general it was decided that SABS will determine the scope whilst Eurocode 8 will provide the additional information not present in SABS. The approach that Eurocode 8 follows was simplified and adapted for South African use. Whether the changes to the code are realistic and relevant for South African conditions remains to be tested. It is also necessary to assess whether buildings that were constructed to the specifications of the now superseded SABS still meet the updated requirements of SANS. Above all, it is necessary to determine whether existing buildings can withstand a moderate intensity earthquake.

Various factors that influence the design base shear force for which structures are designed together with the changes and additions made during the revision of SABS will be discussed in Sections 2.4.1 through 2.4.7. This will highlight the possible pitfalls in using SANS for seismic design and also indicate some differences between the SANS and SABS codes.

2.4.1 Peak Ground Acceleration and Load Combinations

Earthquakes cause ground motion that can be recorded by measuring the ground acceleration over the duration of the seismic event. The magnitude of the acceleration peaks give a measure of the intensity of the earthquake. Since structures are excited through motion at the base of the structure (i.e. ground motion), the earthquake acceleration profile gives a direct measure of the excitation that a building will undergo. This is not the case with Richter magnitude, because the energy released by an earthquake will not be directly related to ground excitation, and therefore not necessarily be an accurate measure of the excitation that a buildings will be subject to. The peak ground acceleration (PGA) is the maximum peak acceleration value

measured at the surface during an earthquake. It is commonly used as a basis for seismic design.

SANS includes a seismic hazard map of South Africa. The map contains two zone types, namely: type I (Natural seismic activity) and type II (mining induced activity). Figure 2.4 displays the locations of the above mentioned zones. The map has been generated using PGA values with an exceedance probability of 10% for a 50 year period. This relates to a seismic event with a 475 year return period, a common design standard also used in Eurocode 8. The seismic hazard map used in SABS shows a PGA value of $0.2g$ for the Cape Town area (where earth gravity acceleration; $g = 0.98m/s^2$). This has been replaced in SANS with an updated map that shows a reduced PGA of $0.15g$ for the same area. Figure 2.5 shows the PGA contours of a portion of the Western Cape as it appears in SANS (left) and SABS (right). Both SANS and SABS specify that a *design* PGA value (a_g) of 0.1g should be used for the design of all buildings located in zone I, irrespective of the larger PGA values shown on the seismic hazard map in Figure 2.5.

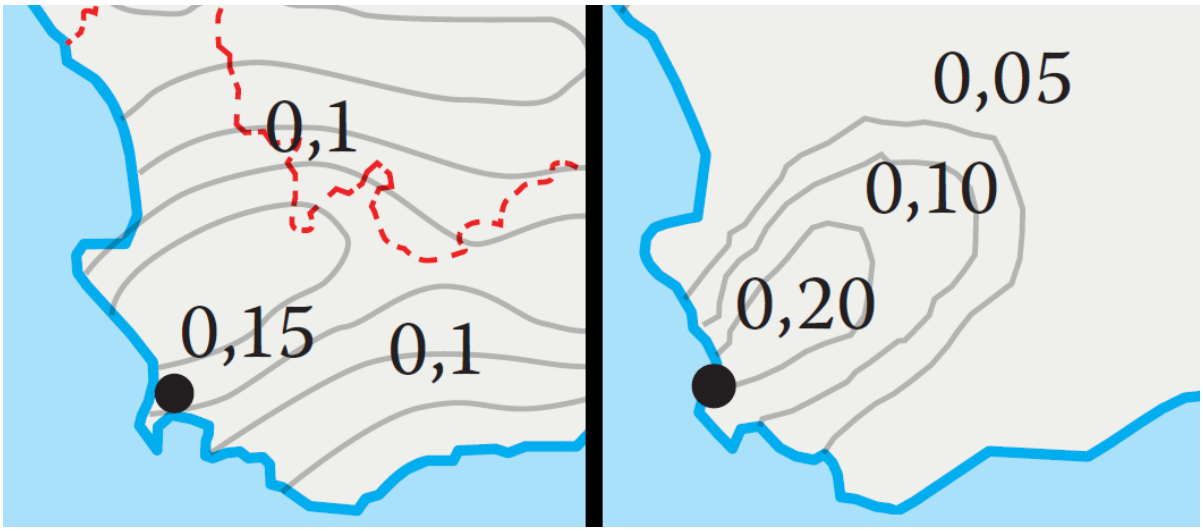

Figure 2.5: PGA contours of a portion of the Western Cape as published in SANS 10160-4 (2009) (left) and SABS 0160 (1989) (right).

Whether the reduced PGA value used for design purposes is sufficiently large is questionable. Kijko et al. (2002) calculated that the Tulbagh earthquake of 1969 had a corresponding PGA value of: $0.13g \leq PGA \leq 0.26g$. Kijko et al. (2002) continues to show that a return period of 475 years corresponds to a PGA value in the range $0.13g \leq PGA \leq 0.23g$ with a mean value of $0.18g$ for the Tulbagh area. This is much larger than the design value published in both SANS and SABS. The SANS revision committee initially considered using a value of 0.15g, as shown in Figure 2.5. Wium (2010) explains that designers regarded the PGA values in SABS to be unrealistic. Many design engineers suggested that a lower PGA value be specified for the Western Cape, since larger PGA values would lead to more expensive and over conservative designs. With many stakeholders, risks involved and impacts on the local economical environment to consider, the working group was not able to make a final decision on a design PGA value to be used for the drafting of the new SANS code. Thus, the design PGA value of 0.1g was retained. The redundancy factor, defined in Section 2.4.2, was implemented in SANS 10160-4 to address this issue.

SABS specifies a load combination of $1.2DL+1.6SL$; where DL = Dead Load and SL = Seismic Load. Most other codes such as Eurocode 8 consider seismic actions as an accidental load case with a $1.0DL + 1.0SL$ load combination. In the past, designers typically preferred to use the smaller load combinations provided in Eurocode 8 along with the design PGA value (0.1g) specified in SABS for their design. In SANS, the load combinations were lowered to meet the requirements of Eurocode 8, i.e. $1.0DL+1.0SL$. This was an important step to prevent designers from using portions of different design codes out of context which could result in under designing a structure.

2.4.2 Redundancy Factor

In structural design, redundancy refers to the practice of adding more load resisting structural elements to a structure than is required as a minimum. Shear walls are the primary load resisting element responsible for resisting ground excitation during seismic events. Adding additional shear walls, or increasing the dimensions of shear walls will increase the redundancy of a structure. This is essential since it adds additional capacity to resist seismic loads even after damage has occurred. Every earthquake is unique. This means that a building can easily be subject to larger displacements, forces or unforeseen actions than it is initially designed for. Adding additional redundancy is essential in allowing a structure to resist these unexpected loads.

The redundancy factor accounts for redundancy of structural elements, such as shear walls, in the structure. The redundancy factor (ρ) was taken from UBC (1997) and incorporated in SANS. The UBC places a limit of $1.0 \leq \rho \leq 1.5$ on this factor. SANS limits the redundancy factor to: $1.2 \leq \rho \leq 1.5$. The redundancy factor is a function of shear wall cross sectional area and length. By increasing the amount of shear walls, the redundancy factor can be reduced. The redundancy factor is used along with the design PGA when calculating the design seismic load. Increasing or decreasing the redundancy factor will directly increase/decrease the design seismic load and effectively increase/decrease the design PGA. The redundancy factor was incorporated into SANS to account for the reduced PGA value of $0.1g$ and to encourage redundant design. If a structure does not have sufficient redundancy, a large ρ value of 1.5 is specified, effectively resulting in an increased design PGA value of $0.15g$. Increasing the amount of shear walls and the length of shear walls will allow for the redundancy factor to be reduced. With the inclusion of proper redundancy in the design, the factor can be reduced to a minimum value of 1.2, resulting in a design PGA value of $0.12g$. This assumes that shear walls are properly designed to code requirements.

Wium (2010) explains that increasing the design PGA value indirectly through the obscure use of the redundancy factor is not ideal. The use of the redundancy factor will achieve adequate results if the entire code is used for the design i.e. using the equivalent lateral static force method and incorporating the redundancy factor into the design. Unfortunately many designers use finite element software by simply assigning a PGA value of 0.1g together with load factors taken from the code. By using this approach they often overlook the redundancy factor. This dilemma is created when using portions of the code out of context. It is recommended that the

designer uses the product of the PGA value and the redundancy factor when using an alternative design method; i.e. $g = PGA \times \rho$.

2.4.3 Response Spectrum and Soil Factors

Design codes implement design response spectra to calculate the response that a structure with a given natural frequency and ground type will have to a ground acceleration produced by an earthquake. Response spectra were developed to accommodate many different structures and ground types. A response spectrum is constructed by measuring the maximum response of a single-degree-of-freedom (SDOF) system with a specific natural frequency when subject to a given ground motion. This is repeated using various SDOF systems, each with a different natural frequency, and applying time series of many recorded earthquakes. The maximum response is measured for the different natural frequencies. The response results are statistically manipulated and smoothed to produce elastic response spectra. Response spectra are constructed for a specific damping value.

During an earthquake, as seismic shock waves move from the focus through the different soil layers, they are refracted and reflected. Soil layers of different densities and hardness amplify and damp the waves before they finally reach the surface (Tomaževič, 1999). The influence that the ground has on seismic waves is taken into account by specifying ground types in the design codes. That being said, only a small portion of the energy released by an earthquake causes shock waves. Large amounts of energy is dissipated through the crushing of rock close to the focus. In general, the movement of waves through the softer soil layers absorbs many of the stochastic portions of the wave to produce longer periods of strong motion with increased amplitudes of vibration. Movement through harder soil and bedrock preserves the stochastic parameters (Tomaževič, 1999). This behaviour greatly influences the response spectrum obtained for different ground types.

SANS identifies four ground types (type 1 to 4) indicated in Table 2.3, taken directly from Eurocode 8 where it is tabulated as type A to D. Ground type is classified according to the average S-wave propagation velocity in the upper 30m of the soil profile ($v_{s,30}$), Standard Penetration Test blow-count (N_{SPT}) and the un-drained shear strength of soil in kPa (c_u). Tests should be carried out for a building site to determine $v_{s,30}$. If this is not possible, the Standard Penetration Test can be used.

Eurocode 8 has three additional ground types (E, S1 and S2). Ground type E is defined as: a soil profile consisting of a surface alluvium layer with $v_{s,30}$ values of type C or D and thickness varying between about 5 and 20 meters underlain by stiffer material with $v_{s,30} > 800m/s$. This ground type is represented by a separate spectral response curve with a very large response at low periods that quickly dissipates as the period increases. Apart from ground type E, Eurocode 8 also includes two special ground types S1 and S2. This represents soil with a high plasticity index and water content (S1) and deposits prone to liquefaction (S2). The code specifies that special studies are required for ground types S1 and S2. There is no mention of ground types S1, S2 and E in SANS. There is little information available on the topic of liquefaction in South

Table 2.3: Ground types as published in SANS 10160-4 (2009).

Ground type	Description of stratigraphic profile	Parameters		
		$v_{s,30}$ m/s	N_{SPT} blows/30cm	c_u kPa
1	Rock or other rock-like geological formation, including at most 5 m of weaker material at the surface.	> 800	-	-
2	Deposits of very dense sand, gravel, or very stiff clay, at least several tens of m in thickness, characterised by a gradual increase of mechanical properties with depth.	360 - 800	> 50	> 250
3	Deep deposits of dense or medium dense sand, gravel or stiff clay with thickness from several tens to many hundreds of m.	180 - 360	15 - 50	70 - 250
4	Deposits of loose-to-medium cohesion-less soil (with or without some soft cohesive layers), or of predominantly soft-to-firm cohesive soil.	< 180	< 15	< 70

Africa and on the occurrence of liquefaction at low PGA values; **this indicates that further research is required.**

Different response spectra are created for each ground type. The spectra are then normalised with respect to PGA to produce normalised elastic response spectra. The normalized design response spectra that are used design in SAN 10160-4 are shown in Figure 2.6

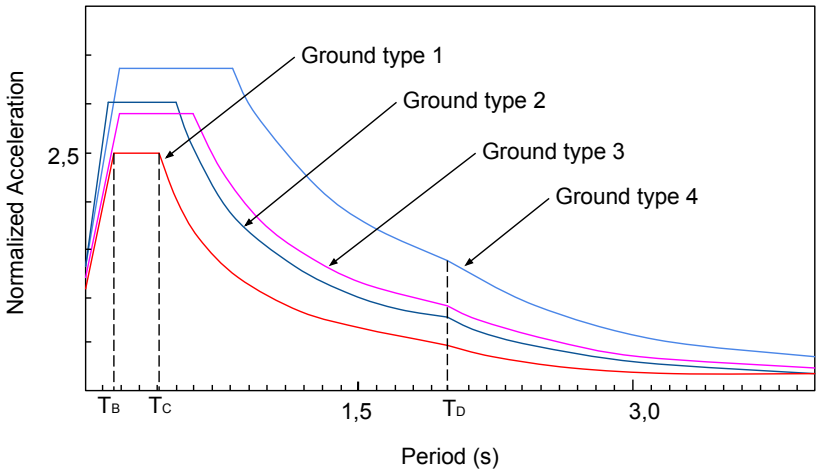

Figure 2.6: Normalised design response spectra for 5% damping and a behaviour factor q = 1 as published in SANS 10160-4 (2009).

Section 2.4.5 discusses the procedure for determining the natural period of vibration of a structure. This is used along with subsoil class and design ground acceleration values to determine the elastic response. SANS contains four response spectra, one for each ground type, indicated in Figure 2.6. It is therefore necessary to determine the ground type of the site that a building occupies in order to choose a relevant response spectrum. The code stipulates that the most unfavourable response curve (the curve representing the largest response for a given natural frequency) should be used when the site conditions are not fully known or when site investigations do not enable any profiles to be used. Design response spectra included in SANS are constructed for a 5% damping ratio. They are normalised with respect to design acceleration and behaviour factor (discussed in Section 2.4.4) so that they can be applied to different design

ground accelerations and building types.

2.4.4 Behaviour Factor

In general, masonry is regarded as a brittle material. Empirical data have, however, shown that masonry does indeed demonstrate some ductile behaviour during seismic excitation. The ductility of the structure will enable it to displace more than is predicted with a linear elastic representation, without needing to resist a larger force. Non-linear characteristics of masonry can be sufficiently accounted for by performing a direct non-linear dynamic analysis of the structure as explained in Section 2.8.2. This is a complex and time consuming analysis method. Design codes, including SANS suggest the use of simple linear elastic methods. Non-linear effects will be represented through the use of the behaviour factor.

To understand the purpose of the behaviour factor, it is necessary to look at the way in which structures dissipate energy during an earthquake. Figure 2.7 shows a typical response graph of an URM structure along with a simplified linear elastic–perfect plastic envelope.

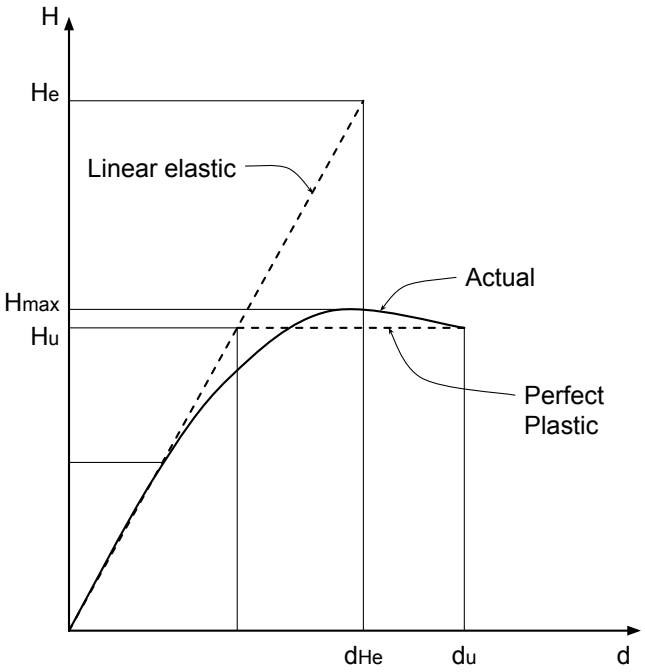

Figure 2.7: Structural resistance diagram indicating the actual as well as linear elastic - perfect plastic material behaviour in order to define the behaviour factor (q) (Tomaževič, 1999).

During an earthquake, the structure is subjected to displacements at it's base. As the structure responds to the earthquake, it dissipates energy, represented by the area under the building response graph. Due to the non-linear nature of materials, a building is able to undergo larger displacements after yielding has occurred, without needing to resist a large increase in stress. The amount of displacement that a structure can undergo before failure depends on the ductility of the material. It is therefore possible to design a structure for the ultimate design load (the load at which maximum displacement has occurred) instead of the elastic seismic load (the load at which the ultimate displacement will occur if the structure remains elastic) (Tomaževič,

1999). The ratio of these two forces ($q = H_e/H_u$) is termed the behaviour factor, and is listed in SANS. URM buildings have a behaviour factor of 1.5 tabulated in SANS. **These factors where taken directly from SABS without any experimental verification.**

Tomaževič, Bosiljkov, and Weiss (2004) performed experimental tests on 2 and 3 storey building models to verify that a value of 1.5 is indeed accurate for masonry. The research shows that the behaviour factor is dependant on the material quality, construction methods and structural system used. It is also shown that the value of 1.5 is conservative and that certain structural layouts will produce larger values. This means that a well constructed URM building constructed using high quality materials would be able to undergo larger deflections than calculated using the code. This emphasises the need for good construction practices and a sound conceptual design as discussed in Section 2.4.6. The response spectra are reduced by applying the behaviour factor to account for non-linear behaviour.

2.4.5 Natural Period of Vibration

SANS provides a simplified formula for the calculation of the fundamental period of vibration (T) for buildings up to 40m in height. The majority of URM buildings in South Africa fall in this category. The formula provided by SANS for URM buildings is given by Eq. 2.1.

$$T = C_T \times h_t^{3/4}, \tag{2.1}$$

The values of C_T and A_C is obtained from Eqs. 2.2 and 2.3:

$$C_T = \frac{0.075}{\sqrt{A_c}} \tag{2.2}$$

$$A_C = \sum \left[A_i \left(0.2 + \left(\frac{L_{wi}}{h_t} \right)^2 \right) \right]. \tag{2.3}$$

A_C – Total effective area of shear walls on the first storey of the building.

A_i – Effective cross section area of wall i on the first storey.

h_t – Height of the building from the foundation or top of a rigid basement.

L_{wi} – Length of the shear wall i in the first storey in the direction parallel to the applied forces with the restrictions that L_{wi}/h_t shall not exceed 0.9.

Equation 2.1 is a very crude formula for the determination of the natural frequency. The formula assumes a regular structural layout with uniform storey mass and stiffness along the height of the structure. In addition, it assumes that the lateral load-resisting structural elements are continuous along the height of the structure. This means that the natural frequency can be completely underestimated, especially if a structure has abrupt changes in shape, mass and stiffness along it's height.

SANS allows for the use of alternative methods. The code specifies that a natural period computed by an alternative method may not exceed 1.4 times the period calculated using Eq. 2.1. This is due to many designers using finite element software to determine the natural period of a building. Normally, when a building is modelled, only the structural components are modelled. Masonry in-fills and other non-structural elements are not considered. These elements provide additional stiffness to the structure. By underestimating the stiffness of a structure, the natural period obtained can be unrealistically large, leading to an unconservative design. Figure 2.6 shows that increasing the natural period of vibration could result in a reduced building response used for design. Limiting the natural period will prevent this. In addition, SANS notes that the stiffness and strength properties of all elements that significantly influence the mass and stiffness of the structure and that influence the distribution of forces are to be included when using alternative design methods. Unless specifically calculated using a non-linear approach, the stiffness of cracked elements should be taken as half of their original stiffness. Due to the brittle nature and low tensile resistance, URM buildings should be assumed to be cracked during seismic analyses.

2.4.5.1 Rayleigh Method

The Rayleigh method is an alternative approach for determining the natural frequency. It is based on the principle of conservation of energy and is given by Eq. 2.4.

$$\frac{1}{T_1} = f_1 = \frac{1}{2\pi} \cdot \sqrt{\frac{\sum_{i=1}^{n} F_i d_i}{\sum_{i=1}^{n} m_i d_i^2}} \tag{2.4}$$

m_i – mass of the i^{th}-storey located at height h_i.

d_i – horizontal displacement of the i^{th}-storey due to lateral force F, computed using a FEM program or another appropriate method.

F_i – lateral force acting on the i^{th}-storey with $\sum F_i = F$.

Lateral static forces are applied to the structure. The total lateral force F is distributed along the height of the structure according to Eq. 2.5.

$$F_i = F \cdot \frac{m_i h_i}{\sum m_i h_i} \tag{2.5}$$

The magnitude of the total lateral force is not important and can be substituted with a unit load. The relative magnitudes and distribution of the force components F_i must be maintained. For regular buildings, the mass of the storeys will approximately be the same. This allows the distribution of lateral forces given by Eq. 2.5 to be simplified as a triangular distribution. Displacements resulting from the lateral force are calculated for each storey. This is used along with the distributed forces and storey masses to calculate the natural frequency of the structure.

The Rayleigh method provides a simple alternative to using the crude SANS approach and can be used to check the validity of the natural frequency obtained from FE software.

2.4.6 Basic Design and Detailing Principles

One of the major improvements of SANS over SABS is the inclusion of general seismic design requirements for good design practice. Tomaževič (1999) explains that many modern buildings have sufficient strength to resist moderate intensity earthquakes because of the improvements in masonry materials and construction methods over the years. Quite often failure in URM structures is instead a result of irregular shapes and asymmetrical distribution of stiffness as well as other basic conceptual design and detailing flaws. In fact, a building's ability to resist larger base shear forces does not necessarily equate to better seismic performance. This is perhaps the reason why many historical URM buildings have endured earthquakes despite not being designed according to modern seismic codes (Bruneau, 1994).

Wium (2010) explains that SANS was revised with a philosophy of improving conceptual design and detailing practice so that buildings can more effectively resist earthquakes. The guidelines already present in SABS were supplemented and clarified using the design requirements of Eurocode 8. The application of these guidelines would allow a designer to reduce the redundancy factor resulting in a reduced design base shear force. The basic detailing requirements as put forth by SANS in section 5.1 of the code (relevant to multi-storey buildings in zone I and II) will now be discussed as this is essential, not only for design purposes, but also for evaluating existing structures.

2.4.6.1 Structural Simplicity, Uniformity, Symmetry and Redundancy

Buildings should be designed with direct paths for the transmission of seismic forces. This leads to improved seismic performance as well as simplifying the analysis and modelling process. All elements along a load path, including connections should be designed to transfer the expected seismic loads. A structure should also be designed to be uniform with respect to the distribution of stiffness and mass. In non-uniform buildings, the seismic energy developed during an earthquake will not dissipate uniformly over the structure, leading to stress concentrations in certain regions and eventual collapse. The fact that earthquakes are tri-dimensional should be taken into account when designing buildings to resist seismic forces in both principal directions to avoid collapse about the building's weak axis. An asymmetric design will lead to the formation of torsional moments that should be avoided. SANS explains that torsional moments will develop stresses in unexpected locations within the building structure.

Structural regularity is common in URM structures, even if they are not specifically designed for seismic loads. This is because simple regular structures carry vertical loads very effectively. Figure 2.8 indicates various ways in which structural regularity can be achieved by applying the following design practices (Tomaževič, 1999).

Symmetrical lateral stiffness and mass in both orthogonal directions, shown in Figure 2.8a

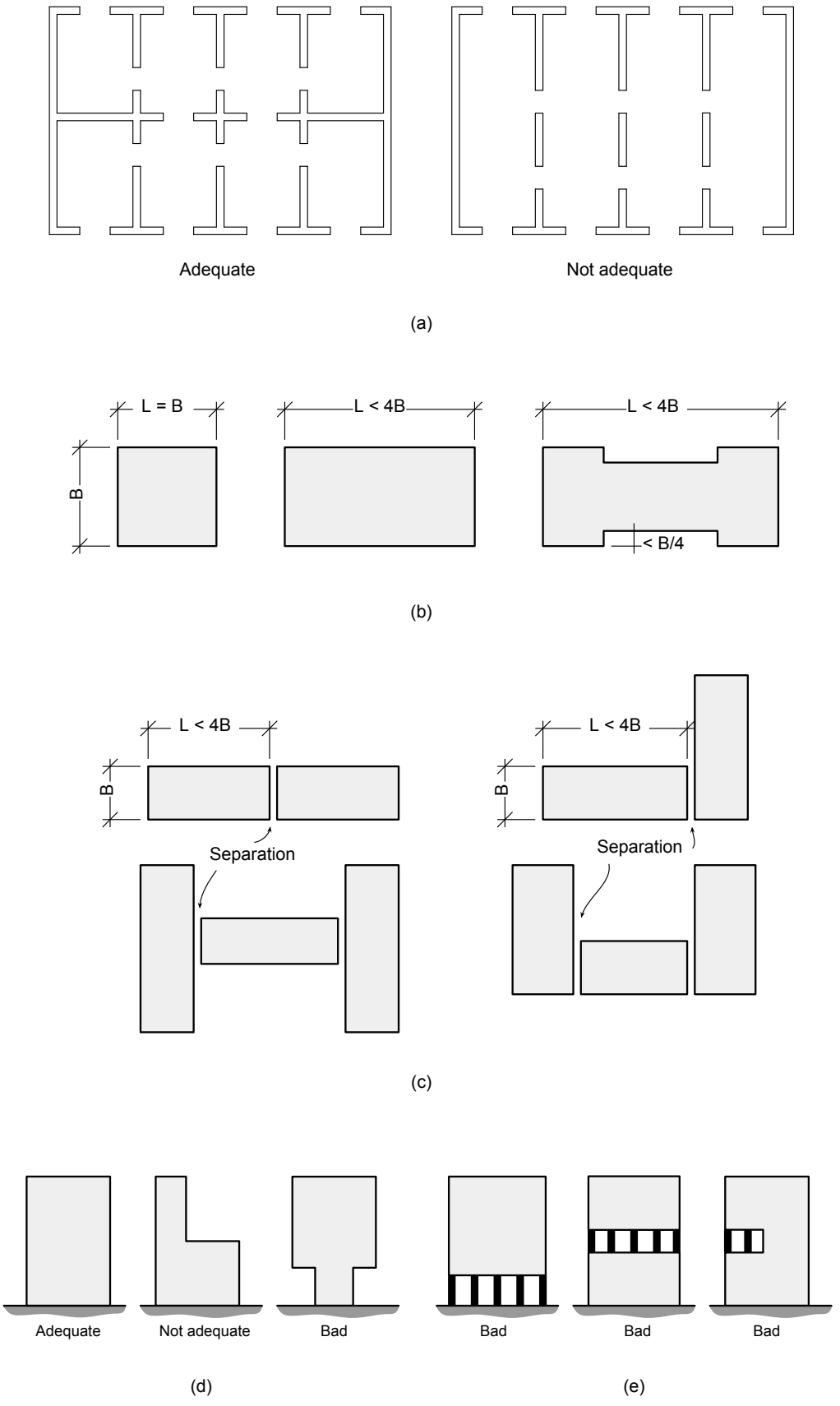

Figure 2.8: Summary of the basic conceptual design requirements for seismic design. (Tomaževič, 1999)

(left), can be achieved by providing the same amount of structural walls in both directions. Figure 2.8a (right) shows a building that is stiffened in the north-south direction, but not in the east-west direction. The plan shape of buildings should be a simple square shape (Figure 2.8b). When longer rectangular buildings are designed, limiting the length to less than 4 times the width, or separating the structure into shorter parts can achieve the same result. Separation techniques can also be used to divide L and U-shaped buildings into rectangular shaped parts (Figure 2.8c). It is important to note that when uniformity is considered, it refers to uniformity in both elevation and plan (Figure 2.8d). The use of different construction materials in different parts of the building such as the inclusion of soft stories as seen in Figure 2.8e should be avoided in seismic areas.

2.4.6.2 Floors, Walls and Openings

Floors and roofs act as horizontal diaphragms. They are responsible for transferring horizontal forces that act on the building to the shear walls, where they are in turn transmitted down to the foundations. It is essential that floors have adequate in-plane stiffness to transfer forces while limiting out-of-plane deflection. Connections to vertical elements such as shear walls should be sufficient to transfer horizontal loads from floor diaphragms. Simply supported connections without floor-to-wall anchors do not adequately transfer horizontal forces and should be avoided. SANS 10160-4 specifies that floor-to-wall connections should be able to transfer a load of at least $15a_g kN/m$. In addition, the floor and roof diaphragms should be designed to transfer a lateral force of $0.5a_g * w$, where w is the weight of the diaphragm and attached elements. Enough capacity should be provided to transfer forces between the structural elements, such as shear walls located above and below the diaphragm. Providing sufficient diaphragm capacity will ensure that the vertical elements in the building act as a unit by distributing horizontal forces to structural members in relation to their stiffness and allowing for the redistribution of forces from damaged elements to undamaged elements.

Openings greatly affect in-plane stiffness and resistance capacity of URM walls and especially shear walls. During seismic excitation, stress concentrations form at openings causing cracking and failure. Ideally openings should be located in walls that carry smaller vertical loads and be symmetrically distributed in plan to provide uniform stiffness. In addition, openings should be less than a third of the wall area. This requirement is rarely met in modern buildings where large window areas are the norm. SANS suggests that horizontal bed joint reinforcement be provided, even in URM buildings.

SANS 10160-4 specifies in Section 10 that non-structural elements should be designed to resist horizontal loads relative to the element weight and PGA as a result of inertia. This is extremely important since non load bearing infill walls could also experience large lateral loads despite not being part of the load resisting system. The out-of-plane resistance of masonry will be discussed further in Section 2.6.4.

2.4.7 Other Important Changes

SANS requires that a building is designed for accidental eccentricities during seismic action. This was included to ensure that buildings will sufficiently resist torsional effects. A minimum eccentricity of 5% must be applied to the centre of mass of each floor in both orthogonal directions when designing a structure.

For vertical ground motion, SANS requires that the vertical component only be taken into account for accelerations where $a_g > 0.25$. This is due to the smaller magnitude of the vertical component of ground motion compared to horizontal components. The vertical component only becomes noticeable for large earthquakes. Since a maximum PGA value of 0.15g can be expected in South Africa based on the seismic hazard map provided (Figure 2.5), the vertical component need not be considered for South African purposes.

2.5 Un-reinforced Masonry as Construction Material

Masonry structures can be divided into three main types: reinforced, confined and unreinforced masonry (URM) structures. Adding reinforcement to masonry greatly improves tensile strength and the ability of a building to withstand lateral forces. It also enables structural members to undergo much larger displacements before failure and therefore improves ductility. Since earthquakes induce lateral displacements, ductility is an important factor in providing seismic resistance. URM has many advantages including: low cost, adequate thermal insulation and the ability to effectively carry vertical loads. URM buildings of two to five storeys in height are very common in South Africa, especially in residential areas. These areas can be densely populated. The Cape Flats, and surrounding areas are excellent examples of 3 to 5 storey URM buildings situated closely together. URM is an acceptable construction material if large lateral loads are not present. Unfortunately, earthquakes are characterized by large lateral displacements and loads.

SANS 10164-1 (1980) is the current design code used for structural URM design. The code follows a limit state design approach and is applicable to the design of structural URM elements in buildings that are not located in seismic prone regions. The additional requirements and recommendations in SANS 10160-4 should be used along with SANS 10164-1 for the design of buildings in seismic prone areas. **Although research on the use of URM in seismic prone areas in South Africa is lacking, extensive research was done in other countries with similar seismic conditions.**

2.5.1 Material Strength Properties

When the strength of masonry is determined, it can be analysed on two levels: the strength of the bricks, mortar and masonry as separate materials, or the strength of the structural masonry element such as a wall or column (Tomaževič, 1999). When an analysis is performed on a masonry structure, the following material properties are important:

E – modulus of elasticity (Young's Modulus)

ν – Poisson's ratio

f – compressive strength

f_t – tensile strength

f_v – shear strength

$\sigma \leftrightarrow \epsilon$ – stress strain relationship

G – shear modulus

ρ_m – mass density

SANS 10164-1 (1980) provides tables and formulae to determine the material properties of masonry. These are crude methods applicable to masonry design and rely on the use of material and load partial safety factors during limit state design. In addition to the empirical formulae provided, various experimental methods are presented in order to directly determine material properties. Although the empirical formulae along with material partial factors are acceptable for use during design, they can be very conservative or even unconservative when analysing an existing structure. Experimental data should therefore be obtained where possible in order to accurately determine the building's seismic resistance capacity. The various material properties listed above will be discussed in the following sections with reference to the values presented in SANS 10164-1.

2.5.2 Elastic Modulus

The elastic modulus (Young's Modulus - E) represents the elastic stiffness of a material. When linear elastic behaviour is assumed, the Young's Modulus is obtained from the slope of the elastic portion of the stress strain diagram. SANS 10164-1 does not provide any empirical data on the determination of E. Eurocode 6 presents Eq. 2.6 as the empirical relationship between the characteristic compressive strength (f_k) and Young's Modulus.

$$E = 1000 f_k, \tag{2.6}$$

In addition, Eurocode 6 suggests that the shear modulus (G) be taken as 40% of E. Tomaževič (1999) shows through experimental results that the values of G can be much smaller than 40% of E with results falling between 6% and 25%. In addition, the Young's Modulus shows large variations ($200 f_k \leq E \leq 2000 f_k$) due to the broad range of compressive strengths of different masonry types commonly in use. It is therefore suggested that experimental results be used to determine E.

The elastic modulus will depend on the strength of the brick units and mortar, unit bond and interlocking but also the aspect ratio of brick units and construction quality, both affecting

the elastic stiffness of a structural element. Table 2.4 summarises various values for Young's Modulus obtained by other authors through the testing of clay brick masonry prisms.

Table 2.4: A summary of various elastic moduli of standard clay brick masonry as reported by various authors.

Author	**E (GPa)**
Griffith, Vaculik, Lam, Wilson, and Lumantarna (2007)	3.54
Bothara, Dhakal, and Mander (2010)	6.1
Griffith, Lam, Wilson, and Doherty (2004)	9.4 ± 5.3
Kaushik, Rai, and Jain (2007)	3.6–5.2 (strong mortar) 3.3–4.7 (intermediate mortar) 1.8–2.6 (weak mortar)
Yi (2004)	8 and 6.9
Dhanasekar and Haider (2008)	2.46 (parralel to bed joint)
Calderini, Cattari, and Lagomarsino (2009)	2.8
Calvi and Magenes (1991)	2.991
Ip (1999)	4.3–7.1 (strong mortar) 2.8–5.7 (weak mortar)

It should be noted that the values represent masonry of various strengths, highlighting the large range of possible values. This makes the analysis of a building with uncertain material properties exceedingly difficult. Fortunately the seismic response of a structure does not depend primarily on the E-modulus, since the structure will quickly transition from elastic into plastic response.

Ip (1999) performed an experimental study and computer simulation in order to examine the effect that mortar and brick strengths have on the Young's modulus of masonry. Specifically, the study aims to provide insight into the variation of masonry properties for different combinations of strong/weak mortar and strong/weak masonry units. The author explains that the strength of mortar in the masonry assemblage can be significantly less than results obtained through experimental testing. This is due to the ability for clay bricks to absorb moisture from the mortar, leading to insufficient hydration of the cement and therefore reducing strength. Stockl, Beckhaus, and Fritsche (1998) mentions the drastic impact that the choice of testing method can have on the Young's modulus of mortar, stating that variations of up to 10 times the measured value could be obtained when using different testing methods. Ip (1999) finds however, that mortar strength has a very small influence on the elastic modulus of the resulting masonry assemblage. The Young's modulus depends primarily on the properties of the masonry units. Even with this knowledge, the results are very inconsistent. It is concluded that the elastic modulus should rather be determined through experimental testing of a masonry wall, than attempting to calculate the value using Eq. 2.6, or similar formulae.

2.5.3 Poisson's Ratio

Poisson's ratio (ν) is an important material property required to define elastic material behaviour. It represents the ratio of the transverse strain to axial strain and is a measure of the

degree to which a material will expand laterally when undergoing axial deformation. A larger Poisson ratio will lead to larger lateral expansion when a material is axially compressed. As with all the other masonry material properties, ν will depend on the separate values of brick and mortar units. Ip (1999) confirms that Poisson's ratio is a critical material property with a large impact on the behaviour of masonry as material. By studying the relationship between the Poisson ratios of brick and mortar, a value of 0.15–0.2 is suggested for URM (Ip, 1999). Concrete masonry typically has a value closer to 0.2 and clay brick masonry a value of 0.16. The relative difference between the Poisson ratio of brick and mortar is more important than the magnitude since the non-uniform deformation of mortar and brick can have a large influence on the resulting masonry strength. This is further discussed in Section 2.5.4.

Many other authors have obtained different values for ν. A summary of various values obtained by different authors is shown in Table 2.5.

Table 2.5: A summary of Poisson ratios for clay brick masonry suggested by various authors using a range of different testing techniques.

Author	**Poisson Ratio (ν)**
Ip (1999)	0.15–0.2
Bakhteri, Makhtar, and Sambasivam (2004)	0.25
Bosiljkov, Totoev, and Nichols (2005)	0.17–0.29
Dhanasekar, Kleeman, and Page (1985)	0.19

Despite the importance of Poisson's ratio in material behaviour, there is still no precise method for determining the effective Poisson ratio of masonry, due to the complex interaction between brick and mortar. In addition, the measurement of separate Poisson ratios of mortar and brick within a masonry assemblage remains difficult. This is further complicated due to the drastic increase in ν when micro cracks form in mortar during the compression of masonry (Ip, 1999). A value of 0.2 or 0.25 is commonly used for analysis, comparable to values used for reinforced concrete analysis.

2.5.4 Compressive and Tensile Strength

The compressive strength of masonry is dependant on the strength of the mortar and brick units that combine to form the material. SANS 10164-1 specifies the strength of masonry in tabular form for different mortar grades and brick strength ratings as seen in Table 2.6.

Table 2.6: The compressive strength of standard format bricks as documented in SANS 10164-1.

Mortar class	Nominal compressive strength*, MPa, of structural units complying with the requirements of SABS 227, SABS 285, or SABS 1215, as applicable							
	3,5	7	14	17	21	28	35	49
I	2,0	3,2	5,6	6,5	7,5	9,3	11,1	14,4
II	2,0	3,1	5,1	5,7	6,6	8,0	9,3	12,0
III	1,7	2,6	4,2	4,7	5,3	6,2	7,2	8,8
*Linear interpolation for intermediate compressive strengths of structural units is permitted.								

Various attempts have been made in literature to provide an empirical formula to calculate the characteristic compressive strength of masonry (f) using the characteristic compressive strength of the bricks (f_b) and mortar (f_m). The relationship which is commonly used to determine f is given by Eq. 2.7.

$$f = K {f_b}^{\alpha} {f_m}^{\beta} \tag{2.7}$$

f – Characteristic Compressive strength of masonry.
K, α, β – Statistical parameters that are calibrated to fit experimental data.
f_b – Characteristic compressive strength of bricks.
f_m – Characteristic compressive strength of mortar.

Values for K, α and β are statistical parameters, calibrated to fit experimental data. Eurocode 6 specifies values of 0.6, 0.65 and 0.25 for K, α and β respectively. It is important to note that the choice of α and β values indicate that the brick strength has a larger influence on the masonry than the mortar strength. This is confirmed by Kaushik et al. (2007) who proposed values of 0.63, 0.49, and 0.32 for K, α and β respectively.

The ultimate compressive strength of masonry, whilst important for modelling material behaviour, should be used along with a suitable elastic/plastic material model in order to define the post crack material strength. The simplest material model, is an ultimate strength cut-off model, which assumes failure when the ultimate compressive or tensile strength is reached. This assumption can be conservative if an element shows good energy dissipation in the plastic region. A structure should be further analysed using alternative methods that take strength degradation into account such as a direct plastic analysis or the use of a structural behaviour factor. Plastic material behaviour is discussed in Section 2.5.6.

Ip (1999) explains that an increase in mortar strength will have a very minor influence on the masonry compressive strength. Other factors play a much larger roll. When mortar strength is increased by adding more cement to the mix, not only will the workability of the mix be negatively affected, but the occurrence of shrinkage will also be exaggerated. Emphasis should rather be placed on the increase of workability to ensure the proper placement and bonding of masonry elements as well as monitoring the water absorption rate of masonry to ensure that the masonry is properly hydrated.

Compressive testing of masonry is conducted experimentally through the testing of masonry

prisms. A masonry prism is a small element that is constructed from several layers of masonry bricks. The exact dimensions of the prism depends on the testing procedure used and is specified in material testing codes. This allows the compressive strength of masonry to be determined at a small scale (Ip, 1999).

Drysdale and Hamid (1979) performed 146 axial compression tests on concrete masonry prisms. The experimental results show that mortar has increased strength in a masonry prism when compared to mortar tested separately. This behaviour is also confirmed by other authors (Ip, 1999; Kaushik et al., 2007; McNary & Abrams, 1985) who explain that it is due to the difference in deformation properties (specifically Poisson's ratio) of brick units and mortar. Figure 2.9 shows the forces acting on brick and mortar layers when placing masonry under compression.

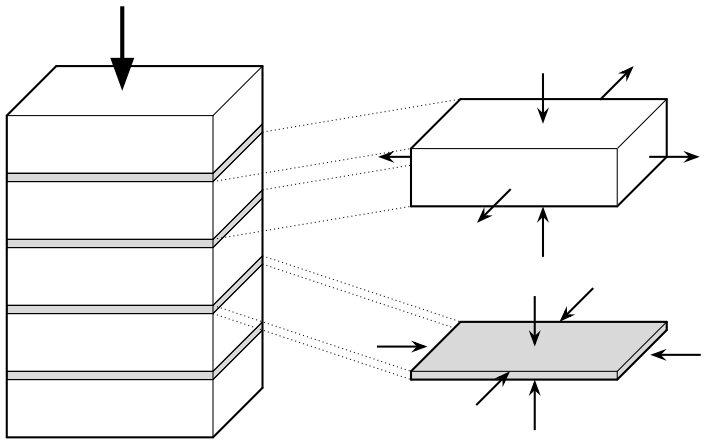

Figure 2.9: Internal confining forces acting on brick and mortar layers inside an URM prism under compression (Ip, 1999).

Mortar has a higher Poisson ratio than clay bricks. When compression is applied to masonry, the mortar will attempt to expand laterally, while the masonry units do not. This is exaggerated by the micro-cracking of mortar, further increasing the Poisson ratio. The bond between brick and mortar creates a confining force on the thin mortar layer preventing it from expanding. At the same time, the shear forces acting on the brick layer will cause it to develop tension forces in the horizontal plane as it expands. This places the mortar layer in a state of tri-axial compression, thereby increasing the compressive strength. The brick units, on the other hand, will have a reduced strength since failure due to tensile splitting will occur.

Increasing the mortar strength will have little impact on the compressive behaviour and weak mortars will not necessarily lead to weak masonry in compression. This is shown by Ip (1999) who noted that increasing the mortar strength by 685% only increased the masonry strength by 15%.

Masonry tensile strength presented in SANS 10164-1 ranges from 0.4–0.7 MPa for the formation of horizontal cracks (0.3–0.5 and 0.25–0.40 for type II and III mortar respectively) and 1.1–2.0MPa in the case of vertical cracks (0.9–1.5 and 0.8–1.2 for type II and III mortar respectively). The tensile strength is not specified for direct tension since URM structures are normally designed so that members are not in direct tension. The tensile strength is dependant

on the moisture absorption rate of the brick units.

2.5.5 Shear Strength

During seismic excitation, shear stresses will develop in a building in addition to compressive and tensile stresses. If the shear stresses developed in a material exceeds the shear resistance, cracking and shear sliding failure could occur. Due to the non-uniform nature of masonry, the material will have different shear strengths in different directions. Shear strength along the mortar bed joints can more easily be measured than diagonal shear strength passing through both bricks and mortar. According to SANS 10164-1, the shear strength along the bed joint of unreinforced clay brick masonry in South Africa can be calculated using Eq. 2.8,

$$f_v = 0.35 + 0.6 \cdot g_a \tag{2.8}$$

with g_a = design vertical load per area wall section. A maximum shear strength of $1.75MPa$ is specified. Equation 2.8 assumes a Mohr-Coulomb friction model when defining shear strength. The model (shown in Eq. 2.9) defines shear strength as function of vertical stress (σ_v) using a cohesion factor (c) and friction factor ($\tan\phi$).

$$f_v = c + \tan\phi \cdot \sigma_v \tag{2.9}$$

An increase in σ_v will result in an increased frictional resistance provided by the element resulting in an increased shear resistance. The cohesion factor represents the shear strength of a material under zero vertical stress. This means that walls at the upper part of the structure will have a reduced shear resistance due to the lower vertical stresses. At the bottom of the structure, larger shear stresses can be expected along with larger shear resistance due to large vertical stresses. The c and $\tan\phi$ values proposed by SANS 10164-1 is 0.35MPa and 0.6 respectively. Atkinson, Amadei, Saeb, and Sture (1989) performed 56 cyclic shear tests on various clay brick masonry specimens. Testing shows that values of c vary widely among different specimens. Average peak values of 0.8MPa were obtained for new bricks and strong mortar (1:1.5:4.5 cement:lime:sand) and 0.2MPa for old bricks and weak mortar (1:2:9). Once the peak strength values are exceeded, the shear strength of masonry degraded with a residual strength of 0.038MPa observed for both new/strong and old/weak brick/mortar specimens. The results for friction values are more consistent, ranging from 0.64 for weak mortars to 0.75 for strong mortars. The above mentioned results are comparable to the values presented in SANS 10164-1. It is clear that masonry has very little residual strength during cyclic loading. This means that structural elements can be assumed to fail once the peak shear strength has been reached.

Diagonal shear strength of masonry is not determined directly. Tomaževič (1999) shows that the diagonal shear strength of masonry is dependent on the tensile resistance of masonry. Shear failure will occur as a result of large principle tensile forces forming perpendicular to the plane of maximum shear stress when a wall panel is subjected to large shear forces. It is therefore a

valid assumption to limit the diagonal shear strength of a masonry wall by the maximum tensile resistance of the masonry material since shear cracks will form once the tensile stress has been exceeded. The tensile strength of masonry is discussed in Section 2.5.4.

2.5.6 Plastic material behaviour

Masonry remains elastic until cracking occurs. It is a relatively brittle material that shows large stiffness reductions after first crack. Once cracking in initiated, masonry behaves plastically, meaning that the energy put into the material will not be recovered during unloading. Instead, permanent deformations will remain. The post cracking plastic behaviour is especially important in seismic loading since it enables a structure to absorb the energy of the seismic event.

Kaushik et al. (2007) performed a variety of tests on 84 brick masonry prisms to determine the stress-strain behaviour of clay brick masonry in India. Standard size bricks (110x230x75mm) were used to construct masonry prisms. Bricks from four different manufacturers were tested in combination with three mortar strength grades. The mortar mix proportions (cement:lime:sand) include strong (1:0:3), intermediate (1:0.5:4.5) and weak (1:0:6) mixes. A number of important findings regarding masonry plastic behaviour are presented. The average compressive stress-strain behaviour of masonry prisms constructed with three mortar grades are compared in Figure 2.10.

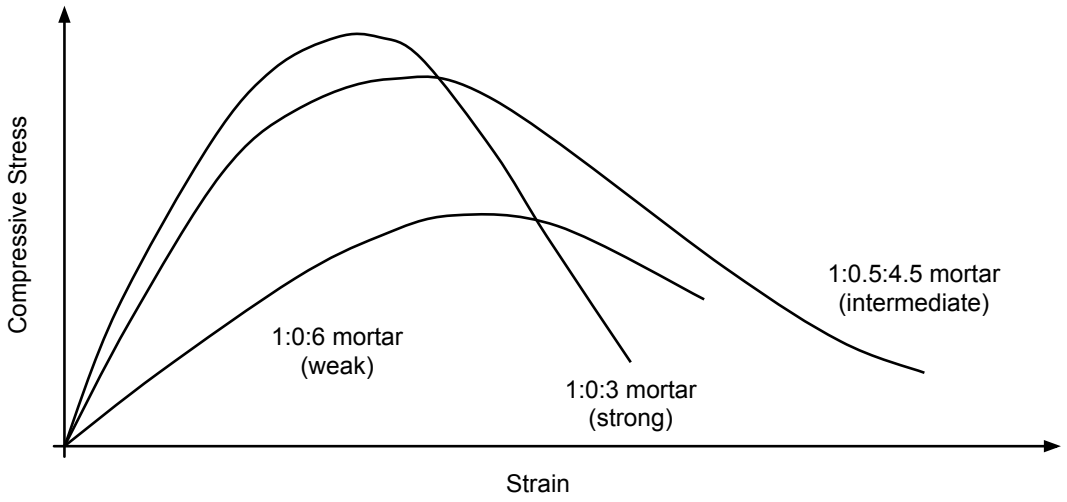

Figure 2.10: Comparison between the stress-strain curves of masonry prisms constructed using different mortar strengths and tested in compression (Kaushik et al., 2007).

Kaushik et al. (2007) shows that strong mortar masonry consistently fails at smaller strains when compared to weaker mortar grades. Tests show that strong mortars show only a small increase in the ultimate compressive strength of masonry prisms when compared to intermediate mortars, but cause behaviour to be more brittle. The ductility of masonry is significantly increased by the addition of lime to mortar mixes. This is not common practice in South Africa, especially not when high strength mortar is specified. By analysing test data, a simplified tri-linear stress-strain model is presented. Several limit states are identified and used to construct the tri-linear

model. The important limit states are:

0.75f – Initiation of significant splitting cracks corresponding to the end of the initial linear region at a strain $\epsilon_{0.75f}$.

f – Ultimate masonry compressive strength occurring at ϵ_f.

0.5f – Stress at maximum dependable masonry compressive strain $\epsilon_{0.5f}$.

0.2f – Stress at ultimate masonry compressive strain ϵ_{max}.

Both Kaushik et al. (2007) and Ewing and Kowalsky (2004) show similar strain values at the various limit states, however different strains were recorded for (ϵ_f). Figure 2.11 shows a comparison of the strain results suggested by Kaushik et al. (2007) and Ewing and Kowalsky (2004).

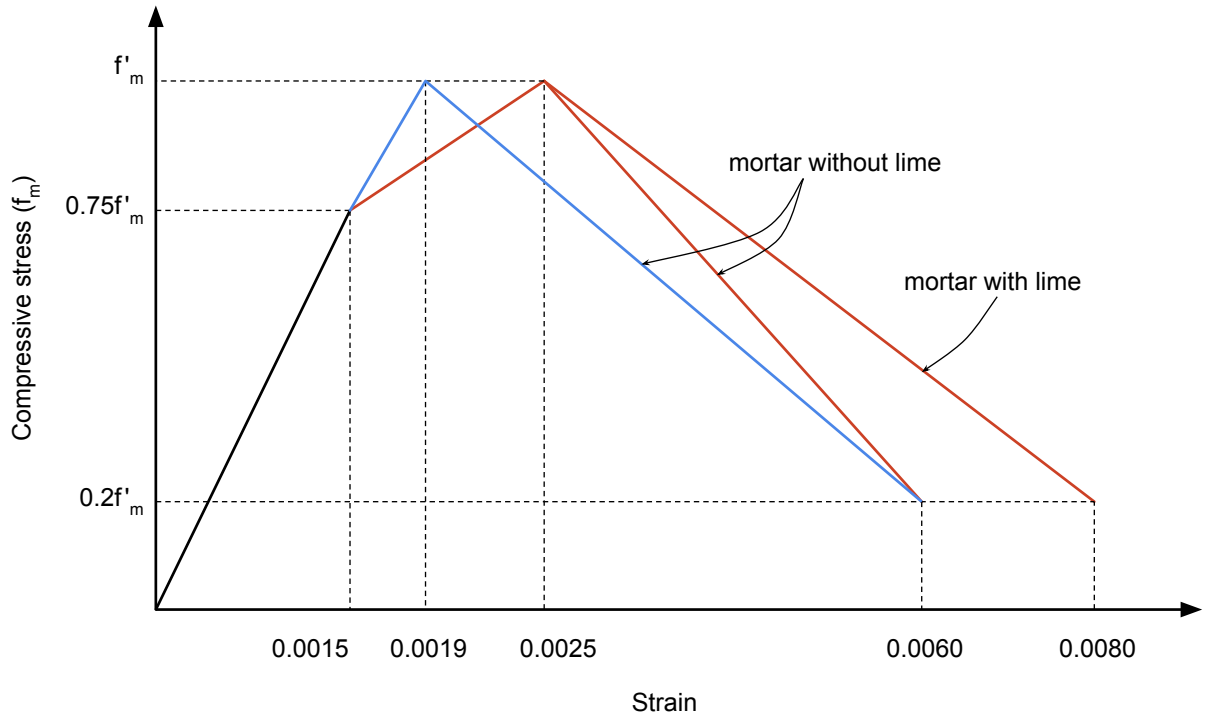

Figure 2.11: A comparison between the tri-linear approximation of the stress-strain behaviour of masonry in compression as determined by Kaushik et al. (2007) (red) and Ewing and Kowalsky (2004) (blue).

Ewing and Kowalsky (2004) performed compressive tests on 15 URM prisms to determine the stress-strain behaviour. Tests included single and double-leaf URM prisms. Results obtained are similar to those presented by Kaushik et al. (2007), however different strains are measured at ultimate compressive strength. An average strain of 0.0017 (maximum of 0.0019) is measured by Ewing and Kowalsky (2004) while a much higher average strain of 0.0025–0.003 is reported by Kaushik et al. (2007). This shows more brittle behaviour for the specimens tested by Ewing and Kowalsky (2004). An explanation can be found when looking at the materials used. The average compressive strength of bricks commonly used in India, as tested by Kaushik et al. (2007), are much lower than the bricks used by Ewing and Kowalsky (2004). The model presented by Kaushik et al. (2007) can easily be adapted to reflect the behaviour obtained for stronger bricks. The other strain values are comparable.

Little research has been performed on the tensile plastic material behaviour of

URM. Dhanasekar and Haider (2008) present the stress strain behaviour of URM with an ultimate tensile strength of 0.6MPa. This is comparable to the tensile strengths presented in Section 2.5.4. The stress strain curve is adapted and simplified to a piece-wise linear graph in Figure 2.12.

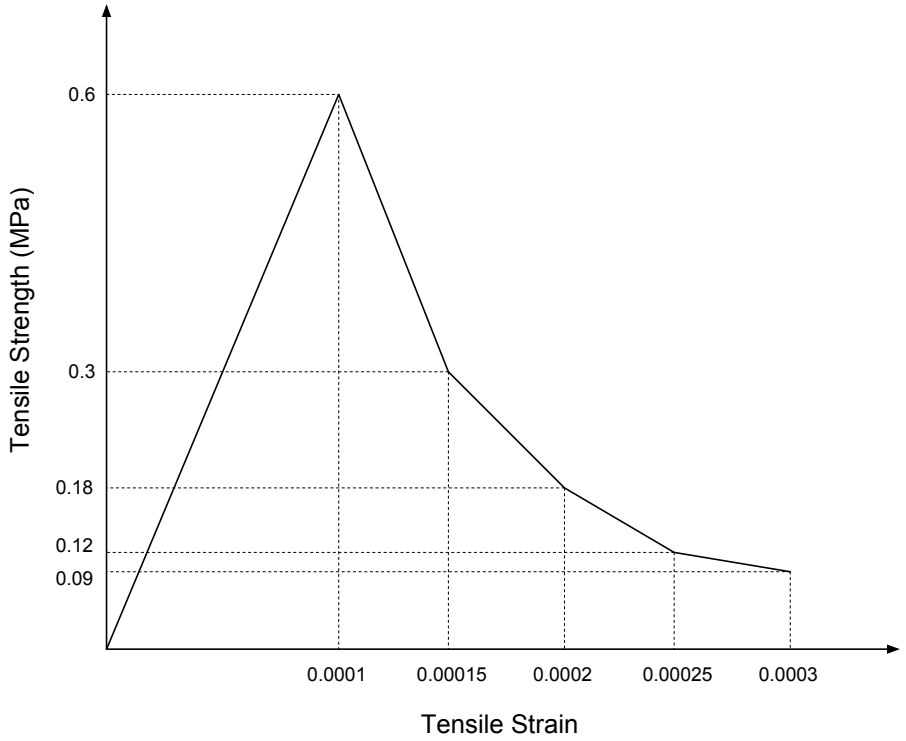

Figure 2.12: Tri-linear approximation of the stress-strain behaviour of masonry in tension, adapted from the material behaviour presented by Dhanasekar and Haider (2008).

The tensile behaviour of the URM material remains linear until the ultimate tensile strength f_t is reached. Thereafter, material strength is drastically reduced until failure occurs at a strain of 0.0003. URM has much less deformation capacity in tension with a maximum stain of only 5% of the ultimate compression strain. It is clear that masonry is much more brittle in tension than in compression. Tomaževič (1999) states that failure will occur once the strength of a structural member has degraded to 80% of the maximum strength. This is the point at which the material will be unable to reliably undergo further deformation without risk of structural collapse.

2.5.7 Masonry Properties in South Africa

There is very little research data available on URM use in South Africa. The little information that is available is in the form of design codes and manufacturer data sheets, all of which is empirical in nature. This information is intended for use in design and offers little aid when performing analyses of existing buildings. The data does not provide insight into the behaviour of existing masonry structural elements under different complex loading conditions. Research regarding the effect of construction quality on material strength, is scarce. As was seen in Section 2.5.4, data on the strength of masonry and mortar as separate materials are of little use when analysing a structural element on a macro scale. SANS 10164-1 (1980) covers URM

design in South Africa.

2.5.7.1 Mortar types

Mortar is made by combining three basic materials: cement, lime and sand. The use of lime is optional in South Africa, but produces favourable properties when used in a mortar mix as discussed in Section 2.5.6. SANS 10164-1 defines three basic mortar types, categorised by compressive strength. Table 2.7 lists mortar types along with minimum compressive strength and approximate mix proportions required to meet the strength requirements.

Table 2.7: Classification of mortar into three basic types by SANS 10164-1 (1980) along with the approximate mix ratios of cement:lime:sand required to meet the strength ratings (Clay Brick Association South Africa, 2002).

Mortar Type	Laboratory Strength	Work Strength	Mix Proportions (Cement:Lime:Sand)
I	14.5 MPa	10 MPa	1 : (0–0.3) : (3–4)
II	7 MPa	5 MPa	1 : (0–1.2) : 6
III	2 MPa	1.5 MPa	1 : (0–2.4) : 9

Class I mortar is used for load bearing applications where structural members are required to resist large stresses such as load bearing walls in multi-storey buildings. This class mortar is used in combination with high strength masonry units. Class II mortar is the standard mortar strength grade used for normal load bearing applications and commonly used in two storey buildings. Class III is a weak strength mortar used in lightly stressed walls such as internal walls and single storey load bearing walls that are not exposed to dampness. The bond of mortar to brick units has a large influence on the tensile and shear strength of masonry.

2.5.8 Masonry Construction Techniques

Various wall types are used to construct URM buildings in South Africa. These range from single-leaf walls used for non-load bearing applications to double-leaf and cavity walls. Figure 2.13 shows cross sections of four wall types commonly used to construct URM buildings both in South Africa, and abroad (Eurocode 6).

Single-leaf walls (Figure 2.13.a.) can be one or two bricks wide but are bonded so that there is no cavity or continuous vertical joint. Double-leaf walls (Figure 2.13.b.) have two leafs that are arranged to form a 25mm gap. The gap is filled with mortar and the leafs tied together using wall ties. The wall ties do not mean that the wall can be considered reinforced since the ties simply allow the leaves to act as a unit when resisting loads.

In coastal areas, masonry perimeter walls are normally built as cavity walls (Figure 2.13.c.) with two 110mm masonry leaves and a 50mm gap. The wall leaves are tied together with metal ties so that the wall leaves resist loads as a unit. If insufficient ties are provided, the wall will have a reduced out-of-plane strength since the leaves will act separately. The cavity has the

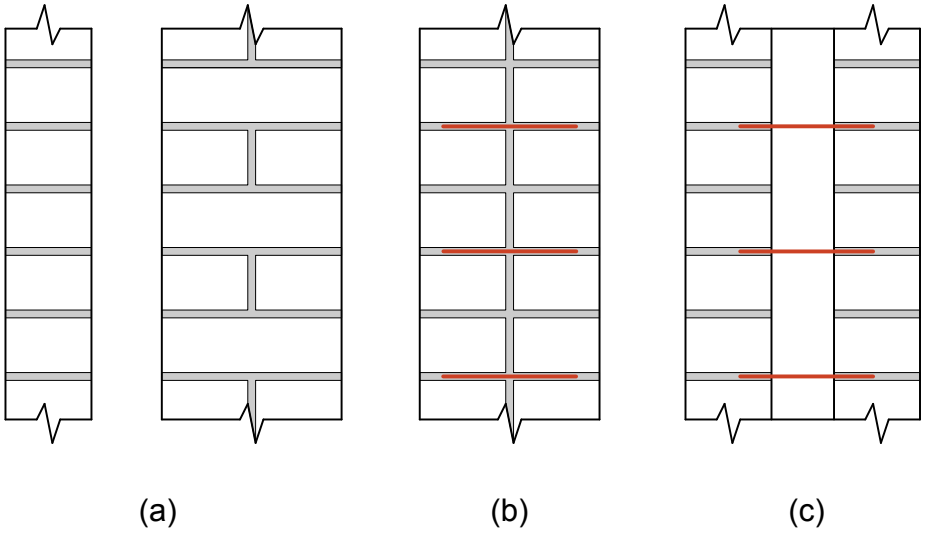

Figure 2.13: Cross sections of common wall types used in URM construction, including (a) single-leaf, (b) double-leaf and (c) cavity wall (Eurocode 6).

purpose of providing good insulation from dampness and rain. Weep holes are provided to allow moisture within the cavity to drain and damp proof courses (DPC's) are placed at surface bed level, floor level and at window openings to keep moisture from entering the structure (Clay Brick Association South Africa, 2002). DPC's can often be a weak point for an URM wall since the bond between masonry and the DPC layer could be less than the bond between adjacent masonry units. The behaviour of DPC layers and their effect on shear strength is discussed in Section 2.5.9.1.

Internal walls are designed to be non-load-bearing and are therefore designed to only carry the weight of the wall. They also provide lateral support to the out-of-plane perimeter walls. To prevent the crushing of the weaker internal walls, they are detailed so that a gap is left between the top of internal walls and the bottom of the overhead floor slab. This allows the floor slab to deflect without exerting forces on the internal walls.

The floor to wall connections in URM structures are normally not required to transfer large horizontal forces. It is common practice to detail the floor to wall joint with a slip joint that allows the floor to expand under temperature changes to improve serviceability. This is achieved by placing a softer material such as bitumen impregnated soft-board between the inner leaf of the cavity wall and the floor slab (Clay Brick Association South Africa, 2002). The floor slab will only rest on the inner of the two wall leaves. This connection is commonly used in areas where seismic activity is not expected. In the case of seismic prone areas however, this type of movement joint is unacceptable since the floor is expected to transfer large horizontal loads. Sufficient wall-to-floor connections aren't always provided since the restraining action of positive floor connections will inhibit the expanding capacity of the floor, leading to serviceability concerns (A. W. Page, 1996). The connection design requirements of floor-to-wall anchors is discussed in Section 2.6.2.

2.5.9 Other Considerations

2.5.9.1 Damp-Proof Courses

Damp-proof courses (DPC's) are used in URM walls to prevent moisture from entering a building. They are placed near the base of walls, above openings and at certain floor-to-wall connections. Membrane type DPC's are commonly used in South Africa. They are placed between two brick layers and are normally laid on the masonry units with mortar on top. This creates a plane of possible weakness when considering shear resistance since the bond and friction properties of DPC layers are different from that of brick and mortar (A. W. Page, 1996).

Sliding shear performance of URM is discussed in Section 2.5.5. Shear resistance is represented using a Mohr-Coulomb friction model represented by Eq. 2.9. The model can be adapted to represent shear behaviour of DPC layers by adjusting the cohesion factor and friction factor. A. Page (1995) experimentally determined values of the friction factor for a number of different DPC types. Values range from 0.26–0.59. The shear bond strength of the mortar-DPC joint (cohesion factor) has values of 0.01–0.07. A. W. Page (1996) suggests however that the cohesion factor should be ignored for design purposes.

Friction factors of all the DPC types were lower than the value of 0.6 specified for mortar in SANS 10164-1. In addition, the cohesion strength at DPC joints were negligible with average values 90% lower than that of mortar joints. The reduced strength of the DPC joint should be taken into consideration when analysing a structure for sliding shear failure.

2.5.9.2 Construction and Manufacturing Quality

Construction quality affects the strength of URM structures on many levels. Proper quality control and material testing at various stages of construction is necessary to ensure that the constructed building has the same strength as the design. Bruneau (1994) emphasises the relationship between material/construction quality and damage for different PGA values, stating that failure can occur at PGA values of less than 0.1g if poor construction methods are applied. Lane, Watermeyer, and De Villiers (1991) report that investigations in Australia have indicated a 38-45% reduction in brickwork strength under unsupervised conditions.

Manufacturers in South Africa have to meet certain requirements regarding quality control in order for them to be SABS accredited. Good quality control standards can be maintained during the manufacturing process due to the limited amount of external factors that influence the manufacturing process. The same can not be said for quality control during construction where many environmental and external factors play a role.

SANS 10164-1 accounts for construction quality by increasing the material partial safety factor (γ_m) depending on the control applied. $\gamma_m = 2.9$ for good construction control and $\gamma_m = 3.5$ when inadequate control is present. This will lead to a masonry strength reduction of approximately 9% under bad construction quality control. Further research is needed to quantify the construction quality in South Africa.

2.6 Seismic Performance of URM

2.6.1 URM Structural System

URM buildings use shear walls and floors to resist vertical and horizontal loads. Walls that lie parallel to the earthquake excitation are called in-plane walls and walls that lie perpendicular to the excitation are called out-of-plane walls. These structural elements are connected in order to effectively transfer and dissipate forces. Structural walls are designed to be either load-bearing shear walls that carry vertical as well as in-plane loads or non-load bearing walls that do not carry vertical loads, but provide lateral bracing to other load bearing walls. Horizontal loads are carried by the floors and roofs to shear walls that are placed in both orthogonal directions. Infill walls that are constructed to compartmentalise the structure do not form part of the primary structural system. They provide some lateral support to the structural system.

Due to the inherently low tensile strength of URM, buildings are designed to avoid tensile forces as far as possible. In addition, URM buildings are designed to respond primarily in the elastic range due to the non-ductile behaviour of URM, resulting in a small amount of dependable plastic strength. Ductile behaviour should not be disregarded when performing an analysis of an existing building. Analysing a structure in only the elastic range, could lead to conservative estimates of the seismic performance.

The ductility of a structure allows structural walls to resist vertical loads while undergoing cracking and displacements. It also allows damaged walls to redistribute forces to undamaged structural elements. During the cracking and deformation process, energy is dissipated. This behaviour will continue until a structural element forms a mechanism after which collapse will occur. This means that the resistance of a structure can be verified by calculating the resistance at which a failure mechanism will develop. The formation of a mechanism will cause local collapse if it develops in a non-critical structural element. It could cause global collapse if a critical structural element forms a mechanism. This is to be avoided.

URM buildings are designed with a specific load path. All forces acting on the structure are transmitted and dissipated along the load path to the foundations. Structural elements that form part of the load path must be designed to resist all possible forces that they can experience. Connections must have sufficient capacity to transfer forces between elements along the load path. Failure can therefore be caused by the failure of structural elements (walls and floors) or the failure of the connection between these elements.

URM buildings are very effective at resisting vertical loads. Loads applied to floor and roof slabs are transferred to load bearing walls which transfer the load to the foundations. Horizontal loads are resisted in-plane by shear walls. The floors act as diaphragms to redistribute the horizontal loads from weaker (less stiff) elements to stiffer shear walls as shown in Figure 2.14.

This means that sufficient shear walls are required in both orthogonal directions in order to transfer horizontal loads to the foundations. When a structure undergoes face loading, the loaded element will undergo out-of-plane deformation. The resulting forces are distributed via

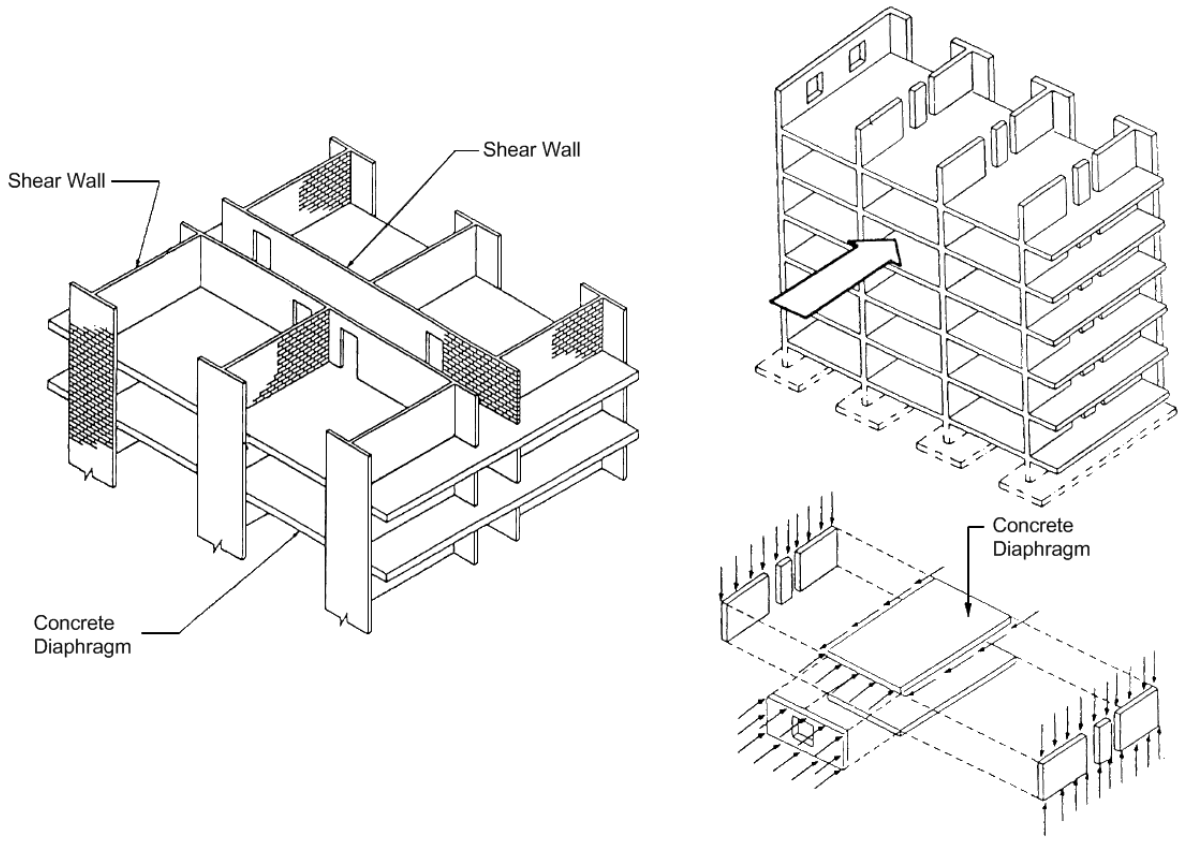

Figure 2.14: Basic representation of an URM structural system (A. Page, 1995).

the floor diaphragm (located above and below the out-of-plane loaded element) and lateral bracing walls to the shear walls and finally to the foundations. The out of plane failure of walls can be prevented by reducing the horizontal distance between lateral supports and also by reducing the vertical dimensions between diaphragm supports (A. Page, 1995).

2.6.2 URM Seismic Failure Modes

If an analysis of an URM structure is conducted, it is important to note the possible failure modes. All the applicable failure modes should be accounted for or eliminated in order to obtain realistic results. Bruneau (1994) has grouped seismic failure of URM structures into various categories, based on observations from previous earthquakes:

- **Lack of anchorage:** This refers to the anchorage of floors and roof to walls of the URM building. In some cases the floors may be simply supported. This can lead to the floors slipping off their support, causing collapse. If insufficient anchorage is provided, the exterior walls will behave as cantilevers with an increased risk of out-of-plane failure. SANS 10160-4 (2009) specifies that floor diaphragms should be designed with effective connections to the structural system to allow horizontal forces to be transferred. In addition, for elements not forming part of the main structural system, sufficient anchorage should be provided to resist a lateral force of at least $15a_g$ kN per meter of wall. With a design value

of $a_g = 0.1$ being used, this relates to 1.5 kN/m of lateral force.

- **Anchorage failure:** If anchorage is not specifically designed for seismic action, it could lead to anchorage failure. This should not occur if the code requirements for anchorage are followed.
- **In-plane failures:** Normally caused by large bending or shear effects. This is common in the spandrels and piers of façade walls. Walls with in-plane failure cracks will fortunately resist gravity loads to some extent. Shear walls are specifically designed to carry horizontal in-plane loads. If a wall is not designed to carry in-plane loads, or if shear walls are not adequately designed, in-plane failure could occur.
- **Out-of-plane failure:** This failure type depends largely on the lateral support provided by structural walls and the diaphragm behaviour of floors. If insufficient lateral support is provided, walls will behave as unrestrained cantilevers, greatly increasing the probability of out-of-plane failure. This method of failure can also happen when cavity walls are improperly bonded along their collar joints. This lack of bonding will cause each layer to behave as a separate thin wall, increasing probability of failure.
- **Combined in- and out-of-plane effects:** This is a result of earthquakes being bi-directional in nature. When in-plane shear cracks form in an URM wall, the out-of-plane behaviour of the cracked sections will be greatly reduced.
- **Diaphragm related failures:** Diaphragm failures occur mainly in historical URM buildings with wooden floors. Although the failure of a concrete diaphragm is rare, the rotation and movement of flexible diaphragms can cause damage at wall corners.

A significant amount of research was performed on the behaviour of structural masonry walls during earthquake excitation. The in-plane and out-of-plane resistance of masonry walls will be discussed in Sections 2.6.3 and 2.6.4 respectively. Yi (2004) presents general rules for determining the locations where cracks are likely to form during a seismic event. A summary of typical cracking locations is shown in Figure 2.15.

The presence of openings in perimeter walls will lead to the formation of stress concentrations at the corners of the openings. This causes cracks to form diagonally from the corners of openings to the edge of wall elements. Once cracking has occurred, the different elements will separate from the structure and act as separate bodies leading to the formation of collapsing mechanisms. Sliding shear can typically occur at the horizontal cracking locations indicated in Figure 2.15. Crushing and diagonal shear failure of these elements is also common.

It is important to note that different experimental methods often yield different results due to the amount of variables that effect URM seismic performance. This makes the task of determining seismic resistance of masonry very difficult. Determining the hysteretic effects of seismic events on masonry, such as the degradation of stiffness and energy dissipation capacity is especially difficult. In order to obtain these characteristics, parameters such as the displacement patterns applied during experiments must be carefully chosen. Tomaževič (1999) illustrates that the use of different time histories can yield significantly different displacement patterns. Also, due to

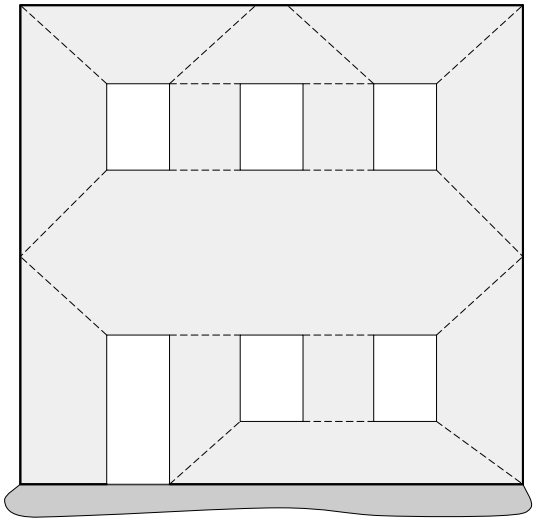

Figure 2.15: Common locations where cracks are likely to form during seismic excitation of a perforated structural wall (Yi, 2004).

the complex nature of masonry as material, it is often necessary to make assumptions regarding the elastic, homogeneous and isotropic properties of the material at a global level. Simplification of the problem is especially important when a large structure is to be analysed.

2.6.3 In-plane Seismic Resistance

Tomaževič (1999) defines three basic failure modes that are applicable to in-plane failure of structural URM walls: sliding shear, shear and flexural failure as shown in Figure 2.16.

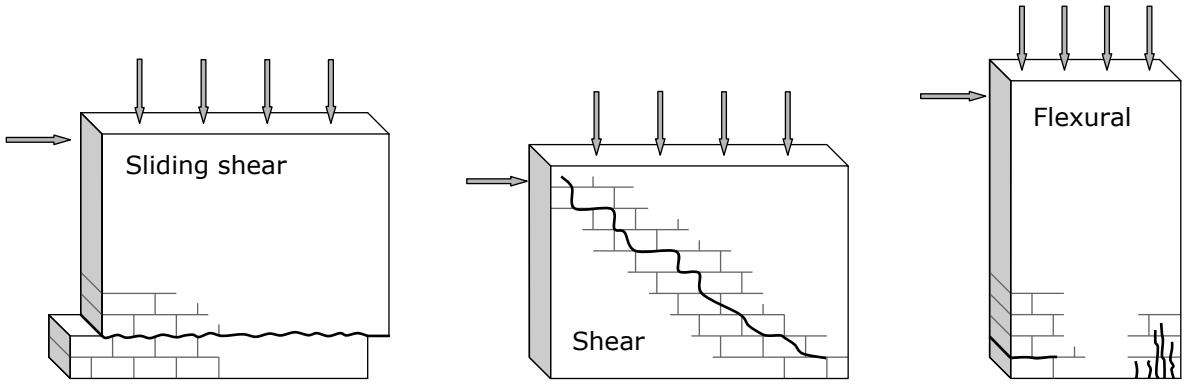

Figure 2.16: Typical in-plane failure modes of structural masonry walls (Tomaževič, 1999).

Sliding shear can occur if insignificant vertical loads act on the wall and if poor quality mortar is used. It is also a common failure mode at DPC levels. Shear failure occurs when the principle tensile stresses that develop within the wall are larger than the tensile resistance of the masonry materials and the interface between the mortar and masonry units. Cracks will follow the weakest path, either along the mortar joints or through the masonry units. In the case of masonry columns or other masonry walls with similar aspect ratios and when improved shear resistance is present, the crushing of compression zones at wall edges will indicate flexural failure.

When a masonry element undergoes in-plane seismic excitation, its stiffness will gradually degrade as damage occurs. The effect that stiffness degradation has on the element can be determined by analysing the element using finite element (FE) software when implementing non-linear material behaviour. Experimental data can be used to determine the hysteretic behaviour of masonry walls. If the experimental behaviour of an element is known, the results can be used to calculate the properties and resistance of similar masonry elements.

Tomaževič (1999) suggests an idealisation of hysteretic behaviour by using a bi- or tri-linear approximation of an experimentally determined resistance envelope. This allows experimental data obtained by applying lateral dynamic loads to a wall to be used to determine the resistance and stiffness degradation of a wall element. The tri-linear approximation, shown in Figure 2.17, consists of three basic limit states representing the behaviour of a wall element:

- **Crack limit:** Formation of significant cracks occur when d_{cr} is reached, corresponding to a resistance H_{cr} and a change in stiffness (slope of envelope).
- **Maximum resistance:** The maximum force resisted by the part under consideration (H_{max}) with a displacement $d_{H_{max}}$
- **Ultimate state:** The maximum displacement reached with a resistance of $H_{d_{max}}$.

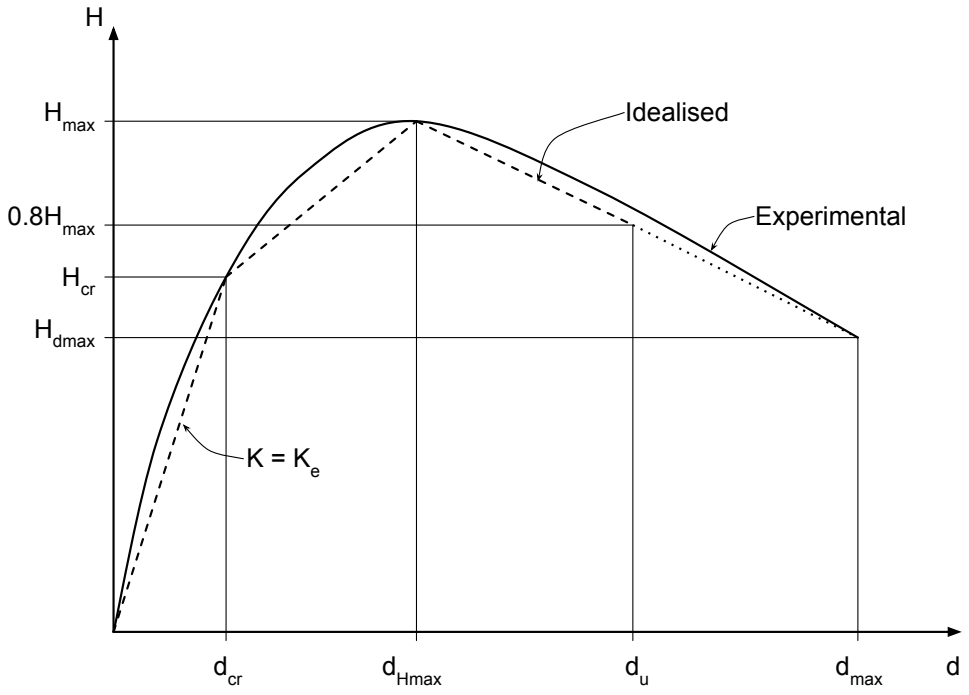

Figure 2.17: Simplification of non-linear resistance of masonry walls through a tri-linear relationship (Tomaževič, 1999).

The envelope, shown in Figure 2.17, consists of three straight line segments, each with it's own stiffness. The initial line has a slope given by the secant stiffness at the crack limit (K_e) as presented in Eq. 2.10.

$$K_e = \frac{H_{cr}}{d_{cr}} \tag{2.10}$$

The maximum resistance of a wall element is taken directly from experimental data as the largest force that the wall was able to resist. Tomaževič (1999) suggests that H_{cr} be estimated using Eq. 2.11.

$$H_{cr} = 0.7H_{max} \tag{2.11}$$

After the maximum resistance is reached, the wall will undergo severe strength degradation whilst allowing further displacement. $H_{d_{max}}$ is taken as 80% of the maximum wall resistance (H_{max}) to limit the damage that walls will be subjected to. However, experiments have shown strength degradation of up to 60% before collapse.

The stiffness of a structural wall can be computed from basic principles by considering a lateral force that will cause a unit displacement. This relates to a stiffness value given by Eq. 2.12.

$$K_e = \frac{GA_w}{1.2h\left[1 + \alpha' \frac{G}{E}\left(\frac{h}{l}\right)^2\right]} \tag{2.12}$$

with $\alpha' = 0.83$ for fixed ended walls and $\alpha' = 3.33$ for cantilever walls. When determining the value of α' for an URM wall, any wall that supports a floor that spans on both sides can be considered fixed. Boundary walls or walls that only support floors on a single side should be considered cantilever.

The stiffness given by Eq. 2.12 is the effective stiffness in the linear region. In the non-linear range, the stiffness degradation can be defined in terms of K_e using two approaches given by Eq.s 2.13 and 2.14.

$$K = \alpha K_e \left(\frac{d}{d_{max}}\right)^{\beta} \tag{2.13}$$

$$K = K_e - \sqrt{aI_d - b} \tag{2.14}$$

Values of $\alpha = 0.3$ and $\beta = -0.85$ is suggested by Tomaževič (1999) when using Eq. 2.13. α should not be confused for α'. Equation 2.14 determines the stiffness through the use of a damage index I_d representing the extent of damage. Values for I_d are listed in Table 2.8. Parameters a and b represent stiffness degradation and should be determined experimentally.

Table 2.8: Damage index values (I_d) for use in Eq. 2.14.

I_d	Extent of damage
0.25	Crack limit.
0.50	Network of diagonally oriented cracks. Point of maximum resistance.
0.75	Masonry units being crushed in middle of wall while units and grout split at the compression zones.
1.00	This relates to the collapse of the wall at a point where the stiffness is only about 2-5% of K_e

The shear resistance of URM walls can be modelled by an appropriate theory discussed by Tomaževič (1999). By considering basic elastic theory, it can be shown that a wall with a vertical load, N, and lateral load, H, will develop a principal compression stress presented in Eq. 2.15,

$$\sigma_c = \sqrt{\left(\frac{\sigma_0}{2}\right)^2 + (b\tau)^2} + \frac{\sigma_0}{2} \tag{2.15}$$

and a principle tensile stress given by Eq. 2.16.

$$\sigma_t = \sqrt{\left(\frac{\sigma_0}{2}\right)^2 + (b\tau)^2} - \frac{\sigma_0}{2} \tag{2.16}$$

By substituting the average shear stress at maximum resistance, the tensile strength of masonry can be determined from Eq. 2.16 to yield Eq. 2.17.

$$f_t = \sigma_t = \sqrt{\left(\frac{\sigma_0}{2}\right)^2 + (b\tau_{H_{max}})^2} - \frac{\sigma_0}{2}. \tag{2.17}$$

The symbols used in Eqs 2.15 to 2.17 are defined as:

σ_0 $= N/A_w$ is the average compressive stress when applying a vertical load N,

$\tau_{H_{mas}}$ $= H_{max}/A_w$ is the average shear stress at the point when maximum resistance is obtained,

A_w is the cross section area of the wall in plan,

b is the shear distribution factor of the wall, obtained by evaluating the aspect ratio of the wall such that an aspect ratio of $h/l = 1.5$ will yield $b = 1.5$.

The lateral shear resistance of masonry can be expressed as a function of the geometry and the ratio of the vertical and lateral load to yield Eq. 2.18.

$$H_{s,w} = A_w \frac{f_t}{b} \sqrt{\frac{\sigma_0}{f_t} + 1} \tag{2.18}$$

When determining design shear resistance to a certain design seismic action, f_t is replaced with f_{tk}/γ_M, the material safety factor. For design purposes, σ_0 is replaced with σ_d, the design compression stress. It is evident that $\tau_{H_{max}}$ is obtained by dividing Eq. 2.18 by the wall area A_w, yielding Eq. 2.19.

$$f_v = \tau_{H_{max}} = \frac{f_t}{b} \sqrt{\frac{\sigma_0}{f_t} + 1} \tag{2.19}$$

Sliding shear occurs primarily in the upper floors of a structure where the vertical load acting on the wall is small and the horizontal acceleration is large. This causes horizontal cracks in the bed joints that lead to the upper part of the wall sliding on the bottom part. Sliding shear can be modelled using the Mohr-Coulomb friction model. The friction model along with the specific

material strength properties relating to shear is discussed in Section 2.5.5. Shear properties of DPC's is discussed in Section 2.5.9.1.

2.6.4 Out-of-Plane Seismic Resistance

Out of plane failure of masonry walls is a common failure mode of perimeter walls. In order to prevent this, enough transverse walls should be provided as well as floors that are designed to act as diaphragms. The effectiveness of floor diaphragms are often limited by the type and strength of connections between the floor and perimeter walls. Many URM buildings lack effective floor-to-wall connections, leaving the connection between the perimeter walls and transverse walls to resist out-of-plane failure. de Felice and Giannini (2001) analysed the out-of-plane performance of perimeter walls against failure due to detachment from the transverse wall. This can occur with a vertical crack at the connection to the transverse wall or due to a diagonal crack through the transverse wall. The study shows that larger masonry units provide better seismic resistance than small units (in relation to the wall thickness) due to better interlocking of units. Decreasing the distance between transverse walls increased the seismic resistance of the perimeter walls. Results obtained from a static and dynamic analysis of the walls suggest that a vertical crack at the wall connections is the dominant out-of-plane failure mechanism. Failure of this type can be very common in non-structural façade walls. This type of failure will depend on the vertical tensile strength of masonry, discussed in Section 2.5.4. Cracking at the horizontal plane at floor connections could also lead to failure.

The capacity of a wall can be verified by analysing a wall strip as a beam spanning from wall to wall or floor to floor. From basic principles, the flexural stress in a section subject to moment loading can be expressed by Eq. 2.20 with moment of inertia (I), applied moment (M), compressive or tensile stress (σ) and distance from the neutral axis to outer tensile fibre (y) as input parameters.

$$\sigma = \frac{M \cdot y}{I} \tag{2.20}$$

Rearranging Eq. 2.20 and replacing y and I with the dimensions of a wall strip yields Eq. 2.21.

$$M = \frac{f_t \cdot bt^2}{6} \tag{2.21}$$

M – Moment capacity of the wall for out-of-plane bending.

f_t – Tensile strength of masonry in the horizontal or vertical plane for analysing vertical or horizontal wall strips.

b – Width of the wall strip

t – height of the wall strip perpendicular to the bending axis.

When the basic design principles discussed in Section 2.4.6 are met, out-of-plane resistance of structural walls is usually not critical (Tomaževič, 1999). This assumes sufficient connections between walls and floors. Out-of-plane failure can be an issue if large spans (exceeding 10m) between structural walls are present.

The formulae discussed in Sections 2.6.3 and 2.6.4 are useful for determining the resistance of key structural elements based on experimental data. They have limited application in the analysis of a complete structure where complex interactions occur or when non-linear behaviour should be accounted for. They can however serve as a method for verifying results obtained from a more rigorous analysis.

2.6.5 Floor and Roof Diaphragms

The floor and roof system of URM buildings plays a critical role in transferring forces during seismic events. When vertical imposed loads are considered, the floor and roof elements distribute loads through flexure to the supporting walls, which in turn transfer the loads to the foundation system. When horizontal accelerations are applied to the structure, the floors and roof of the structure act as horizontal diaphragms by distributing the horizontal loads that form at floor level to the in-plane shear walls, in relation to their stiffness, after which the forces are transferred in-plane to the foundations.

In general, floor diaphragms can be classified as either rigid or flexible. Rigid diaphragms (normally constructed from reinforced concrete) have sufficient stiffness to transfer horizontal in-plane loads without undergoing large out-of-plane deflections. If floors are constructed using less stiff materials such as wood, the floor will act as a flexible diaphragm. Flexible diaphragms will exhibit certain distinct characteristics that can significantly influence the behaviour of an URM structural system as mentioned by Yi (2004):

- Rigid diaphragms tend to act as a hinge support at the top and bottom of supporting walls. Flexible diaphragms, on the other hand, act as spring supports. This affects the out-of-plane wall response and can cause damage in the form of pounding and cracking.
- Flexible diaphragms have large deformation capacities compared to diaphragm strength. This causes increased stresses in diaphragm connections. Slipping of floors off of supports can occur.
- Amplification of up to 3 or 4 times the input acceleration can be produced by the diaphragm flexibility in the elastic range. In the plastic range, however, flexible diaphragms show much better hysteretic performance when compared to rigid diaphragms by reducing peak acceleration and velocity responses.
- Flexible diaphragms will not transfer lateral forces as effectively as rigid diaphragms resulting in reduced coupling between parallel in-plane walls.

The stiffness of the floor system will effect the rotational response of a structure. Torsional response occurs when there is an asymmetry in the stiffness distribution or when the stiffness

and shear centres do not coincide. If flexible diaphragms are present, large shear forces will develop in the floor as a result of the unsymmetrical wall resistance. A rigid diaphragm, on the other hand, will rotate as a unit. This will enable the redistribution of forces to other shear walls to assist in resisting the lateral loads. Large torsional forces will however cause out-of-plane forces to develop in the in-plane walls and in-plane forces in the out-of-plane walls. This leads to the simultaneous in- and out-of-plane response of walls which is not ideal.

2.7 Design Methods

In order to perform a thorough analysis and to properly assess the ability of a building to resist earthquakes, it is necessary to study not only the construction methods and materials used, but also the design methods employed. This will highlight possible weaknesses that a particular building might have especially if it originates from an inadequate design concept. Common design approaches will be briefly discussed below.

2.7.1 Static Lateral Force Method

SANS advises the use of the equivalent static lateral force procedure as the standard design method. The method is only applicable when the building responds primarily in the first mode of vibration. This is the case when the following conditions are met:

- The fundamental period of vibration $T \leq 4T_C$ or $T \leq 2.0$ (seconds). T_C is the upper limit of the constant acceleration branch of the response spectrum graph.
- All lateral load resisting systems (walls, cores) run uninterrupted from the base to the top of the building.
- Constant or gradually reducing lateral stiffness and storey mass from the base to the top of the building, i.e. without abrupt changes.
- Sum of setbacks on any storey is less than 30% of the plan dimension of the first storey and less than 10% of the previous storey plan dimension.
- Symmetrical stiffness and lateral resistance in both orthogonal directions without significant discontinuities along the building height.

The above mentioned conditions relate to the seismic design and detailing principles discussed in Section 2.4.6. URM buildings normally have simple geometric and structural layouts, making the static lateral force method ideal. The method, explained in detail in SANS, can be summarized step-wise as follows:

1. Calculate the fundamental period of vibration (T).
2. Determine the ground type.
3. Determine the non-dimensional response of the structure using the design response spectra for the calculated period of vibration while incorporating the behaviour factor.

4. Calculate the design base shear force and resulting design load effect by taking into account the redundancy factor and building importance factor.
5. Distribute the base shear force along the height of the building.

SANS places a storey displacement limit on structures. In addition to being able to resist the base shear force, connections are designed to transmit the horizontal forces imposed by the seismic event. The lateral static force method does not provide response of non-structural elements during excitation. Design codes have additional clauses to dictate the design of non-structural elements.

2.7.2 Displacement Based Design

In general, designers are moving away from the typical force based design methods (such as the method included in SANS) opting instead to use displacement based (DB) design procedures. This is a result of earthquakes being a displacement based phenomenon that relies much more on the ductility of a structure, than its ability to resist large forces.

Initially, a design displacement is determined. Thereafter the building is represented as a SDOF system with a vibration period and effective height determined using displacement spectra for a specific level of damping. The effective (secant) stiffness of the structure is calculated using the mass and vibration period of the structure after which a base shear force is calculated. This is the force that needs to be resisted to enable the structure to undergo the design displacement. Various implementations of DB design methods are documented in literature (Bruneau, 1994; Doherty, Griffith, Lam, & Wilson, 2002; Priestley, Calvi, & Kowalsky, 2007).

2.8 Modelling and Analysis Methods

Numerous modelling and analysis methods can be found in literature. This is due to the highly variable nature of URM material properties, material interactions, failure modes as well as the complexity of seismic loads. There is currently no standard widely accepted method of analysing URM structures. In the past, masonry design has been dominated by empirical methods and rules-of-thumb (Bruneau, 1994). The use of sophisticated numerical tools have recently become popular in the masonry research community. This contrasts the current state of reinforced concrete and steel design where advanced numerical computer models are now the norm. Many researchers have developed numerical methods that attempt to effectively model the failure modes of URM structures. Few of these methods have however been sufficiently tested and implemented. A number of popular modelling and analysis methods will now be described along with their strengths and weaknesses.

There are various analysis types. They can be categorised as either: linear, non-linear or limit analyses. The building can be analysed as a whole, or simply a single structural element. There is also the choice between 2D and 3D analyses. Along with this, the element type must be chosen: eg. shell or solid. Each of these choices impact the quality of the results and computational

demand. The scope of results available for each analysis type will also be affected eg. whether both in- and out-of-plane behaviour is analysed.

An overview of linear analysis procedures is presented in Section 2.8.1. Non-linear material behaviour and analysis procedures is discussed in Section 2.8.2. A comparison between 2D and 3D analyses is presented in Section 2.8.3.

2.8.1 Linear

This assumes linear material behaviour (Hooke's law). Materials remain elastic and cracking is therefore not modelled. It provides a global distribution of reaction forces, stresses and displacements. Linear analyses are useful for identifying possible points of failure. Linear analyses will accurately predict the behaviour of non-ductile materials since failure is assumed to occur once the ultimate strength is reached. It allows the identification of critical elements to be used in a more complex analysis. The two major linear analysis types useful in seismic engineering are linear static and modal dynamic analyses. Although the strength degradation of the material is not taken into account by linear material models, damage can be implemented by assuming a reduced stiffness during analysis. This is the method commonly suggested by design codes such as SANS 10160-4.

2.8.1.1 Linear Static

A static analysis can be used to model a critical snapshot of a single point in time response of a structure to an earthquake. This can be adapted to give good results on the capacity of a structure to resist seismic loads. It is however unable to capture dynamic properties of a structure such as resonance and damping. During the analysis, lateral forces are applied along the height of a building. A linear or modal displacement gradient is assumed so that the applied forces vary from a minimum at the base of the building to a maximum at its apex. Forces are generally applied as concentrations at the slab level of each floor since the floor acts as a diaphragm for the distribution of horizontal forces. This is useful when performing a simplified two-dimensional (2D) analysis. Alternatively the forces can be applied directly to the walls, if the walls are represented using shell or solid elements in the case of a 3D analysis. This has the advantage of accounting for openings, but requires more computing power. The forces are applied to the walls in proportion to the weight and stiffness of each wall element. The static lateral force method is a popular example of a static simplification of dynamic problems.

Although a linear static method can provide a good estimate of stress distribution and forms the basis of the lateral static force design method (Section 2.7.1), it is insufficient for analysis since it does not take resonant behaviour or the failure of non-structural walls into account and will not present the true dynamic behaviour of a structure.

2.8.1.2 Modal Dynamic Analysis

A modal dynamic analysis (modal superposition analysis) is an effective way of modelling the dynamic behaviour of a structure. It involves the determination of a finite number of vibration modes of the structure. The modes that are used in the analysis is normally only a small subset of the total amount of modes. All modes with a mass participation factor of 5% and larger should be considered. Sufficient modes should be considered so that a total mass participation of 85% is accounted for. The building is excited by applying an acceleration time-history to the base. The response of the building in its various modes is added through superposition to calculate the total building response at each time step. However, since the building behaves in the linear range, the stiffness and mass matrices do not need to be re-calculated at each time step. This has a large impact on computational time. This method provides accurate results if a structure shows dominant behaviour in its lower modes and if sufficient modes are taken into account to represent the dynamic behaviour of the structure. The modal dynamic analysis does not allow for non-linear material models and strength degradation to be taken into account. It does however allow non-linear geometry (P-Δ) effects to be taken into account.

2.8.2 Non-Linear Analysis

A non-linear analysis can refer to either non-linear material modelling or geometric non-linearity. Non-linear material modelling requires the modification of the material properties to include post yield behaviour. Various failure and yield theories can be implemented to simulate post-yielding and cracking behaviour. Geometric non-linearity refers to the redistribution of forces as a structural member deforms. This leads to the incorporation of $P - \Delta$ effects and loss of equilibrium/collapse detection. It is essential to include geometric non-linearity if slender elements are modelled and when large displacements are expected or eccentric loading plays a role.

Different approaches to modelling masonry at the material level will be discussed in Section 2.8.2.1. This includes the micro and macro material modelling appoaches. Thereafter two macro material models will be presented: the Smeared Crack model (Section 2.8.2.2) and the Damaged Plasticity model (2.8.2.3). In order to implement a non-linear material model, an implicit dynamic analysis must be performed, discussed in Section 2.8.2.4.

2.8.2.1 Material Modelling Overview

URM consists of masonry bricks with mortar in-between the brick elements. This leads to a structural unit (e.g. a masonry wall) consisting of multiple materials that need to be modelled. When considering material modelling, there are two basic strategies: micro and macro modelling. This relates to the different ways in which the constituting elements are represented. Since URM consists of masonry blocks and mortar, it would seem logical that the two separate materials be modelled as separate features. This is however extremely computationally intensive and not viable for the analysis of large masonry structures. It becomes a viable option only

when examining a specific wall or critical structural element in an URM building or verifying experimental results on a small scale.

Micro modelling refers to the approach of representing masonry and mortar as separate features, each with their own material properties. In addition, the interaction at the interface between the masonry and the mortar is represented. Using micro modelling, the exact location of failure cracks can be determined. In addition, the damp proofing layers can be added with separate friction coefficients (Lourenço, 1996).

With macro modelling, the mortar and masonry is represented as a single material. There is no longer a distinction between separate masonry units and mortar, but rather the material has a combined stiffness and strength behaviour. This is an effective method when the structural elements are large enough so that the stress distribution along an element are uniform.

Since masonry will easily crack during seismic excitation, it is necessary to account for the formation of cracks. This can be done by modelling discrete cracks, smeared cracks or simply by reducing the material stiffness. Discrete cracks involve the modifying of the model geometry to create cracks. Yi, Moon, Leon, and Kahn (2006) performed an analysis on a two storey URM building. Possible crack locations were identified from building behaviour during past earthquakes. A discrete crack model was implemented with cracks modelled using contact elements. This is computationally intensive and impractical when analysing a large structure. A smeared crack approach (discussed in Section 2.8.2.2) is an alternative method of representing cracks at the integration points of the material by modifying the stiffness matrix once cracking has occurred. It is much more computationally efficient than discrete crack approaches. This makes the smeared crack approach an attractive choice when creating a macro material model. Complicated crack models can often lead to difficulties in convergence during analysis and have many input parameters that are difficult to determine experimentally, making a standard plastic model that reduces the material stiffness as damage progresses a simple alternative.

2.8.2.2 Smeared Crack Model

The smeared crack approach (as implemented by ABAQUS finite element software) works by creating cracks at locations where the stresses reach a *crack detection surface*. A popular crack detection surface (cracking failure criterion) is the William-Warnke failure criterion for the modelling of brittle materials (also implemented in the ANSYS finite element software). The effect of cracks are implemented at each integration point by modifying the material stiffness and stresses at that point. In addition, the orientation of the crack is calculated after which the stress and strain vectors are orientated to lie in the new crack coordinate system. After a crack has formed, a damaged elasticity theory governs the material. Tension stiffening is taken into account whereby the material is allowed to resist some stress and dissipate energy after cracking so that the stress-strain curve slowly decays to zero. In this way, the formation of cracks is smeared over the material at integration points rather than the formation of visible discrete cracks. Compressive stresses are modelled by an applicable elastic-plastic yield theory such as the Drucker-Prager yield criterion (Truong Hong & Laefer, 2008; Zucchini & Lourenço, 2007).

The smeared cracking model requires the following input:

1. Young's modulus;
2. Poisson ratio;
3. Any constitutive model assigned for values of tension and corresponding plastic strain rates;
4. Tension stiffening or tension strength decay after cracking;
5. The following Failure ratios:
    - Bi-axial *to* uni-axial ultimate compressive stress;
    - Absolute value of: uni-axial tensile stress at failure *to* uni-axial compressive stress at failure;
    - Magnitude of principle plastic strain at ultimate stress in bi-axial compression *to* uni-axial compression;
    - Principal tensile stress value at cracking in-plane stress, when the other non-zero principal stress component is at the ultimate compressive stress value *to* tensile cracking stress under uni-axial tension.

The smeared crack approach therefore offers a convenient way of modelling the formation of cracks due to tensile stresses in masonry structures. It is more computationally efficient than discrete crack approaches since cracking is introduced in the calculations at the integration point and therefore does not lead to the formation of additional degrees-of-freedom (DOF). The method has therefore been widely implemented (Ballio, Calvi, & Magenes, 1993; Lotfi & Shing, 1991; Romano, 2006; Syrmakezis, Chronopoulos, Sophocleous, & Asteris, 1995).

The method is however not without its drawbacks. The various disadvantages include: mesh-size dependency of numerical solutions, failure to capture certain failure modes such as diagonal shear cracks and rocking/sliding failure, directional bias and stress locking (Lotfi & Shing, 1991). The model requires a number of input parameters that need to be experimentally verified for different types of masonry. The lack of comprehensive experimental data relating to the use of the smeared crack approach is a major drawback. If incorrect material data is used as input parameters for a complex material model, the results obtained are questionable. This means that a simple plasticity model is a good alternative.

2.8.2.3 Damaged Plasticity

The damaged plasticity material model implemented in ABAQUS is based on models proposed by Lubliner, Oliver, Oller, and Oñate (1989) and Lee and Fenves (1998). It allows plastic behaviour of concrete and other brittle materials to be modelled. The main failure modes relating to brittle materials such as tensile cracking and compressive crushing is taken into account by reducing material stiffness. The model is capable of representing material damage for use in implicit dynamic analyses with parameters specifying cyclic loading and unloading

material behaviour. A damaged plasticity model is valid for brittle materials under low confining pressures (less than four times the ultimate uni-axial compressive strength), such as structural elements found in standard building structures. Under high confining pressures, a brittle material will not behave as expected and will instead behave as a ductile material since a confining pressure would limit crack propagation (Simulia Corp, 2010).

The plastic material representation of the damaged plasticity model is best described by considering a tension-compression-tension loading cycle as shown in Figure 2.18.

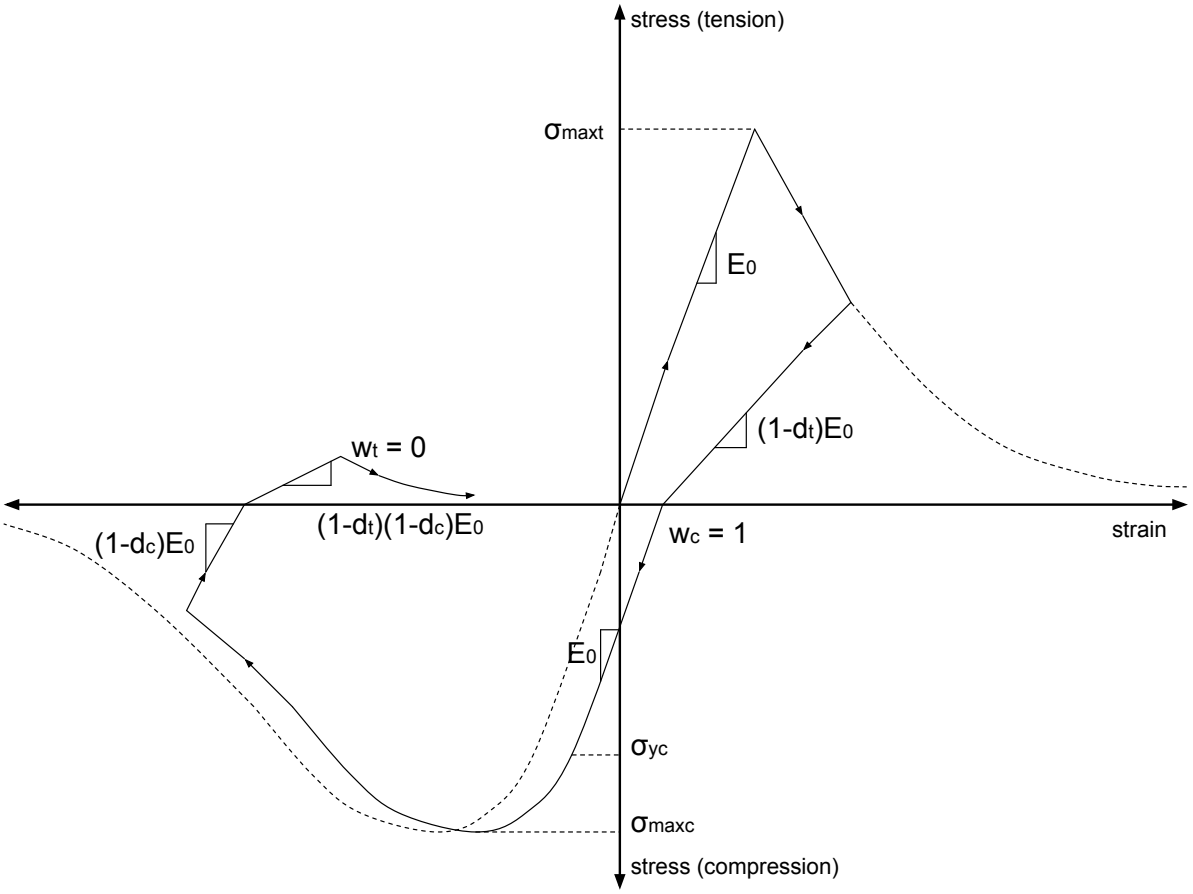

Figure 2.18: Stress strain diagram indicating part of a tension and compression load cycle when modelled using the concrete damaged plasticity material model (Simulia Corp, 2010).

There are various material characteristics that the damaged plasticity model assumes. Young's modulus (E_0) will have the same value for both compression and tension. Material response will remain linear until yielding has occurred. Separate stress-strain curves dictate material behaviour in tension and compression. Tensile behaviour is characterized by linear behaviour until the yield stress, corresponding to the maximum tensile stress (σ_{maxt}), is reached. At this point cracking will occur leading to strain softening behaviour until collapse. Compressive behaviour shows strain-hardening after first crack until σ_{maxc} is reached after which gradual strain-softening occurs. The Maximum yield strength in compression should be approximately 10 times or more than the maximum in tension.

Considering the case where a cyclic load is applied to a material, the stress strain graph will follow

the shape shown in Figure 2.18. Elastic response will be maintained until σ_{maxt} is exceeded. A reduction in material strength will follow with increases in strain. Once unloading occurs, the tensile stress and strain will decrease. The slope of the unloading branch of the tensile stress strain diagram will have a slope defined by E_0 before first crack. If cracking has occurred, the stiffness of the material will decrease as damage occurs. The extent of damage is specified using damage factors for tension (d_t) and compression (d_c) (Lee & Fenves, 1998; Lubliner et al., 1989). Values for d_t and d_c is specified as input parameters at the start of an analysis as a function of plastic strain. Damage factors can be determined from cyclic experimental results. A damage factor has a value of zero if the material is in its undamaged state with increasing values indicating increased damage and therefore reduced material stiffness.

Damage in tension is as a result of cracks opening in the material. Once the material is unloaded in tension and loaded in compression, the cracks will close thereby recovering the stiffness in compression. Stiffness recovery is specified through a stiffness recovery factor for compression (w_c) and tension (w_t) independently with a value of $w_c = 1$ indicating stiffness recovery and $w_c = 0$ resulting in no stiffness recovery (Lee & Fenves, 1998; Lubliner et al., 1989). For masonry it is assumed that compression stiffness is recovered even if tensile cracking has occurred. This is achieved by assigning $w_c = 1$. Cracking that occurs during crushing as a result of compression loading will however further reduce the tensile stiffness therefore requiring $w_t = 0$. This means that the stiffness in tension after the initial cycle will be calculated as $(1 - d_t)(1 - d_c)E_0$. This shows that tensile stiffness will be reduced by both the tensile damage and compressive damage parameters.

Material yielding during multi-axis loading is controlled by a yield function proposed by Lubliner et al. (1989) with modifications by Lee and Fenves (1998). The yield function requires certain input parameters to model brittle yield behaviour. Suggested values based on experimental results is presented in Table 2.9 (Lubliner et al., 1989; Simulia Corp, 2010).

Table 2.9: Defualt suggested parameters to be used in the damaged plasticity model for brittle materials (Lubliner et al., 1989; Simulia Corp, 2010).

Symbol	Description	Value
ψ	Dilation angle	36–40
ϵ_{ecc}	Flow potential eccentricity	0.1
σ_{b0}/σ_{c0}	Ratio of initial equibiaxial compressive yield stress to initial uniaxial compressive yield stress	1.16
K	Ratio of the second stress invariant on the tensile meridian to that on the compressive meridian at yield	0.667

A viscosity parameter is provided to introduce visco-plastic regularization into the material equations if convergence is an issue. This will allow calculated stress values to fall outside the yield surface for a small time period after which the results are corrected. Increasing the viscosity parameter in relation to the analysis time step will improve convergence while decreasing accuracy. A value of 0 will ignore visco-plastic regularization and therefore not influence results

(Simulia Corp, 2010).

The damaged plasticity model provides a simple model to take stiffness degradation into account without introducing cracking.

2.8.2.4 Implicit Dynamic Analysis

In order to include a non-linear material model in the analysis it is necessary to perform an implicit dynamic analysis. During the analysis, the equilibrium equations will be implicitly solved at each time step taking the change in stiffness and mass of the model into account. This allows the material properties to undergo large changes during time steps. The modes of the structure do not need to remain constant since resonant behaviour will be accounted for during the solution, based on the current state of the structure at each time step. This method will be able to capture unexpected excitation at higher modes and the change of natural frequencies as the material stiffness degrades. The primary disadvantage of performing an implicit analysis is the high computational demand, especially for large models and long time-histories.

2.8.3 2D and 3D Analyses

Genna, Di Pasqua, Veroli, and Ronca (1998) performed several analyses on an old masonry monastery. The author shows that a full-scale non-linear analysis of the building is very computer intensive. The building is therefore reduced to a plane problem in order to reduce the model size. Finally a small structural element is analysed in order to perform a full non-linear analysis including the modelling of connections including cracking and crushing of the material. A plane model has various drawbacks, of which the primary one is the lack of out-of-plane response. This can be a problem when diaphragms are expected to be non-rigid. The writer goes on to show that a no-tension model is utterly unrealistic and should be avoided. The importance of taking the effects of cracking into account is highlighted by the analysis.

Yi et al. (2006) performed a 3D elastic analysis on a two-storey building. Due to the weak diaphragm of the building, there was little coupling between parallel in-plane walls. This led to the conclusion that a 2D analysis is sufficient if torsional effects do not play a role and if flange effects are taken into account in the 2D-model. After performing both a 2D pushover analysis and a full 3D non-linear analysis, it was concluded that the full 3D model provides better results, but at a large (in the order of 10 times increase) cost in computational power.

2.9 Summary

In this chapter, literature regarding the properties and behaviour of masonry relating to both construction and analysis has been presented. A brief background of earthquakes in South Africa and the seismic loading codes that governs the design in South Africa was discussed. The literature suggests that there is great uncertainty regarding the performance of URM during seismic events. This is especially the case in South Africa.

South Africa has many areas that are at risk of low to moderate intensity earthquakes. Several earthquakes with a Richter magnitude between 5.1–6.5 that occurred in South Africa have been documented. The Tulbagh earthquake of 1969 is one example of an earthquake that caused extensive damage that occurred in the Western Cape. If such an earthquake occurred in the Cape Town Business District, the damage could be severe. Little is known about the precise location of faults and the exact seismic risk of South Africa. Determining a seismotectonic model of the country has yet to be completed and the current hazard profiles are instead based on the analysis of the main tectonic structures as well as present day seismicity correlations (Singh et al., 2009). This leads to uncertainty regarding the current seismic hazard of South Africa. Although earthquakes have been recorded, they are very few due to the long return period associated with seismic events.

The current seismic loading code, SANS 10160-4, expanded on the seismic provisions of SABS 0160. Wium and van Zijl (2005) suggest that many engineers regarded the code as being over conservative and unrealistic. This provides uncertainty to whether buildings designed to SABS 0160 meet the necessary seismic requirements currently contained in SANS 10160-4. Many buildings were also constructed before SABS 0160 came into effect. SANS 10160-4 provides a seismic hazard map that indicates a PGA value of 0.15g for certain regions of the Western Cape. Kijko et al. (2002) reports that a mean PGA value of 0.18g could be expected in the Tulbagh area. SANS 10160-4, however specifies a design PGA value of 0.1g for the seismic regions of the Western Cape. Wium (2010) explains that the design acceleration value was adopted from SABS 0160 without adjusting it since the revision committee was unable to make a final decision as a result of many external factors that needed to be taken into consideration. The reduced design PGA is remedied through the use of the redundancy factor. The redundancy factor increases the design PGA value to 0.15g if insufficient shear walls are provided. When sufficient shear walls are present, the value of the redundancy factor can be reduced. It was therefore deemed necessary to consider earthquakes with a PGA of up to 0.15g when analysing an existing structure.

The literature highlighted the need for a structure to meet basic conceptual design principles. Whether current URM structures meet these guidelines must be evaluated. SANS takes plastic behaviour of URM into account through the use of the behaviour factor. Masonry is a brittle material with limited post cracking capacity. This must be taken into account when analysing current structures. Research regarding the seismic performance of URM is lacking. Significant research has been done in other countries. This allows local structures to be analysed by using experimental data from other countries.

The material strength of masonry is highly variable. This includes both the material strength and stiffness. This is further impacted by the inability of masonry testing techniques to give consistent results. The uncertainty regarding material strength and random nature of seismic loading means that the determination of the seismic resistance of current structures is not straight forward. There are many techniques that have been used to design analyse URM. SANS 10160-4 relies on the static lateral force method for design. The method relies heavily on the value of the natural frequency of the structure. The formula provided is however crude and

the accuracy of its results are questionable. There is no widely excepted method for analysing masonry and few methods have been developed that take the many failure modes into account. Newer methods can be very complex and cumbersome and have not been sufficiently tested to validate the results. It is therefore necessary to gradually analyse a structure using sufficient checks to validate results.

The current project will aim to address the uncertainty relating to the performance of standard three storey URM buildings. This will be achieved by selecting material data representative of older URM structures, applying earthquake time-histories representative of the Western Cape seismic hazard and interpreting the results with respect to the many failure modes of URM buildings. The results will expand the current knowledge regarding local seismic resistance of structures. This is necessary since an earthquake is capable of causing severe damage to areas where seismic design has not been sufficiently accounted for.

Chapter 3

Model Calibration

3.1 Introduction

The finite element method (FEM) is a powerful tool for solving static and dynamic problems. It is implemented in most modern structural analysis software packages. Software packages, such as ABAQUS, have built-in models for many materials and material behaviours. Other materials, such as URM, need to be implemented by adjusting the input parameters of an existing material model. In order for the software to provide accurate and useful results, it is of prime importance that the input data for a specific problem is calibrated using experimental data. If this is not done, the FE analysis results are questionable.

In Chapter 2, literature was presented to gain an understanding of the behaviour and properties of URM on a broad scale. URM is a non-homogeneous anisotropic material as explained in Section 2.5. For this study, the masonry material will be modelled on a macro-scale, i.e. the properties of the combined brick and mortar assemblage will be applied to structural elements in an ABAQUS model, without modelling separate brick and mortar layers. A macro-material approach, discussed in Section 2.8.2.1, is more suited to modelling an entire structure since the computing requirements are vastly reduced. It was further shown in Section 2.6.1 that in-plane shear walls along with the floor diaphragms form the primary load resisting system. The anisotropic properties of URM and the aspect ratio of URM walls will cause them to have much less stiffness in the out-of-plane direction. It is necessary to account for the difference in in-plane and out-of-plane behaviour by assigning different stiffness values to the in- and out-of-plane walls.

In this chapter, a finite element model will be developed and calibrated using specific experimental data from various researchers. This will be done initially using a basic structural wall to calibrate out-of-plane wall stiffness in Section 3.2.1 after which a full masonry structure will be used to calibrate the in-plane wall stiffness in Section 3.2.2. Input parameters that will be calibrated include the elastic material properties (elastic modulus, Poisson ratio and general wall stiffness) for use in an elastic time-history analysis. In addition to the elastic material properties, the plastic material properties will also be addressed in Section 3.2.3 to be used in a non-linear

analysis. Finally, the damping of masonry buildings will be discussed in Section 3.3.1. This is a critical input parameter when performing dynamic analyses. Once the FE model is calibrated, the full structure can be modelled and analysed.

3.2 Material Strength Property Calibration

Material property calibration involves determining input values that accurately describe the material behaviour. Properties such as density can be easily determined using experimental methods. A mass density value of $1950kg/m^3$, as suggested by Yi (2004) will be used for URM. Other authors and design codes confirm that a general density of 1800–$1950kg/m^3$ can be used for clay brick masonry (AS/NZS 1170.1, 2002; Griffith et al., 2007; SANS 10160-2, 2009; Simsir, Aschheim, & Abrams, 2004; Vaculik, 2012). The determination of the mass matrix is straight forward when using standard shell and beam elements. Any FE software should not have trouble calculating accurate mass values. Determining the stiffness of structural elements is more complicated. FE software will be able to successfully determine the model stiffness if accurate geometry, material strength properties and a suitable mesh is provided. Various material properties of an ABAQUS model will initially be calibrated in the elastic range using experimental results. Thereafter a plastic material model will be presented.

3.2.1 Elastic Out-of-plane Calibration

Griffith et al. (2007) performed cyclic tests on a series of URM walls to determine the out-of-plane force-displacement behaviour and wall strength. The authors explain that seismic forces are carried by shear walls in-plane, which form the primary load path. Due to the acceleration that a building undergoes during an earthquake, inertia forces develop in orthogonal spanning walls that are not part of the primary structural system. These walls will undergo out-of-plane deflections. If these walls are slender and sufficient lateral support is not provided, failure due to out-of-plane collapse could occur. This is further exaggerated by the low tensile strength of masonry and the inclusion of large openings in the building perimeter walls. The combination of small aspect ratio in plan, low tensile strength and lack of unit interlocking will cause masonry walls to be less stiff in the out-of-plane direction than in the in-plane direction.

The difference in in-plane and out-of-plane stiffness will be addressed at the material level by assigning different E-modulus values for in-plane and out-of-plane walls. This allows the difference in stiffness to be taken into account on a macro-material level. Masonry walls are typically thin shell elements that respond out-of-plane through flexure. The flexural response will cause stresses and strains to develop in the plane of the wall. This in turn is affected by the elastic modulus in the plane of the wall. A single elastic modulus will be assigned to out-of-plane walls to represent the out-of-plane flexural stiffness. This will be obtained from experimental results of similar sized URM walls. The elastic modulus of the ABAQUS model will therefore be adjusted until the flexural response and therefore out-of-plane wall stiffness matches the stiffness of the experimentally tested wall.

Research into the lateral strength of URM specific to South African materials and conditions is limited. Instead researchers must rely on test data from other countries with possible adjustments made for South African construction practices. There are numerous examples of experimental tests on the static out-of-plane behaviour of one-way spanning URM walls in literature (Ghobarah & El Mandooh Galal, 2004; Hendry, 1973; Lawrence, 1983; Simsir et al., 2004). Most of these tests were performed on single walls in one-way bending with various techniques used to simulate different boundary support conditions. More recently, Griffith et al. (2007) performed lateral displacement tests on clay brick URM walls with portions of the lateral walls included to simulate the effect of two-way bending. This is especially useful since it provides more realistic and practical data on the response of out-of-plane masonry walls in a building structure. By including portions of the in-plane walls, the lateral support fixidity is accounted for while still allowing the in- and out-of-plane wall connection to respond realistically. It was therefore decided to use the experimental results presented by Griffith et al. (2007) to calibrate the out of plane properties of URM. It is necessary to calibrate the stiffness properties of a single out-of-plane wall since the large stiffness of in-plane walls will dominate global building stiffness behaviour when considering a full structure.

Griffith et al. (2007) performed lateral displacement tests on eight URM walls with different combinations of openings and vertical loads. The walls represent various wall types found within a standard masonry structure. The walls shown in Figure 3.1 were selected to calibrate the material data for the current project.

Both walls are 4.0x2.5m in elevation, 110mm (single brick width) thick and have identical support conditions. The wall and brick dimensions are similar to that of typical single leaf walls in residential URM structures in South Africa. The building selected for the current project, has typical dimensions of 3–4m between lateral walls, similar to the walls tested by Griffith et al. (2007), as shown in Section 4.2. On the vertical edges, the test walls are supported by short lateral walls shown in Figure 3.1c to effectively simulate the connection between in- and out-of-plane walls in URM buildings. At the horizontal edges, the experimental walls are supported as a pin connection to represent the floor-to-wall connections that allow rotation when a rigid floor diaphragm is present. One of the walls has a single 1.2x1.0m window opening (12% opening ratio, Figure 3.1b) typically found in perimeter walls while the other wall is solid.

The walls were constructed using standard size cored clay bricks with dimensions of $230 \times 110 \times 76$mm. Material tests performed by Griffith et al. (2007) on 8 masonry prisms constructed using the same material, determined a masonry compressive strength of 16MPa, tensile strength of 0.6MPa and E-modulus of 3.54GPa. This is consistent with masonry properties in South Africa as discussed in Section 2.5.4. A mortar mix of 1:2:9 (cement:lime:sand) was used for the construction of the test walls in controlled laboratory conditions, which constitutes a weak mortar mix. The bricks used, on the other hand, are of very high quality with a compressive strength of 54MPa. Vertical loads of $\sigma_v = 0.1$MPa and 0.05MPa were applied to the wall without openings whereas a vertical load of $\sigma_v = 0.01$MPa was applied to the wall with the window opening. This leads to three wall alternatives to be considered. During the experimental procedure performed by Griffith et al. (2007), a distributed face pressure was applied to the inside

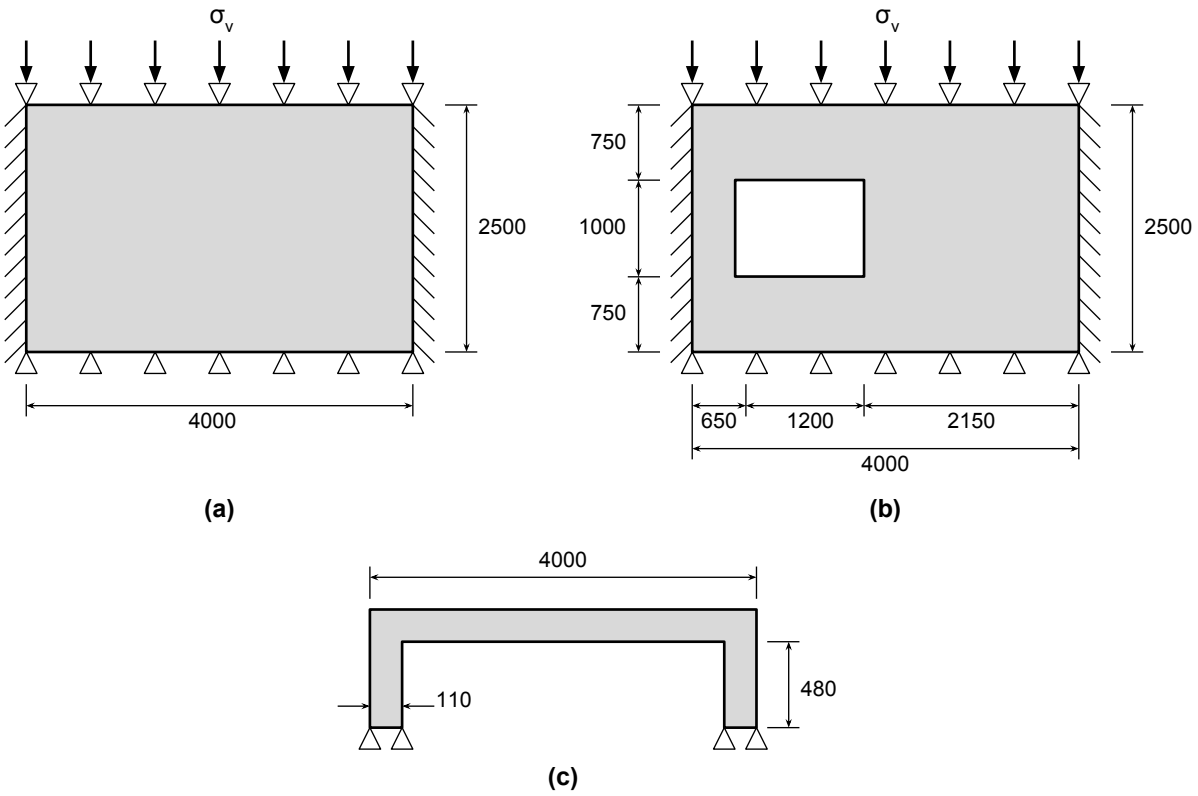

Figure 3.1: Elevation and plan views of the different walls used to calibrate the out-of-plane URM material properties. The elevation views of: (a) the solid wall, (b) the wall with a window opening and (c) the plan view of the walls, are shown. All dimensions in millimetres. (Griffith et al., 2007)

face of the wall causing it to deflect out-of-plane. After every load cycle, the wall was unloaded after which the cycle was repeated with an increased face pressure. Displacement was measured at the centre of the wall face to produce force-displacement ($F - \Delta$) curves.

The material properties determined by Griffith et al. (2007), discussed above, along with a masonry density of $1950kg/m^3$ and a standard Poisson ratio of 0.25 are used to model the walls in ABAQUS. The boundary conditions of the ABAQUS model are specified to match the pin and fixed supports of the experimental setup. An increasing lateral face pressure is applied to the wall, to simulate the face pressure of the experimental procedure, after which displacement results at the wall centre are recorded. The single brick width walls with relatively low Young's modulus represent the less stiff infill walls as well as walls not forming part of the primary load resisting system for a given excitation direction. The $F - \Delta$ curves obtained by Griffith et al. (2007) will be used to determine the out-of-plane wall stiffness of the wall and calibrate the ABAQUS model.

The elastic portion of the curves is of major importance since it allows for the calculation of the Young's Modulus. The elastic portion of the $F - \Delta$ curve obtained by Griffith et al. (2007) during experimental testing is not precisely linear, due to early formation of micro cracks during initial loading sequences. For this study, the elastic portions of the curves are approximated as straight lines. The walls are assumed to remain elastic until the first crack causes a significant

change in slope of the $F - \Delta$ curves. The Young's modulus of the ABAQUS model should be adjusted so that the lateral force and resulting wall displacement at first crack, matches the experimental results obtained by Griffith et al. (2007).

Initial analysis results show that accounting for non-linear geometry produced an increase of 7% in wall displacements. This means that the slenderness of the wall when deflecting out-of-plane under combined vertical and horizontal load is sufficient to increase the lateral wall displacement due to second-order effects. Non-linear geometry was therefore included in further analyses. Next, while taking non-linear geometry into account, the Young's modulus was iteratively adjusted from the initial value of 3.54GPa until the numerical $F - \Delta$ results at the elastic limit matched the experimental values. The analysis results are presented in Table 3.1.

Table 3.1: Comparison between the out-of-plane experimental results (Griffith et al., 2007) and FE analysis results.

	Wall	σ_v **(MPa)**	**Lateral Load (kPa)**	**Experimental**	**ABAQUS**	**% difference**
				δ **First crack (mm)**	δ **(mm)**	
Initial ABAQUS	Solid	0.10	4.0	4.0	2.73	-32
test with	Opening	0.10	4.8	5.0	3.77	-25
E = 3.54GPa	Opening	0.05	3.0	3.0	2.35	-22
Revised ABAQUS	Solid	0.10	4.0	4.0	3.8	-5
test with	Opening	0.10	4.8	5.0	5.25	+5
E = 2.554GPa	Opening	0.05	3.0	3.0	3.26	+9

The analysis results indicate that a revised Young's modulus of 2.554 GPa in ABAQUS predicts the experimental displacements within 5% for $\sigma_v = 0.1$MPa and 9% for $\sigma_v = 0.05$MPa. This is considered sufficiently accurate for use in further analyses. The calibrated E-value is 28% less than the value obtained by Griffith et al. (2007) through masonry prism compression testing. This is expected and can be explained by the difference in aspect ratio between the tested masonry prisms and the out-of-plane bending of the wall. This affects the interlocking and cracking behaviour of masonry. The Young's modulus obtained through compressive testing of masonry prisms does not provide a realistic representation of the Young's modulus of a complete wall in the out-of-plane direction. While the response of the wall was essentially linear-elastic, minor cracks have formed leading to a slight reduction in the wall stiffness, and hence a reduced Young's Modulus.

3.2.2 Elastic In-plane Calibration

Once the masonry walls have been calibrated for out-of-plane bending, it is necessary to calibrate in-plane wall stiffness. A test building is chosen to calibrate the ABAQUS material model. The chosen structure, shown in Figure 3.2, is a two-storey URM building previously experimentally analysed by Yi (2004).

The building tested by Yi (2004) was selected for calibration since a number of experimental tests as well as a numerical analysis were performed on the structure with well documented results. The scale of the structure provides results that will more closely represent the results

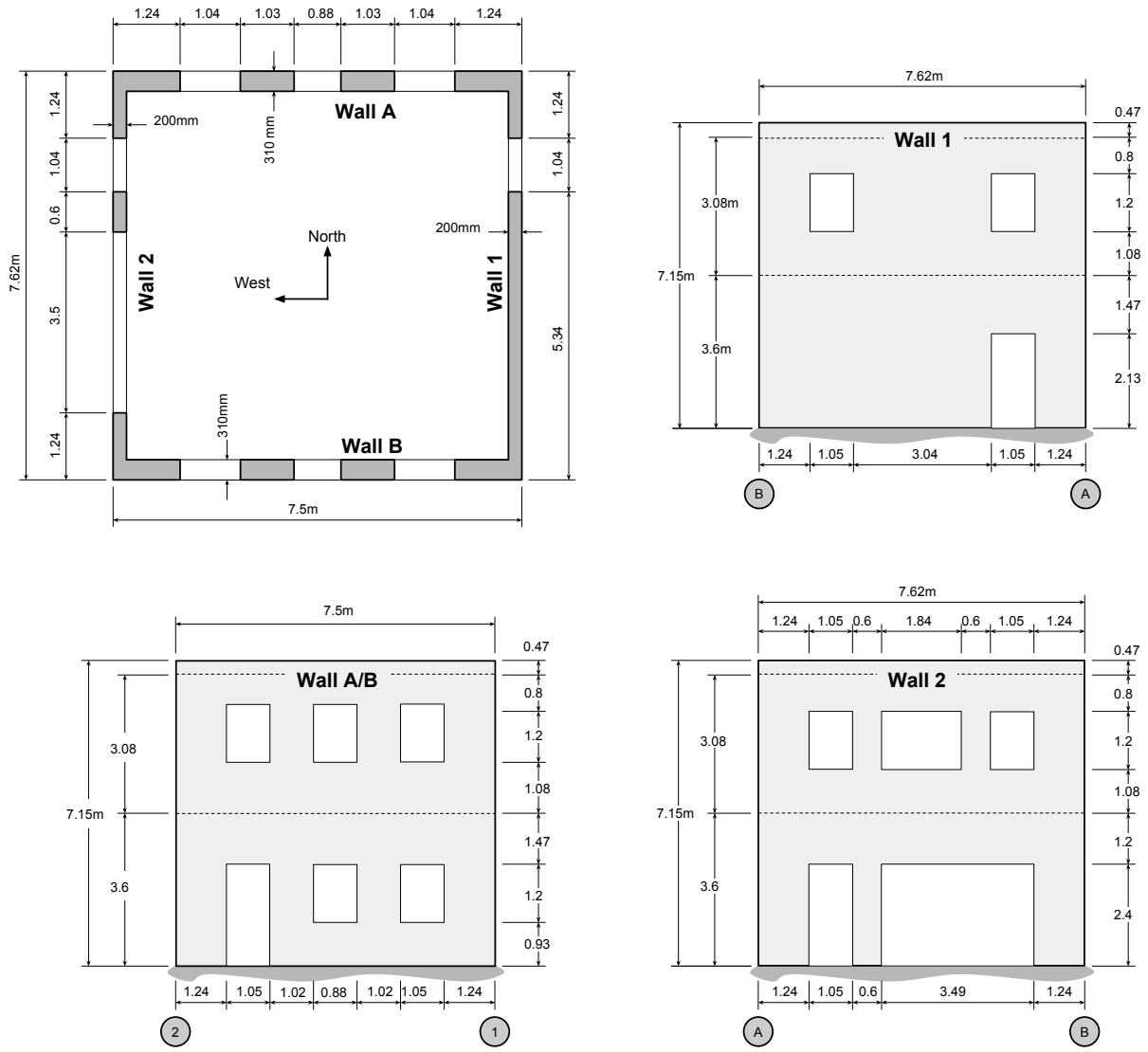

Figure 3.2: Plan and elevation views of the two storey URM building used for in-plane calibration. (Yi, 2004).

of a typical three storey URM structure located in Cape Town and its surrounding areas.

The test building has four walls with various opening ratios. Walls 1 and 2 are 200mm thick (double-leaf) and lie in the North-South direction. They have opening ratios of 9% and 29% respectively. Walls A and B lie in the East-West direction, are 310mm (three-leaf) thick and both have opening ratios of 15%. The structure has flexible wooden floor and roof diaphragms. Yi (2004) performed various lateral static and dynamic tests on the test structure.

Since the in-plane walls provide the majority of the lateral stiffness to the building, it follows logically that experimental lateral $F-\Delta$ curves of a building can be used to determine in-plane wall stiffness. Using a full structure will also account for additional stiffness provided by out-of-plane walls due to coupling and flange effects. The floor diaphragm for the test structure is flexible and therefore only plays a minor role in redistributing lateral loads between in-plane walls. This greatly simplifies calibration of in-plane wall stiffness since the force displacement results will not be severely effected by redistribution of forces through the diaphragm. It provides

further motivation for using the experimental results obtained by Yi (2004) to calibrate the ABAQUS model of the current project.

The test structure is representative of URM structures from the central America region that were built pre-1950. The buildings have flexible wood diaphragms with strong brick - weak mortar material characteristics. This may indicate a relatively weaker mortar than was expectedly used in South Africa during the 1970's. Insufficient experimental data on the strength and stiffness of modern masonry structures and especially structures built during the 1970's in South Africa is available. Globally, research into seismic behaviour of URM is focused on the performance of historic buildings since these buildings are at greater risk of collapse. Some research has also been conducted on the performance of modern URM during past earthquakes. These studies are focused on the behaviour and damage of existing buildings and not strength or material properties of modern URM. Construction of modern URM buildings in seismic active areas remains prevalent, often with little regard given to seismic performance. There are several important differences that need to be taken into account when comparing modern URM buildings to buildings dating pre-1950.

The first major difference is the common occurrence of flexible wooden diaphragms in older buildings. This leads to a structural system that is unable to effectively redistribute loads between in- and out-of-plane walls. Modern URM buildings typically contain reinforced concrete floor systems that act as rigid diaphragms. This greatly enhances the load distribution system of the structure. It is important to note however that floor-to-wall connections play an increasingly important role when the floor diaphragm is expected to transfer large lateral forces during a seismic event. This is reflected in South African design code requirements as seen in Section 2.4.6.2.

Another major difference is the increased mortar strength of modern structures. Yi (2004) explains that a weak mortar mix of 0.5:2:7.5 (cement:lime:sand) with a compressive strength of 0.6MPa was commonly used for building construction pre-1950. This is weak compared to a common mortar ratio of 1:0:3 (cement:lime:sand) that is used for modern structural URM construction. The compression strength of brick units are however consistent with modern brick strengths. As explained in Section 2.5.2, weak mortar will have little influence on the stiffness and compressive strength of masonry walls in the elastic range. An acceptable theory will however be applied to the plastic strength behaviour of the masonry material to take the stronger mortar used in South Africa into consideration. The masonry compressive strength of 10MPa obtained by Yi (2004) is comparable to results from similar masonry types in South Africa, despite the use of a weaker mortar mix.

Compressive testing of 16 masonry prisms by Yi (2004) indicates an E-modulus of 8GPa for the masonry used. This is comparable to results presented by other authors as seen in Section 2.5.2. The significantly stiffer material (when compared to the 3.544 GPa E-modulus obtained by Griffith et al. (2007)) represents the stiff in-plane masonry shear walls that form the primary load resisting system during earthquake excitation. It was shown in Section 2.5.2 that the E-modulus of masonry is subject to very large variations when determined experimentally. As was the case with the calibration process for out-of-plane bending, it is expected that the wall's in-

plane Young's modulus would be less than experimental results obtained from testing masonry prisms. Yi (2004) also performed an elastic FE analysis of the test structure. An E-modulus of 6.895GPa and Poisson ratio of 0.25 were used to define the material model.

An ABAQUS model of the two-storey structure shown in Figure 3.2 is created to calibrate the in-plane masonry properties. Since out-of-plane behaviour of masonry is significantly different from in-plane behaviour, it is necessary to apply different material properties for the in-plane and out-of-plane directions. Out-of-plane wall stiffness was calibrated using experimental data in Section 3.2.1. The calculated E-modulus of 2.554 GPa is applied to the out-of-plane walls. The E-modulus of the in-plane walls will be determined while keeping the out-of-plane wall properties constant.

The experimental building tested by Yi (2004) was excited using actuators located at the second floor and roof levels. The actuators were connected to the in-plane walls and displaced the building while maintaining displacement control to equally displace parallel in-plane walls. The first three loading cycles in the North-South direction are selected for calibration purposes. These cycles are chosen on the basis that the lateral load-displacement results remain linear, therefore indicating elastic response.

Concentrated forces are applied to the ABAQUS model at floor level to simulate the actuators used during the experimental procedure. The elastic modulus of the FE model is adjusted for the in-plane walls so that $F-\Delta$ measurements at the first and second storey match the corresponding elastic limits of the experimental data obtained by Yi (2004). During the analysis the out-of-plane wall properties are kept constant. Experimental $F-\Delta$ results relating to the elastic limit are presented in Table 3.2.

Table 3.2: Maximum force-displacement results for walls 1 and 2 of the test building. (Yi, 2004)

	Force at max. displacement (kN)	**Max. roof displacement (mm)**
Wall 1:	258	0.86
Wall 2:	100	1.17

In order to maintain uniform displacement of parallel walls during the experimental procedure, different loads were applied to each of the walls (Yi, 2004). The loads tabulated in Table 3.2 are applied at floor and roof level of the ABAQUS model with a linear distribution so that the total base shear force amounts to the tabulated values. This results in the following force distribution: $F_{1-1} = 86$kN, $F_{1-2} = 172$kN, $F_{2-1} = 33.4$kN and $F_{2-2} = 67$kN (subscripts indicate the wall number and whether the load is applied at second floor or roof level).

Iteratively adjusting the Young's modulus of the in-plane walls in the ABAQUS model resulted in a value of $E = 5.7$GPa (in-plane) and $E = 2.554$GPa (out-of-plane). The displacement results obtained from the ABAQUS analysis along with the experimental results obtained by Yi (2004) are shown in Table 3.3.

The ABAQUS model displacement of Wall 1 reproduced the experimental displacement results by Yi (2004) within 5%. Using the same Young's modulus, the displacement of Wall 2 was

Table 3.3: Comparison between experimental results obtained by Yi (2004) and calibrated ABAQUS displacement results obtained for this project.

	Experimental displacement (mm)	**Analysis displacement (mm)**	**% difference**
Wall 1:	0.86	0.90	+4.79
Wall 2:	1.17	1.00	-14.84

within 14% of the experimental value. Wall 2 has a very large opening ratio (29%) when compared to Wall 1 (9%). This leads to a far less stiff wall as shown with the large experimental displacements. The FE model was not able to achieve the same lateral displacement for Wall 2 as recorded during the experimental tests. It is assumed that the larger displacements in the experimental results, are caused by the onset of cracking due to smaller wall stiffness. This results in sensitivity to lateral force increase.

3.2.3 Non-linear

Material properties defining the elastic response of URM were calibrated in Sections 3.2.1 and 3.2.2. This will account for material behaviour until cracking has occurred. After cracking, the material response must be specified using an acceptable non-linear material model. In Section 2.8.2.1, various material models available in ABAQUS to represent the non-linear behaviour of masonry was presented. Although the models are intended primarily for concrete behaviour, other brittle materials such as URM can be modelled by inputting relevant plastic material data. For this project, it was decided to model the masonry using a damaged concrete plasticity model as discussed in Section 2.8.2.3. This allows plastic material behaviour to be specified to account for the post cracking behaviour of the masonry including both the post cracking strain-hardening behaviour until the ultimate strength is reached and also the subsequent strength degradation until failure occurs.

The stiffness of the material will reduce until 20% of the ultimate strength is reached after which it will remain constant to allow the analysis to finish. While it was acceptable to use experimental data of weaker masonry to calibrate the elastic stiffness in Section 3.2.1 and 3.2.2, the plastic material data should reflect the ultimate compressive and tensile strength of masonry that is used in South Africa. The plastic material parameters implemented in ABAQUS for this study will now be presented and discussed. This includes parameters necessary to configure the damaged plasticity material model as well as plastic material properties that will define the post cracking behaviour of the ABAQUS model.

General model parameters relating to the yield surface is discussed in Section 2.8.2.3. The parameters along with their values used for calibration purposes in this study are listed in Table 3.4.

All parameters except for the viscosity factor are default values for brittle materials such as concrete and masonry. The viscosity factor was selected to be as small as possible while allowing convergence to occur. Plastic material properties are specified as a function of plastic strain. A

Table 3.4: Parameters to be used in the damaged plasticity model for brittle materials during calibration (Lubliner et al., 1989; Simulia Corp, 2010).

Symbol	**Value**
ψ	39
ϵ_{ecc}	0.1
σ_{b0}/σ_{c0}	1.16
K	0.667
Viscocity	0.001

Young's modulus of 5.7GPa in-plane was determined in Section 3.2.2. This will represent the material stiffness in the elastic range until cracking occurs. The plastic behaviour is based on the linear stress-strain approximations for tension (Dhanasekar & Haider, 2008) and compression (Kaushik et al., 2007) discussed in Section 2.5.6. Stress and plastic strain values are shown in Table 3.5 for compression and Table 3.6 for tension.

Table 3.5: Compressive stress and inelastic strain values for URM.

	Compression Behaviour	
	Stress (MPa)	Inelastic Strain
σ_Y	8.85	0
σ_{max}	11.80	0.001
σ_u	2.36	0.0045

Table 3.6: Tensile stress and inelastic strain values for URM.

	Tensile Behaviour	
	Stress (MPa)	Inelastic Strain
σ_{max}	0.6	0
	0.3	0.0001
σ_u	0.12	0.0002

An element of unit size is modelled in ABAQUS and assigned the plastic properties shown in Tables 3.5 and 3.6. For the elastic properties, a Young's modulus of 5.7GPa and Poisson ratio of 0.2 is assumed. While the one side of the element is fixed, the other side is displaced gradually, first in tension and then in compression to verify that the stress-strain behaviour obtained at the integration point matches the ideal compression and tension behaviour. Results indicate that ABAQUS matches the non-linear results presented in Section 2.5.6 in both tension and compression.

3.3 Dynamic Property Calibration

The material properties calibrated in Section 3.2 represent the behaviour of URM at the material level. When a dynamic analysis is performed on a structure, additional material and structural properties will influence the structure's behaviour. The natural period of the structure is an important property that must be calculated. This will depend on the mass and stiffness distribution of the structure. When a finite element model is created and analysed, it is important to ensure that the natural frequency of the FE model matches that of the building that is being modelled since it will dictate the dynamic response of the structure. Damping also plays an important role in dynamic analyses and must be specified for URM.

Due to the large variations in results and the degree of uncertainty in modelling URM, it is impractical to attempt to match a specific dynamic experimental test result during calibration, unless a large scale experimental test is performed on masonry under local building conditions. To the knowledge of the author, such data is not yet available for South African conditions. It was therefore decided that the dynamic results will be verified by performing a simplified dynamic analysis on a simple spring-mass model of the structure. In a similar way, the natural frequency of the ABAQUS model can be verified using the formula provided in SANS 10160-4.

3.3.1 Damping

Vaculik and Griffith (2007) performed shaketable tests on five half-scale walls. The walls used were similar in layout to the walls used for out-of-plane calibration in Section 3.2.1. This includes walls with and without openings as well as supporting various magnitude vertical stresses. Walls included a portion of the lateral supporting wall to simulate two-way bending similar to wall behaviour in buildings during excitation. The base of the walls were excited by applying various acceleration time-histories of existing earthquakes. Damping ratios were determined for different damage states by measuring the energy dissipated for each acceleration cycle. Damping ratios increased as wall damage progressed. Mean damping ratios of 0.12-0.17 were calculated by Vaculik and Griffith (2007) for fully cracked walls. A general value of 0.05 was confirmed for uncracked walls.

Based on the results presented by Vaculik and Griffith (2007), a damping ratio of 0.1 is assumed for this study. This assumes that URM will tend to crack during earthquakes causing an increase in damping. The increased damping can be attributed to opening and closing of cracks, further formation of cracks and frictional sliding at crack locations. The effect of decreasing the damping ratio will be evaluated through a sensitivity analysis in Chapter 6.

Damping can be specified as a ratio of the critical damping using viscous damping model when performing a linear analysis such as the modal dynamic analysis discussed in Section 2.8.1.2. When a non-linear implicit analysis is to be performed, the material properties will change during subsequent time steps. It is therefore necessary to use an alternative damping model. ABAQUS allows the use of a Rayleigh damping model shown in Eq. 3.1.

$$C = \alpha M + \beta K \tag{3.1}$$

M and **K** are the mass and stiffness matrices of a structure. Rayleigh damping therefore specifies damping as a proportion of the mass and stiffness of the structure. The values of α and β can be calibrated so that the behaviour matches that of a classically damped structure (Alipour & Zareian, 2008). The viscous damping ratio will be matched exactly for two specific modes. Damping for intermediate modes will depend on the Rayleigh model. Alpha and beta values will be determined in Chapter 6.

3.4 Summary

When performing a FE analysis of a structure, it is important to calibrate the model using experimental results to ensure that the FE results obtained are valid. URM is a non-homogeneous material. It is necessary to account for this anisotropy by assigning different material properties in different directions. It was identified that URM has two primary loading directions during seismic excitation that should be accounted for: in-plane and out-of-plane loading. Initially, the material was calibrated for out-of-plane loading by incrementally adjusting the Young's modulus in an ABAQUS model until experimental displacement results presented by Griffith et al. (2007) were matched. Three walls were used for calibration with different combinations of openings and vertical compression. An E-modulus of 2.554GPa was determined for the out-of-plane direction.

Similarly the in-plane stiffness was determined. For the in-plane case, a two storey building was analysed. The out-of-plane walls were assigned an E-modulus of 2.554GPa while the in-plane value was adjusted until the building displacement of the ABAQUS model matched experimental results obtained by Yi (2004). This suggested an E-modulus of 5.7GPa for in-plane URM. The in-plane wall stiffness dominates the structural behaviour. Using a two-storey building allowed the component interactions of in- and out-of-plane walls to be taken into account when determining the E-modulus.

Once the elastic material properties had been calibrated to sufficient accuracy, a non-linear material model was presented. Using a damaged plasticity model, the plastic compressive and tensile behaviour of an element was capable of matching ideal behaviour for uniaxial compression and tension. Finally damping ratios for a viscous damping and Rayleigh damping model was obtained from literature. The calibrated values can now be implemented in a three-dimensional model of an existing building and used to perform both a linear and non-linear seismic analysis.

Chapter 4

Modelling and Elastic Analysis

4.1 Introduction

When performing a full scale analysis of a building, it is important to consistently perform the necessary verifications to ensure that the results obtained are realistic and accurate. The initial preparation in the form of model calibration was performed in Chapter 3. The numerical model was calibrated to match the experimental results obtained from the literature. This provides the necessary material data to perform an analysis.

In this chapter, the modelling process leading up to the initial elastic static analysis will be discussed. There are various important aspects that need to be considered. It is important to maintain a good balance between simplicity for computational efficiency whilst including sufficient detail to ensure the results are relevant. The required accuracy of the results will depend on the analysis type and will be verified in later chapters.

A typical three storey masonry structure from the Western Cape will be selected for analysis purposes. Initially the basic building layout and structural system will be presented in Section 4.2. The plan layout and elevation views of the building are shown with a description of the structural system and locations of structural and non-structural elements. Thereafter the structure will be critically examined according to basic design requirements presented in Section 2.4.6. This is necessary to identify possible conceptual design flaws which could lead to poor seismic performance. This could help in detecting and eliminating certain failure modes in order to reduce the scope of the analysis. Various assumptions that were made in order to simplify the analysis are discussed after which a static analysis is performed to verify the building's behaviour under vertical and horizontal loads. The elastic results are discussed at a global level and possible failure modes are identified. This will provide a solid platform to proceed with a dynamic analysis in Chapter 5.

4.2 Building Layout

The building chosen for analysis is a basic three-storey URM low cost residential apartment building located in the Stellenbosch region in South Africa. A 3D model of the building is shown in Figure 4.1.

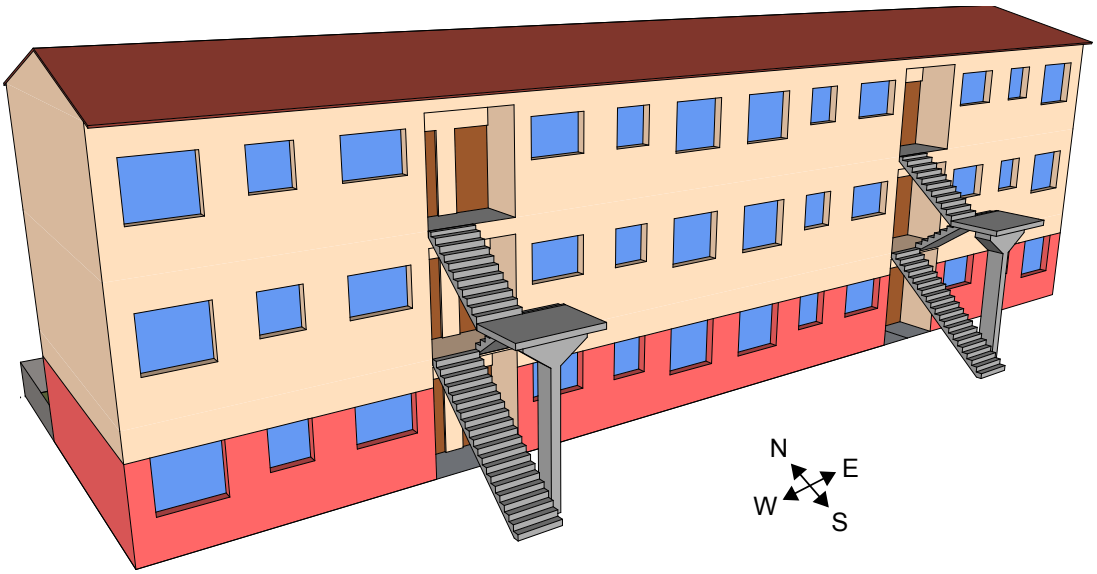

Figure 4.1: A 3D view of the three storey URM apartment building used for the numerical model.

The three storey building is situated in an underprivileged area along with twelve other buildings of the same type, placed in close proximity. This is a common occurrence in the Cape Flats region as well as surrounding communities. These structures are quite often densely populated. The structure has a simple layout and is considered a typical representation of three storey apartment buildings constructed in low-income areas during the 1970's. Figures 4.2 to 4.4 show the front, back and side elevations of the structure.

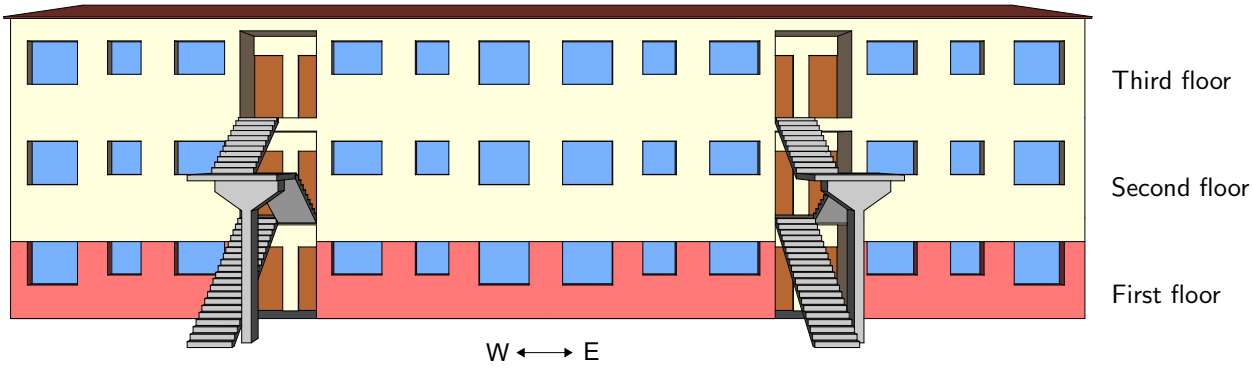

Figure 4.2: Front elevation of the three storey URM building used for the numerical model.

The locations of the first floor (bottom/ground floor), second floor (middle floor) and third floor (top floor) are indicated in Figure 4.2. The building consists of four apartment units per floor with plan dimensions of 7.2x8.0m which are symmetrically arranged about the centre of structure. The building has plan dimensions of 7.2x32m. Access to the units are provided via two external concrete staircases that are attached to the structure at floor levels as seen in

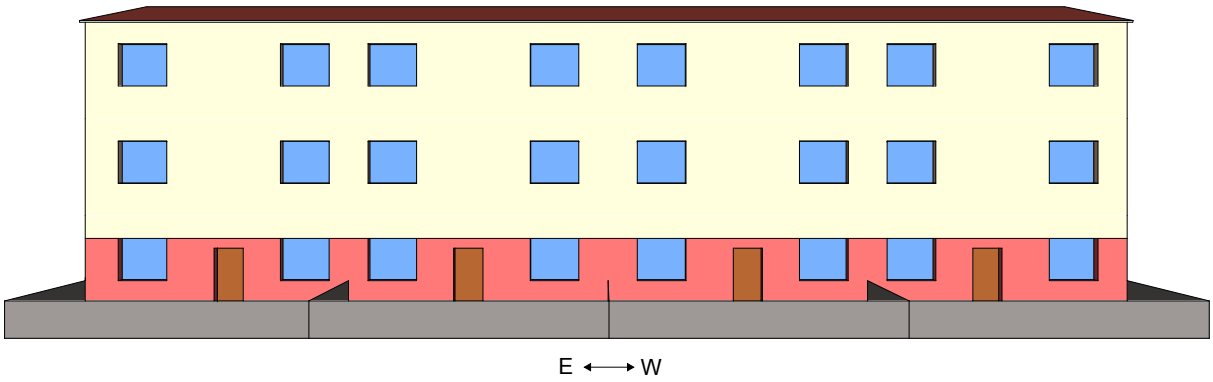

Figure 4.3: Back elevation of the three storey URM building used for the numerical model.

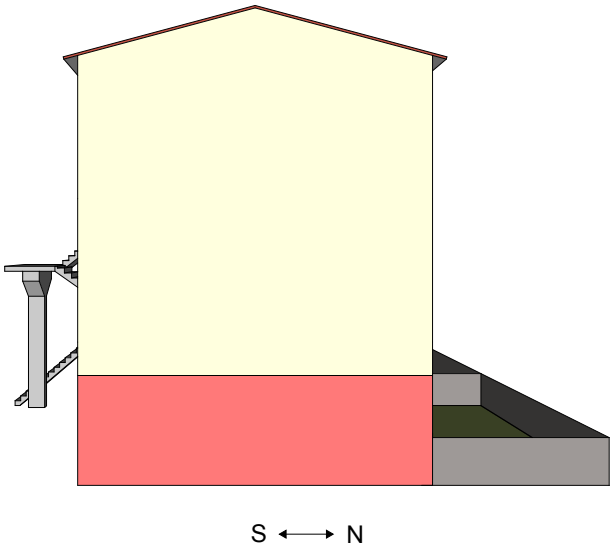

Figure 4.4: Right elevation of the three storey URM building used for the numerical model.

Figure 4.2. The staircases do not form part of the building's structural system, and have their own supporting columns. Standard clay bricks with dimensions of 220x110x75mm are used in the structure. All external walls are cavity walls, which is typical for structures in coastal areas. The cavity walls have two 110mm brick skins and a 50mm cavity which results in a total thickness of 270mm. In addition to the outer perimeter walls, three internal walls spanning in the North-South direction are constructed as double brick width structural walls with a thickness of 230mm. The perimeter walls as well as the double leaf internal walls form the primary load bearing system. A plan view of the building is shown in Figure 4.5.

All load bearing walls are indicated with a hatch pattern. Additional internal walls are provided to partition the apartments. These are single brick width (110mm in thickness) non-load bearing walls. Non-load bearing walls are constructed with a gap between the top of the wall and the overhead slab to prevent crushing of the wall due to sagging of the slab. The internal partition walls do however provide lateral support to the structural walls since they are built into the internal leaf of the structural walls to form a fixed connection. A plan view of a single apartment is shown in Figure 4.6 indicating the dimensions of the internal non-load bearing walls.

Reinforced concrete slabs with a thickness of 250mm form the floor diaphragm system and are

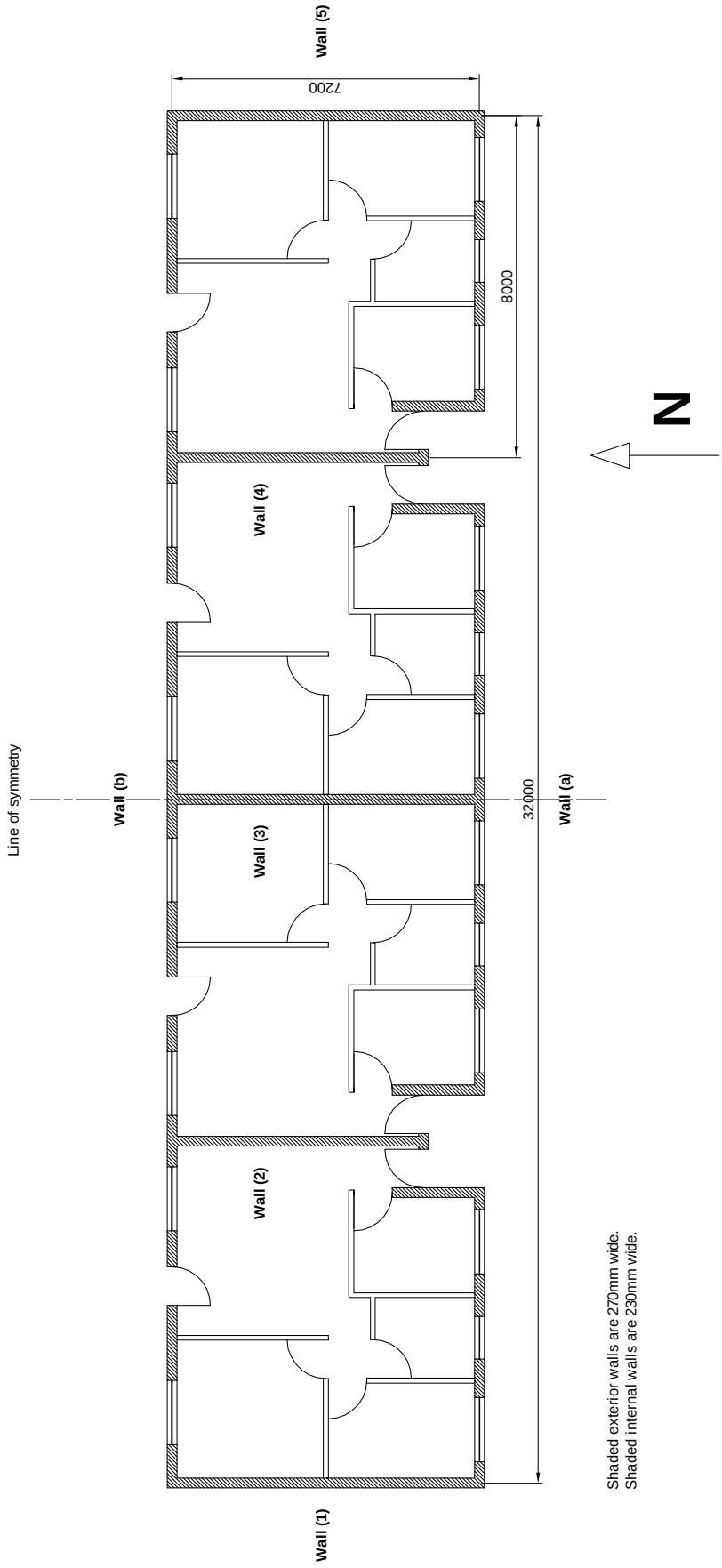

Figure 4.5: First floor plan layout of the URM building with shear walls indicated by the hatch pattern. There are no door openings in wall b on the second and third floors.

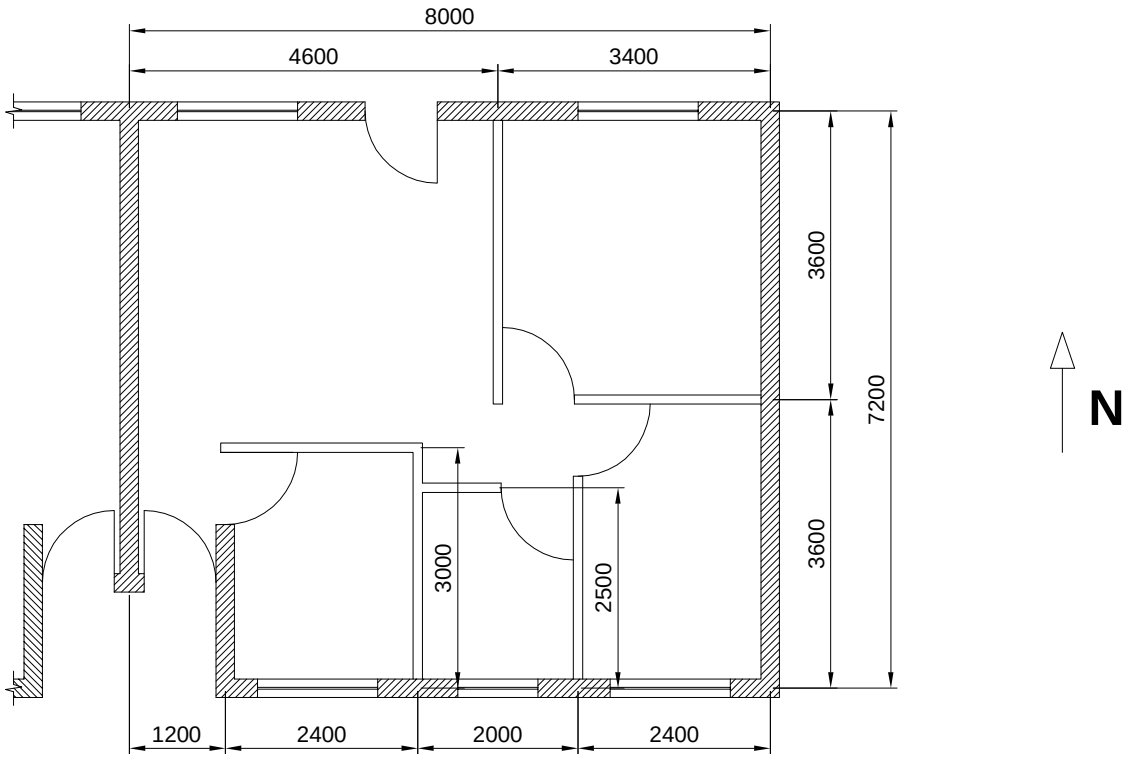

Figure 4.6: Plan layout of a single apartment located in the URM building. Dimensions of internal and external walls are indicated.

situated at the second and third floor. The floor slab is supported by the internal leaf of the perimeter walls as well as the internal structural walls. The connections between floor slab and perimeter walls do not provide moment resistance and is considered to be pinned. Likewise the internal load bearing walls provide pin supports at the slab connections. The building has a basic duo-pitched roof supported by wooden King Post trusses at 1m intervals. Corrugated fibre concrete sheets are used for roof sheeting. The North and South facing walls support the roof while the East and West facing walls are built to form gables that extend to the pitch of the roof. Pre-cast concrete lintels are placed above all openings to support the masonry across the span.

4.3 Review of Basic Design Requirements

It is necessary to analyse the building layout and structural system according to general design requirements as presented in Section 2.4.6. General building layout plays an important role when resisting seismic action in URM buildings.

The building has many window openings in the perimeter walls as well as door openings in the South side of the structure. Additional door openings are present in the first storey on the North side of the building. The East and West facing structural walls do not contain any openings. Figures 4.7 and 4.8 show the dimensions of the openings situated in the North and South facing walls.

The amount of openings in structural walls greatly affect their stiffness when subjected to

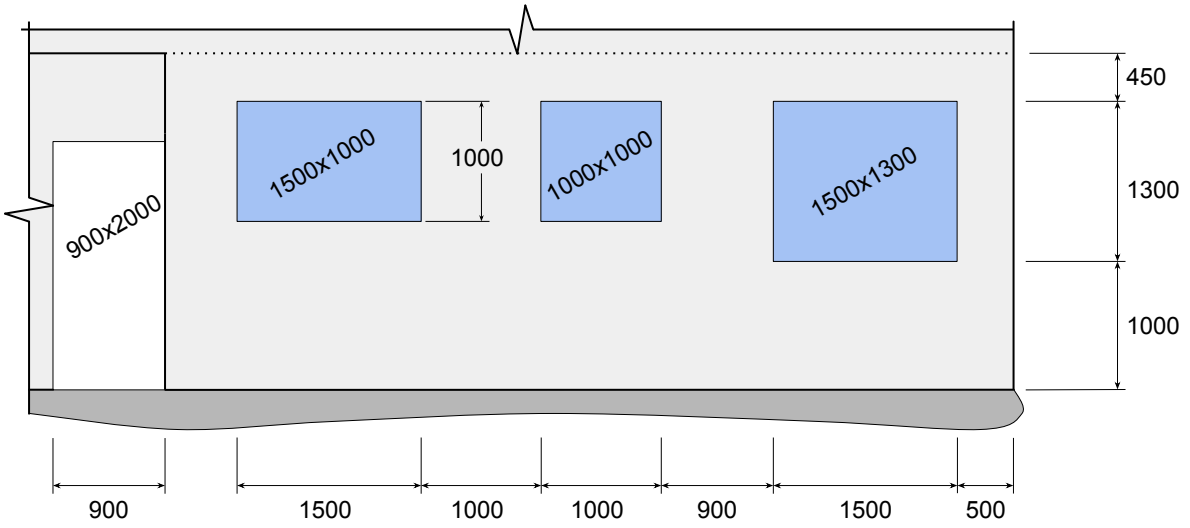

Figure 4.7: Opening dimensions of a single apartment for the South side of the building.

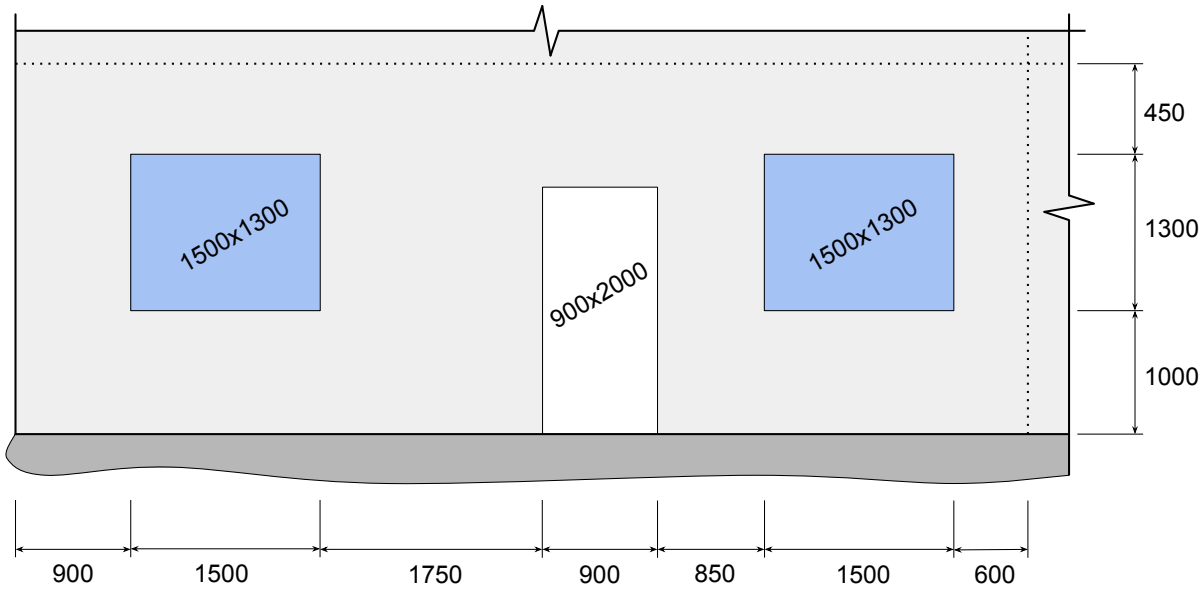

Figure 4.8: Opening dimensions of a single apartment for the North side of the building.

horizontal seismic loads. This is especially the case for window and door openings in the first storey walls since large stresses are expected to develop around these regions. The opening areas and opening ratio's of the various shear walls are presented in Table 4.1.

Table 4.1: Opening ratios calculated using the face area of the structural walls.

Wall	**Total Wall Face Area** (m^2)	**Opening Area** (m^2)	**Opening %**
a	289	75	26
b	289	54	19
1	71	0	–
2	49	0	–
3	67	0	–
4	49	0	–
5	71	0	–

Since walls *1–5*, spanning the North–South direction, do not contain openings, their seismic resistance capacity are completely unhindered. This is beneficial to the building response since uninterrupted masonry walls will have a larger sectional area to resist the horizontal loads. In-plane failure mechanisms involving pier failure due to shear cracking and rocking, are avoided. Walls *a* and *b* on the other hand contain many openings and have opening ratios of 26% and 19% respectively. This is however still less than the recommended limit of 30% presented by SANS 10160-4 and Tomaževič (1999). Stress concentrations at the corners of openings can lead to the formation of diagonal cracks as discussed in Section 2.6.2.

The structural layout of the building is both simple and uniform with symmetry being provided about the centre of the structure. There is a large difference in the opening ratios of the North and South facing walls that will lead to an imbalance in stiffness provided for excitation in the East–West direction. The stiffness remains relatively uniform along the height of the building with a small discrepancy in the form of door openings provided on the bottom floor in the North perimeter wall that are not present in upper storeys. This will cause the wall to have a decreased stiffness at the bottom of the structure. This is not ideal since the first storey must resist larger stresses compared with the upper levels. The distribution of the internal walls are also relatively uniform providing lateral support to the load bearing walls at approximately 3–4m intervals. Walls 2 and 4 are not supported laterally by internal walls. This could lead to increased lateral deformations during excitation in the East–West direction. Good torsional resistance is provided by the long shear walls located at the perimeter of the structure.

The suggested storey limit for URM buildings in areas experiencing PGA values below 0.2g is four storeys. It is also suggested that structural walls be provided at a maximum of 10m intervals. Finally, structural walls are required to have a minimum cross sectional area of at least 3% of the gross floor area (Tomaževič, 1999). All of the above mentioned guidelines are met. At a global level however, the building does not satisfy the requirement of the building length not exceeding four times the width (i.e. $L > 4B$).

4.4 Problem Simplification and Assumptions

URM structures consist of many different structural elements, such as walls and floors, that are connected to make up the building. Each of these elements will be modelled in ABAQUS with connections that reflect the structural behaviour of the elements. Different connection types are shown in Figure 4.9 along with the simplified connections that will be used when modelling the building in ABAQUS. The various assumptions and simplifications made will now be discussed.

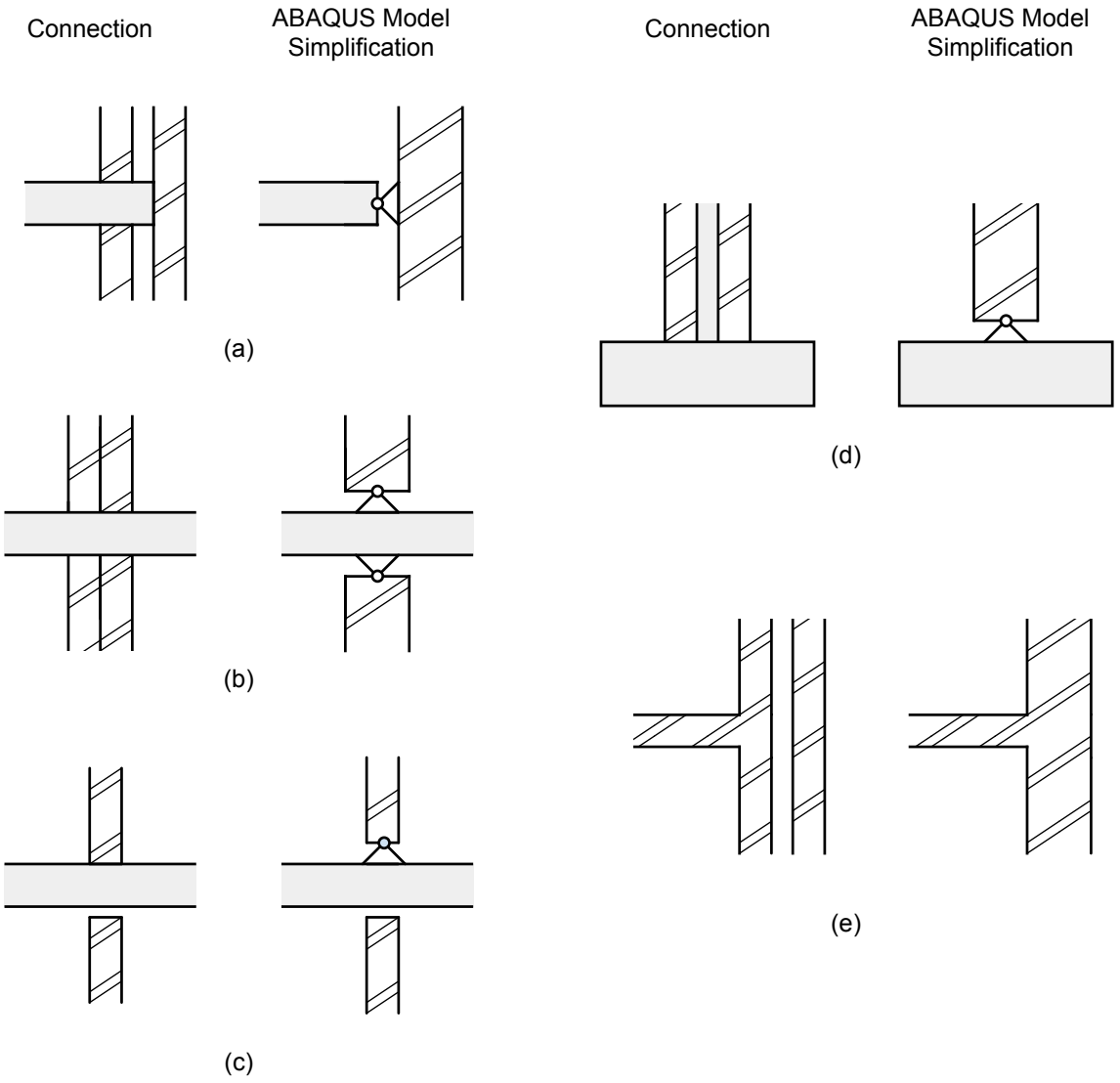

Figure 4.9: Several connections in a typical URM structure along with the simplification made for FE modelling purposes, including: (a) floor connection at external structural walls modelled as a pin connection; (b) continuous floor connection to internal structural walls, modelled as a pin connection; (c) top and bottom of non-load bearing internal walls at slab level, modelled as a pin connection at wall base and not connected to slab at wall top; (d) connection of bottom of walls to foundations modelled as pin connections; (e) plan view of connection between internal walls and internal leaf of external walls modelled as fixed connection.

- All foundations are assumed to be adequate in size and provide sufficient strength to

provide a pin connection to the bottom of the URM walls, shown in Figure 4.9d). It is assumed that wall-foundation connections do not provide adequate moment capacity to provide a fixed connection. Interactions between a specific ground type and building foundations during an earthquake is a complex problem that should be analysed in-depth before specific foundation strength and stiffness values are provided.

- Floors are assumed to remain elastic and rigid. No specific constraints were added to simulate the rigidity, but the geometry and material provided sufficient rigidity to distribute horizontal loads without dramatic deflections. The displacement of floor elements will be monitored to ensure that rigid behaviour is indeed being observed. In addition, the participation of the floor in vibration modes should not dominate the building behaviour. The lack of openings in the floor diaphragm will also ensure that adequate stiffness is maintained.

- Floors will have pin connections to structural walls (Figure 4.9a) and b) and will not be connected to the top of internal walls (Figure 4.9c). The bottom edge of internal walls will be pinned to the floor of a specific storey (Figure 4.9c). The connections are modelled to be perfect pin connections that transfer forces between members without failing. This is a valid assumption if the connections were designed to transfer the seismic loads as presented in SANS 10160-4. The connections themselves will not be modelled and will therefore not develop any stresses.

- The building has a timber roof structure. Normal roof connections are not sufficient to transfer horizontal seismic loads between structural members. It is with this in mind that the stiffness of the roof structure is disregarded for the analysis. The mass of the roof structure will nevertheless be added to the top of the building, but the roof will not form part of the load resisting system.

- Interior walls will have sufficient connection to the perimeter walls (i.e. built into the interior leaf) to provide lateral support to the perimeter walls (Figure 4.9e). This is modelled by fixing the non-load bearing walls to load bearing walls.

- The staircases on the South side of the building will be excluded from the analysis. This is justified by the fact that the connection between the staircase and the building will not enable the transfer of horizontal forces, especially not at a magnitude relevant to the resistance of seismic loads. The staircase has its own supporting structure. It is necessary to analyse the separate staircase structures to evaluate their performance under seismic loading since they are critical elements during the emergency evacuation of the building. This falls outside the scope of the current project.

- The inner and outer leaves of the cavity walls are bound together to act as a single unit. They are therefore modelled as a single 230mm thick masonry wall. This will slightly reduce the aspect ratio of the section for out-of-plane bending due to the distance of the outer compression and tension fibre from the neutral axis, but since the cavity walls are expected to resist forces predominantly in the in-plane direction, it should not have a large effect on results.

4.5 Finite Element Model

The structure was modelled with ABAQUS using predominantly shell elements. S4R (4-node doubly curved shell) elements were used to model the walls and the floors. B31 (2-node linear beam) elements were used to model the lintels above external openings. The beam elements were attached along the length of the beam to the shell edges above the openings.

A 0.25m mesh size was chosen for the entire building. This proved sufficient in size to allow accurate stress and displacement results to be obtained during the elastic analysis when compared to smaller mesh sizes. Although a larger mesh could be specified in the floor diaphragms, due to the expected rigidity of the floor, it was decided to keep the mesh size for all elements constant to facilitate the tying of nodes on different parts of the structure to form pin and fixed connections. Partitions were used to ensure proper alignment of the elements close to the openings in order to obtain a uniform mesh pattern.

As shown in Figure 4.9, pin connections were provided at the bottom of the structure to tie the bottom edge of building walls. This will also form the primary base used to specify the seismic base acceleration. The floor slabs on the second and third floors were connected by pin connections to the supporting load-bearing walls. This is achieved by tying the translational degrees of freedom (DOF) of each floor edge node to the closest node on the wall structure - illustrating the advantage of using a similar sized mesh in both the floors and walls. In a similar way, the displacement DOF of the internal walls are tied to the floors at their bottom edge, while remaining unconnected at their top edge (since they are non-load bearing). Vertical edges of internal walls are tied to the load bearing walls to provide fixed connections allowing them to provide lateral support.

The roof structure was added as a non-structural distributed mass at the top edge of the North and South perimeter walls — allowing for the effect of vertical forces due to roof weight as well as horizontal forces developed during an earthquake due to inertia to be taken into account. Imposed live loads are applied as per the recommendations in SANS 10160-2. A load of 1.5 kPa is used as stipulated for residential occupancy class. When performing a seismic analysis, the imposed load is adjusted using a combination factor of 0.3, resulting in a distributed load of 0.45 kPa applied vertically to the floor slabs. When considering the serviceability limit state to assess floor deflections in Section 4.6, the live load will be applied with a combination factor of 1.0 resulting in a distributed load of 1.5kPa. This will be used along with the load combination factors at serviceability limit, i.e. 1.1DL + 1.0LL.

Two models were created. One for each of the two orthogonal building directions (i.e. North-South and East-West). The stiffness values of the walls are assigned so that the in- and out-of-plane walls have different E-moduli as determined in Chapter 3. Figure 4.10 shows the stiffness distribution for the two models.

The different stiffness distributions for the two models will cause small changes in the mode shapes. It is therefore necessary to create a third model with a constant stiffness distribution to determine whether the mode shapes in the different orthogonal directions are reasonable and

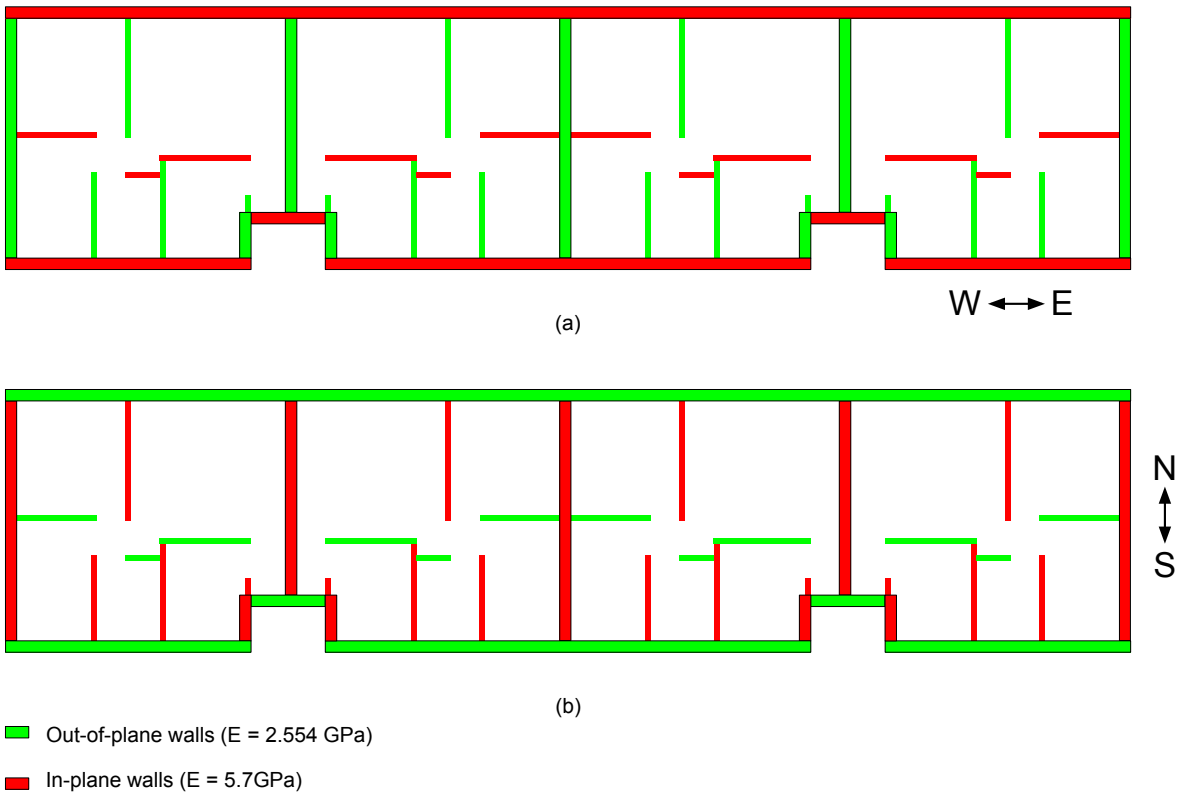

Figure 4.10: Stiffness distribution between in- and out-of-plane walls for an earthquake in the (a) East–West direction and (b) North–South direction. In-plane walls are indicated in red and out-of-plane walls in green.

representative of the building as a whole. This will be discussed in Section 5.4.

4.6 Static-elastic Analysis

As a final step to the modelling process, a static vertical and static horizontal analysis is performed in order to verify that the model behaves as expected. The purpose of the static analysis is to verify the response of the structure to static vertical loads. In addition, a constant static horizontal acceleration is applied to assess the behaviour of the structure to horizontal body forces. The magnitude of the acceleration is not important since the results merely give a distribution of stresses that verify whether the modelling procedure is sound and allow possible failure modes to be identified. In the first case, the building is analysed under vertical gravity and live loads. Load combinations of 1.1DL and 1.0LL are applied to assess the deflection of the floor slab under serviceability conditions. This is necessary to evaluate that the floor diaphragm shows rigid behaviour. Thereafter a static horizontal acceleration of 0.1g is applied to the whole structure. Non-linear geometry is included in the analysis. The model contains a total of 29313 elements and 32852 nodes. The results of the static analyses are summarised in Figures 4.11 to 4.13.

The vertical deflections of both the East-West and the North-South models, shown in Figure 4.11, reach a maximum of 2.3mm at the centre of the slabs in the end apartment units at

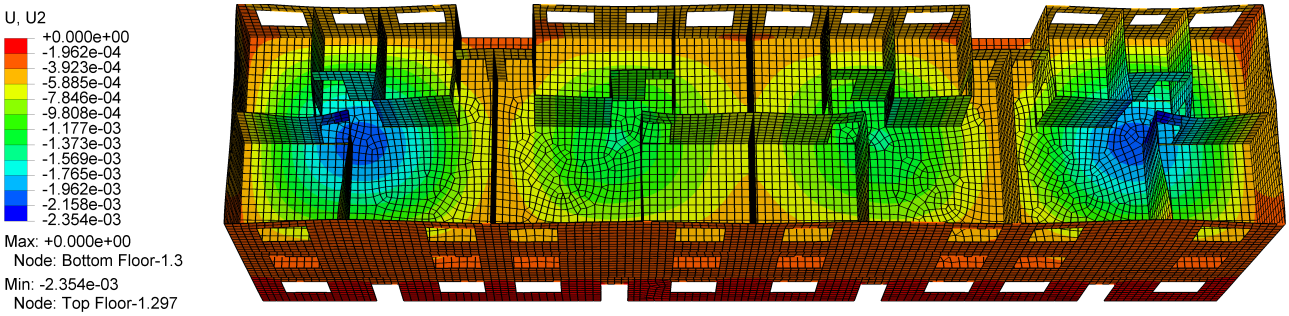

Figure 4.11: Vertical displacements obtained from the static analysis under vertical gravity loads. Maximum displacement of 2.35mm is indicated in blue.

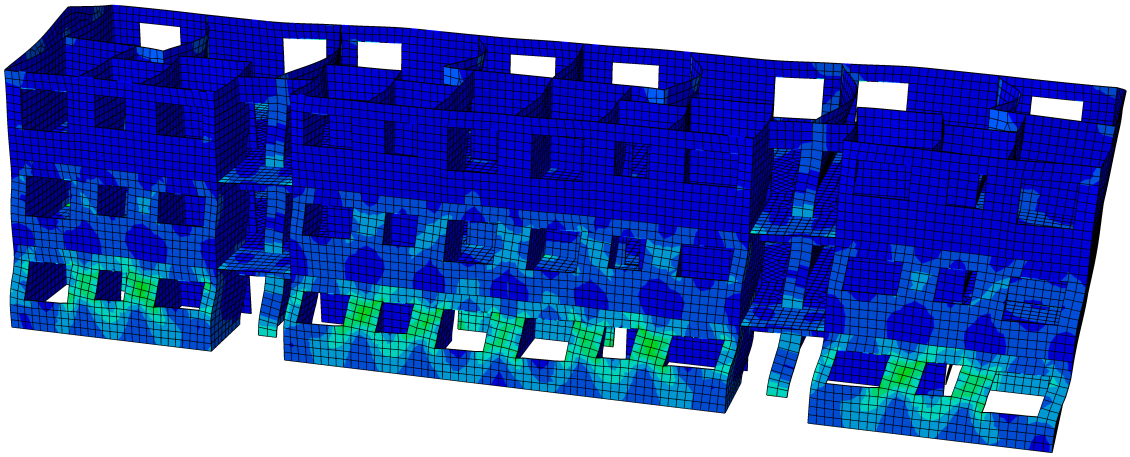

Figure 4.12: Von Mises stress distribution obtained from the static analysis of the East-West model under a horizontal 0.1g acceleration load. Stress concentrations can be seen in the first storey piers in distinctive "X" shapes.

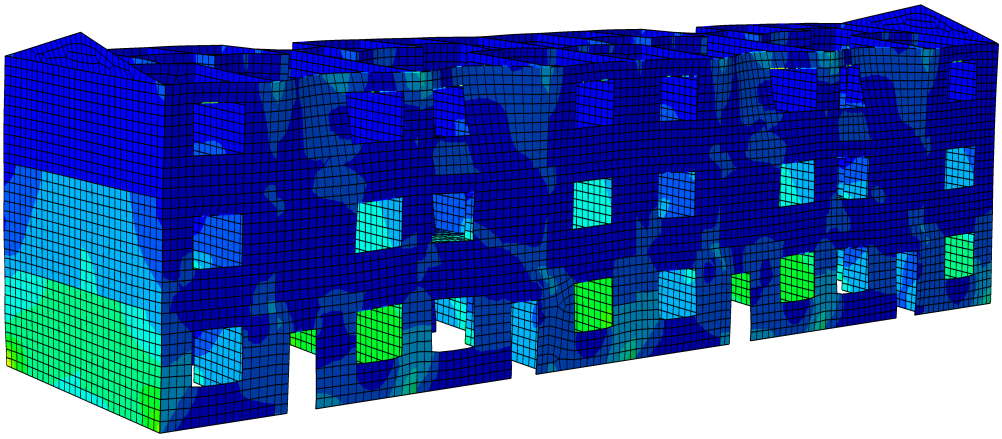

Figure 4.13: Von Mises stress distribution obtained from the static analysis of the North-South model under a horizontal 0.1g acceleration load. Stress concentrations can be seen in green at the base of the shear walls and at diagonal lines from the corners of openings.

the serviceability limit state. This is expected since the floor slab is continuously supported at external and internal structural walls along the length of the building, resulting in maximum displacements forming at the first (or last) span. The deflection is well within the required limit

to prevent the crushing of the non-load bearing walls (generally a 10mm limit) and therefore acceptable.

For the static horizontal analysis (Figures 4.12 and 4.13), the magnitude of stresses is not shown since the stress magnitudes obtained by applying a static horizontal acceleration is of little use. The relative magnitude and distribution of stresses is however shown, with green representing the largest stresses and dark blue the smallest. For static acceleration in the East-West direction, the shear walls contain a large number of openings. Stress concentrations (shown in green) develop in the brick piers that are situated between openings. The largest stresses are located at the bottom of the structure. Stresses form a cross ("X") pattern suggesting shear failure and possible rocking failure of the piers.

For the North-South model, stress concentrations develop at the bottom of the in-plane shear walls as expected. These walls do not contain any openings however. Diagonal stresses appear at the corners of openings, especially in out of plane walls that are connected to in-plane shear walls. This indicates that the out-of-plane walls will act as flanges, as long as the in- and out-of-plane connections are strong enough to resist the bending moments. The size of the flange will however not be large and is limited by the presence of openings close to the edge of out-of-plane walls. This could lead to cracks developing from the corners of openings to the edge of out of plane walls as illustrated in Figure 2.15 (Yi, 2004). The magnitude of the stresses generally decrease towards the top of the building as displacements increase. There are however stress concentrations that form at the connections of walls on the upper storeys due to the relatively larger displacements of out-of-plane walls.

The floor diaphragm shows good in-plane rigid behaviour with negligible out-of-plane deflections produced by horizontal loading.

4.7 Summary

A three storey URM building with plan dimensions of 7.2x32m was chosen for the analysis. It is representative of typical multi-storey URM buildings located in the underprivileged areas in and around Cape Town. The structural layout and details were presented and discussed. The layout of the building was analysed according to the basic design principles discussed in Section 2.4.6. The structure has a simple, consistent and symmetrical layout in plan and along the height. This is beneficial since it improves the seismic performance of the building. Although a large number of openings are present in the North and South facing walls, they are within the limits of SANS 10160-4 for URM design. Shear walls are provided in both orthogonal directions allowing the building to resist seismic events acting at different angles. Shear walls located at the building perimeter will provide additional resistance against torsional response.

Even though the structure was designed before the implementation of SABS 0160, the conceptual layout of the structure meets the recommendations of SANS 10160-4. The simple layout of the building and amount of internal lateral walls are an indirect result of the way in which low-cost residential apartments are designed. A box shape structure with small rooms and basic

symmetrical layout leads to an inexpensive building while at the same time improving the seismic resistance of the structure.

A finite element model was created in ABAQUS using shell and beam elements. Connections were assumed to be adequate in strength to resist seismic forces. Walls were modelled as pin connections at the bottom of the structure. Internal walls were connected with pin connections to floor slabs and fixed at their vertical edges to structural walls. The roof stiffness was neglected and it was added as a non-structural mass to the top of the structure. Floor slabs were tied to the structural walls using pin connections.

A static analysis verified that vertical deflections due to gravity and live loads were within limits. Horizontal static analyses showed stress concentrations in the bottom storey of the structure. This suggests that pier failure will be the dominant mode of failure in the East–West direction. In the North–South direction, diagonal stresses indicated that cracking of out-of-plane walls will lead to the formation of flanges to assist the in-plane walls. Stress concentrations in in-plane shear walls will develop at the bottom heel and toe locations suggesting that flexural failure will be critical.

The finite element model created in this chapter can be used along with the calibrated material model from Chapter 3 to perform a dynamic analysis. The model was verified using static analyses. In addition, critical elements were identified. With the above mentioned assumptions and limitations taken into consideration, a dynamic analysis will be performed in Chapter 5.

Chapter 5

Linear Dynamic Analysis

5.1 Introduction

When analysing a structure, loads can broadly be categorized as being either static or dynamic. A static load remains constant with time whereas a dynamic load varies with time. Many dynamic loads can be sufficiently accounted for by performing a static analysis due to very gradual variations with time or when a load has a large single point in time magnitude that needs to be studied.

Dynamic loads are very different from static loads due to their time-varying nature. In the case of an earthquake, a dynamic acceleration is applied to the base of the structure causing subsequent changes in accelerations, velocities and displacements as well as stresses within the structure as it responds to the excitation. Forces that develop due to inertia play a major role in dynamic problems. Inertia force is a product of a structure's mass and acceleration, $F = m \cdot a$, and is introduced when a structure undergoes a change in acceleration. Other structural properties such as mode shapes, natural frequencies (with effects such as resonance) and damping are important. The dynamic behaviour of a structure is accounted for by performing a dynamic analysis.

An ABAQUS material model was calibrated using experimental data from other authors discussed in Chapter 3. A three storey URM structure was presented in Chapter 4 after which an ABAQUS model of the building was created. The ABAQUS model was validated by performing an elastic analysis. In this chapter, the structure will be analysed in ABAQUS by applying various acceleration time-histories to the base of the structure. Several earthquakes were chosen for analysis based on their Richter magnitude, peak acceleration, velocity and displacement values. The identified earthquakes are presented in Section 5.2.

The initial step in performing a dynamic analysis is determining the natural frequencies of the structure, as discussed in Section 5.3. Thereafter the structure is analysed using a modal superposition dynamic analysis presented in Section 5.4. Finally, the results from the various analyses are presented and discussed with respect to the different possible failure modes of the structure in Sections 5.5 to 5.7. A comparison between the results obtained for the North–South

and East–West models is given in Section 5.8. A linear-elastic material model is used in this chapter. Once the critical elements have been identified, a non-linear analysis will be performed in Chapter 6.

5.2 Selection of Time-histories

A number of earthquake time-histories were selected to represent the possible range of earthquakes that could be expected to occur in Cape Town and its surrounding areas. The time-history data for the Tulbagh earthquake could not be obtained. Since earthquakes are very rare in Cape Town, similar sized earthquakes from other countries were used for the analysis. Initially, a target range that represents the seismicity of South Africa was selected using hazard data of past earthquakes as well as values published in SANS 10160-4. Earthquakes with different properties and acceleration profiles were selected within the identified range.

Section 2.3 shows that earthquakes with Richter magnitudes in the range 5.0–6.5 can occur in South Africa. The seismic hazard map presented in SANS 10160-4 indicates that earthquakes with a PGA of 0.15g could occur in the Cape Town area (see Section 2.4.1). SABS 0160, however, required engineers to only design for a PGA of 0.1g. SANS 10160-4 requires the use of the redundancy factor that increases the design PGA value to a maximum of 0.15g. There are also four major ground types to be considered. The most unfavourable of these ground conditions is Ground type D.

Six different earthquakes were chosen based on the above mentioned PGA and Richter magnitude ranges. The records were taken from stations located in areas with ground types that have similar properties to ground type D tabulated in SANS 10160-4. Earthquakes with different properties were selected so that the seismic response of an URM structure can be evaluated for excitations with different properties. The six earthquakes have maximum PGA values of 0.1g, corresponding to the design nominal acceleration value implemented in SABS 0160. This is the value that would likely have been used to design older structures such as the building considered in the current analysis. If designers were to disregard the redundancy factor of the current code, a PGA of 0.1g would be used for design. The parameters considered when choosing the earthquakes are listed in Table 5.1. In addition to the six earthquakes chosen for the analysis, the Chalfant Valley time-history was scaled to a PGA value of 0.15g and used for an additional analysis. This is the largest PGA value shown on the SANS 10160-4 hazard map and represents the largest expected earthquake in the Cape Town area. It is also equal in size to the design PGA value of 0.1g if it is adjusted using the redundancy factor of 1.5. By considering earthquakes of both 0.1g and 0.15g, the performance of the structure can be evaluated against the requirements of both SABS 0160 and SANS 10160-4 to assess the current state of typical URM buildings in the Cape Town area. The use of the behaviour factor will be considered in Chapter 6.

For each parameter listed in Table 5.1, the selected earthquakes describing the upper limit, lower limit and intermediate values are indicated. In this way, the six earthquakes take a number of different parameters into account that could influence the seismic response of a building.

Table 5.1: Matrix of the parameters considered when choosing the earthquakes for analysis purposes. For each parameter, earthquakes corresponding to the lower limit (L), intermediate (M) and upper limit (H) of the parameter are marked with a cross (X).

Earthquake	Magnitude			PGA			PGV			PGD			Dominant Period		
	L	M	H	L	M	H	L	M	H	L	M	H	L	M	H
Chalfant Valley	X	-	-	-	X	-	X	-	-	X	-	-	X	-	-
Coalinga	-	X	-	-	X	-	-	X	-	-	X	-	-	X	-
Morgan Hill	-	X	-	X	-	-	X	-	-	X	-	-	-	X	-
Loma Prieta	-	-	X	-	X	-	-	X	-	-	X	-	-	X	X
Kobe	-	-	X	-	X	-	-	-	X	-	-	X	-	X	X
Chi-Chi	-	-	X	-	X	-	-	-	X	-	-	X	-	X	X
Chalfant Valley (scaled 0.15g)	-	-	-	-	-	X	-	-	-	-	-	-	X	-	-

Table 5.2 lists the properties of the unscaled earthquakes along with the information of the seismic stations that the records were obtained from.

Table 5.2: Summary of different earthquakes that were selected for a time-history analysis. The earthquakes are of the typical size that could be expected to occur in the Western Cape region.

Name	**Station dist. to hypocenter (km)**	**Magnitude**	**Station Record Data**		
			PGA (g)	**PGV (m/s)**	**PGD (mm)**
Chalfant Valley (1986) California Station: CDMG 54424	19	5.77	0.095	0.063	16.9
Coalinga (1983) California Station: CDMG 36452	55	6.36	0.091	0.108	26.6
Morgan Hill (1984) California Station: CDMG 58375	55	6.19	0.046	0.043	7.5
Loma Prieta (1989) California Station: CDMG 58117	100	6.93	0.100	0.156	43.8
Kobe (1995) Japan Station: OSAJ	51	6.90	0.079	0.183	92.8
Chi-Chi (1999) Taiwan Station: ILA 048	140	7.60	0.090	0.184	196.0

The six earthquakes were selected to have very different acceleration, velocity and displacement profiles. Although the Richter magnitudes of certain earthquakes are relatively large (in the range 6.5–7.6) the PGA values measured at the stations are less due to the distance of the stations from the epicentre. It is therefore necessary to rather consider the PGA value obtained from the acceleration time-history since the building will be modelled using the data obtained at

the location of the seismic station and not the location of the epicentre. The largest earthquake is the Chi-Chi earthquake with a Richter magnitude of 7.6. Due to the magnitude of the earthquake and the quality of the seismic station network in Taiwan, a large number of time-histories are available. A station located 140km from the epicentre was selected since the PGA value is of a reasonable size and can be expected in South Africa. The smallest magnitude earthquake chosen for this study is the Chalfant Valley (1986) earthquake with a Richter magnitude of 5.77. A PGA value of 0.1g was measured at the seismic station located approximately 19km from the epicentre. This illustrates the effect that distance from the epicentre has on PGA at a building site. Small (<6 Richter magnitude) earthquakes are capable of producing PGA values of significant size.

The acceleration, velocity and displacement time-histories of the earthquakes are presented in Figures 5.1 to 5.3. Separate graphs for the different earthquakes are also presented in Appendix A. The acceleration data was obtained from the PEER Ground Motion Database (Pacific Earthquake Engineering Research Center, 2013). Velocity and displacement time-histories were obtained by integrating the acceleration graphs. The graphs give a good indication of the dynamic motion that the earthquake will subject the building to.

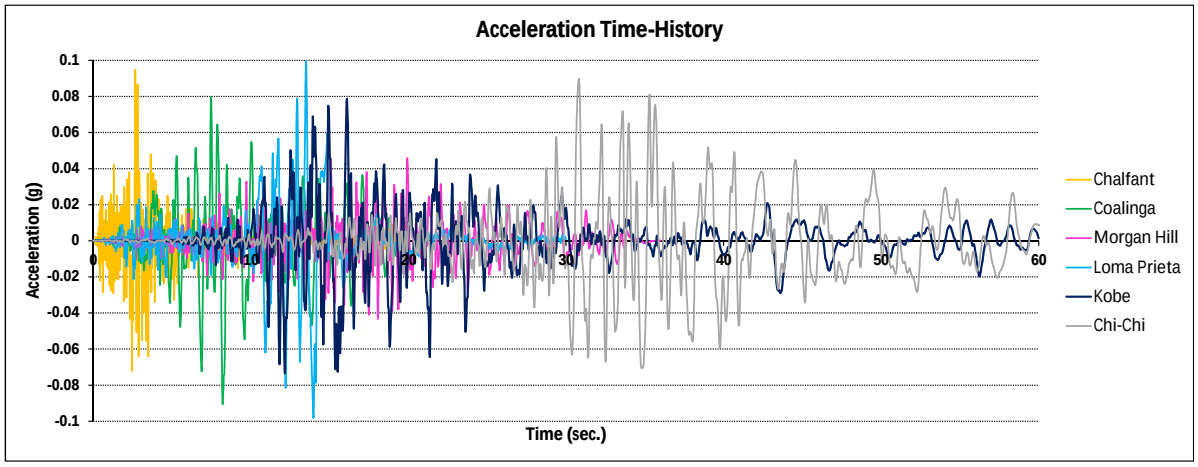

Figure 5.1: Acceleration time-histories of the earthquakes selected for analysis.

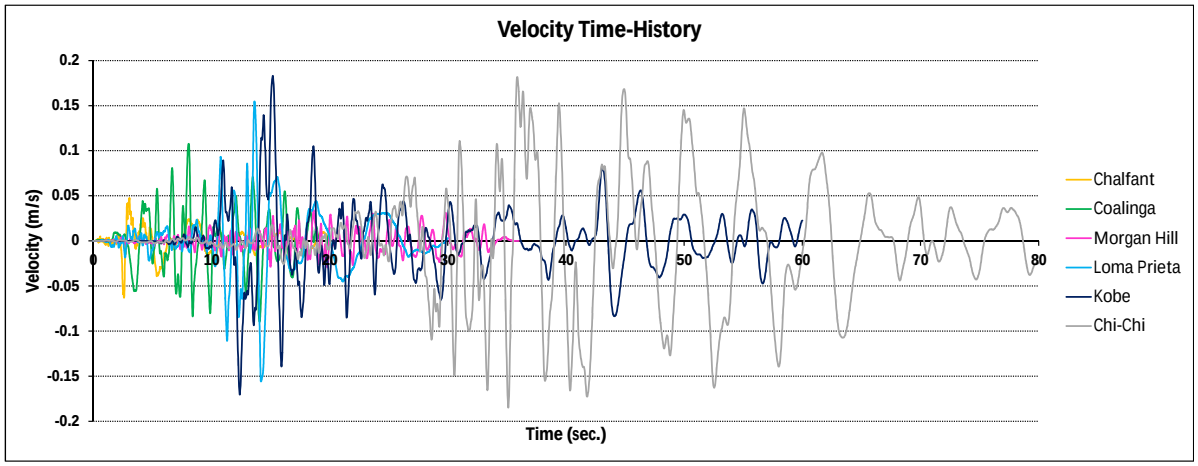

Figure 5.2: Velocity and Displacement time-histories of the earthquakes selected for analysis.

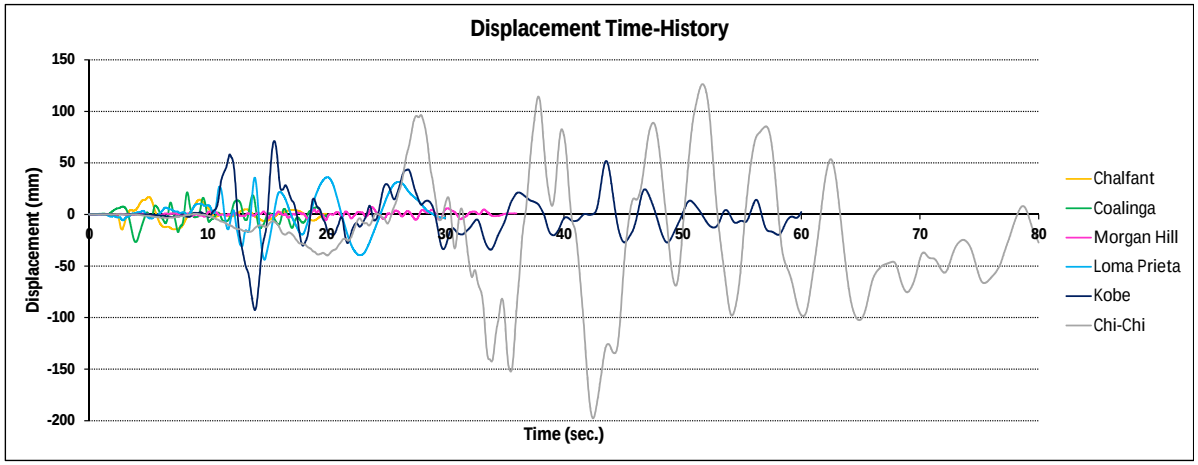

Figure 5.3: Displacement time-histories of the earthquakes selected for analysis.

The Chalfant Valley and Coalinga earthquakes both show moderate peak acceleration values, with very small peak displacements. The highest PGA value is found in the Loma Prieta earthquake shown in Figure 5.1. This leads to large displacement and velocity responses. The displacement peaks show long periods of oscillation. The Chi-Chi earthquake has relatively large peak accelerations, and extremely large displacements. The Kobe earthquake has a PGA of 0.08g, however it also reaches large velocity and displacement peaks. Although the Kobe and Chi-Chi earthquakes show large displacements, they have long periods of up to 5 seconds between peak values allowing stiffer structures with low natural periods to respond without causing excessive deformations. The acceleration response spectra of the six earthquakes along with the design response spectrum for ground type 4 used in SANS 10160-4, is shown in Figure 5.4.

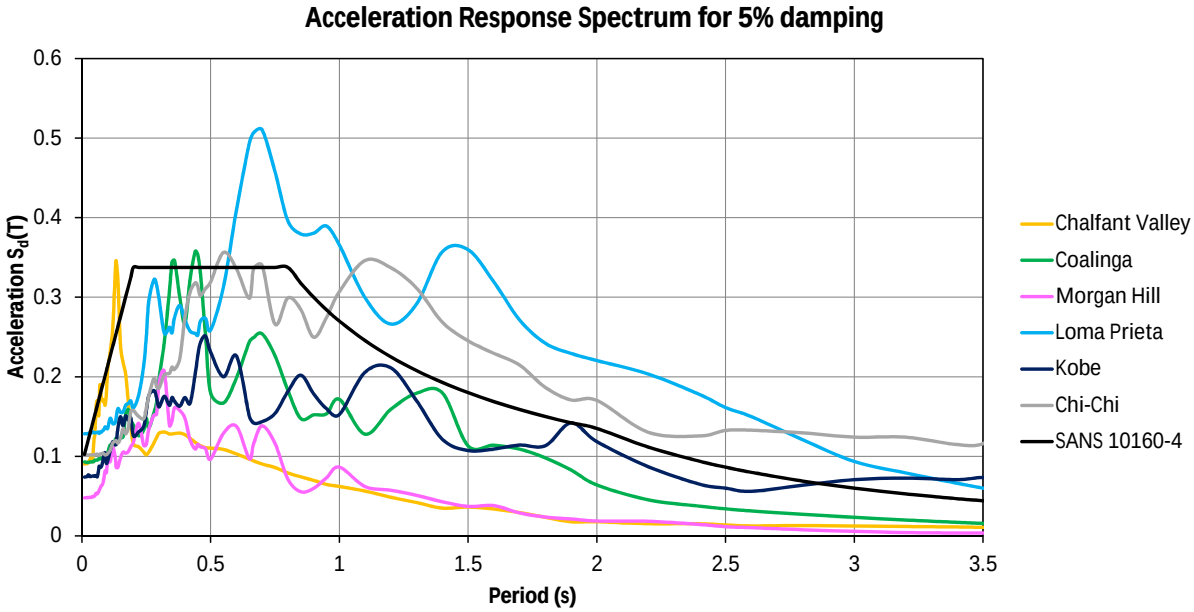

Figure 5.4: Acceleration response spectra for the six earthquakes selected for the analysis. The design response spectrum presented in SANS 10160-4 for ground type 4 is also shown.

A viscous damping ratio of 5% is assumed, as is typically the case when producing design response spectra. From Figure 5.4 the frequency content of the different earthquakes can be

assessed. The Chalfant Valley earthquake responds primarily at lower periods. It is expected that this earthquake will cause increased excitations in short and stiff structures, such as typical three storey URM buildings. The Coalinga and Chi-Chi earthquakes match the design response spectrum in the constant branch of the curve. Both the Loma Prieta and Chi-Chi earthquakes show very large responses at larger natural periods. The Morgan Hill and Kobe earthquakes show smaller responses than the design spectrum. The diverse nature of the earthquake time histories allow a broad range of responses to be studied.

5.3 Natural Frequency Analysis

A natural frequency analysis was performed to determine the mode shapes and vibration frequencies of the structure. Initially, the first 100 vibration modes were determined for each of the East–West and North–South models as well as a third model with uniform stiffness assigned to the in- and out-of-plane walls. The constant stiffness model will serve as a reference to verify the validity of the natural frequency results. A URM structure is expected to respond primarily in the first mode of vibration. The significant modes were identified so that all modes with a mass participation factor of 5% or more are implemented when analysing the structure. In addition, the modes that contribute to 90% of the total participating mass were considered. The first 25 modes were selected based on the above mentioned criteria. Table 5.3 shows a selection of the dominant modes and their properties.

Table 5.3: Summary of the three primary vibration modes along with their corresponding natural frequencies for three different models.

Mode	Description	Frequency (Hz)		
		East–West Model	North–South Model	Uniform Stiffness Model
1	East–West Lateral Displacement	8.80	7.04	9.90
4	North–South Lateral Displacement	8.95	10.17	11.86
10	Torsional Response	9.61	12.16	13.36

Since the East–West and North–South models have different stiffness distributions (representing the reduced out-of-plane stiffness of URM), different natural frequencies were obtained as seen in Table 5.3. A comparison between the modal frequencies of the different models indicates that the structure responds primarily in the frequency range 8.8–13.4Hz. The East–West model will have a dominant first mode of vibration with a frequency of 8.8Hz causing lateral displacement in the East–West direction. The North–South model will have a primary vibration mode at 10.17Hz resulting in lateral displacement in the North–South direction. Torsional modes for the East–West and North–South models occur at frequencies of 9.6Hz and 12.2Hz respectively. The uniform stiffness model shows higher natural frequencies due to the increased stiffness, however, the three models have comparable vibration frequencies with similar mode shapes. It can therefore be concluded that the simplification of the building into two models with different stiffness distributions for excitation in the East–West and North–South directions, will maintain

the mode shapes of the structure without causing significant changes in natural frequencies. The reduced frequencies of the East–West and North–South models will provide a more accurate representation of the mode shapes of the building during excitation than a model with a uniform stiffness.

The primary degrees of freedom (DOF) that will experience excitation are the DOF related to the displacement and rotation in the horizontal plane, since the base excitation will directly excite these DOF. Displacement in the East–West and North–South directions as well as possible torsional behaviour are expected to dictate the building response. Other DOF including rotational and vertical displacement DOF will not be directly excited. They are however included in the analysis since they could cause secondary responses.

5.4 Modal Dynamic Time-History Analysis

There are various numerical analyses methods available to analyse a structure under dynamic excitation. The modal dynamic analysis method is discussed in Section 2.8.1.2. It is a linear dynamic method. Non-linear material models can therefore not be implemented. The method provides an efficient alternative to the complex non-linear analysis methods such as the implicit dynamic analysis and was chosen since it is ideal for evaluating the elastic response of a structure to many different time-histories. It is ideal for structures that respond primarily in the lower modes. The modal dynamic analysis will however not take the post cracking behaviour of masonry into account. The response of the building to the earthquakes selected in Section 5.2 can be determined to assess whether the cracking strength of the material is exceeded in tension, compression or shear. Since URM has limited plastic capacity, the onset of cracking could likely result in structural failure.

Modal dynamic analyses were performed on both the East–West and North–South ABAQUS models, to determine the response of the structure to the acceleration time-histories presented in Section 5.2. The analyses will account for the linear dynamic behaviour of the structure. Non-linear effects such as material stiffness and strength degradation are not taken into account and will require an implicit dynamic analysis. An implicit dynamic analysis will be performed in Chapter 6. The modal dynamic analysis is efficient and suitable for performing a large number of analyses. Results will be accurate if a sufficient number of modes are included to represent the dynamic behaviour of the structure.

The analysis consists of several steps. The results of each step are used as input values for the following step. Initially a static analysis is performed with non-linear geometry taken into account. All static loads are applied to the structure during this step. This includes the vertical gravity load as well as distributed live loads. The step is necessary in order to take non-linear geometry, static loads and the correct boundary conditions at the structure base into account when performing the frequency analysis. The frequency analysis is performed next for the first 25 vibration modes of the structure. These modes make up 90% of the participating mass of the structure. All modes with a participating mass of more than 5% are included in the analysis as

discussed in Section 5.3. The first 25 modes sufficiently represent the dynamic behaviour of the structure, confirming the use of the modal dynamic method. The loads, boundary conditions and non-linear geometry are taken from the base state (static analysis step) and used to determine the modes. All static properties of the structure are captured in the mode shapes. Using the modes as input, a modal dynamic analysis is performed for the East–West and the North–South models.

The acceleration time-histories presented in Figure 5.1 were applied to the base of the structure using time steps of between 0.005 and 0.02 seconds. It is essential that small time increments are used when analysing earthquake time-histories, since the data typically has large oscillation frequencies. Selecting a time increment that is too large, will miss some of the peak acceleration input values and therefore reduce the accuracy of the results. The time steps were taken directly from the recorded earthquake time-histories (PEER, 2013) and were not reduced for analysis purposes. The pinned nodes at the bottom of the building were selected as the primary base for the application of the base excitation.

5.5 Results: East–West

The response of the building to the base accelerations was analysed at key points in the structure. The common failure modes of URM buildings was discussed in Section 2.6.2. Stresses obtained from the dynamic analysis will be compared with the maximum material strength properties to assess whether failure would occur. Large tensile and compressive stresses at the base of the structure can lead to tensile cracking or compressive crushing of the masonry. The capacity of floor-to-wall connections as well as vertical wall connections are verified. Shear failure could also occur since large shear stresses could lead to shear cracks or sliding shear failure. The locations of maximum tensile, compression and shear stresses for the South and North facing in-plane walls along with the cracks that are expected to form are shown in Figures 5.5 and 5.6 respectively.

Damage to in-plane walls is expected to be concentrated on the lower stories of the structure. The stress concentrations show that cracking is likely to initiate at the corners of openings. As discussed in Section 2.6.2, the cracks are expected to propagate diagonally from window openings to the discontinuous edges of the walls. Where openings are situated close together, the cracks will develop between the openings to separate the piers into separate rocking elements. These piers will form a rocking mechanism if the tensile stresses at the crack locations are exceeded. In addition, the piers will be subjected to diagonal shear forces that can cause shear failure. This further illustrates why openings should be avoided in the main structural elements.

The results of the modal dynamic analysis will be discussed further in Sections 5.5.1 to 5.5.3 for the analysis in the East–West direction. Results of the analysis in the North–South direction is discussed in Section 5.6. The common failure modes of masonry will be examined by comparing th stresses obtained through the analysis with the maximum material strength of URM, presented in Section 2.5.1. Structural design codes such as SANS 10164-1 use material partial

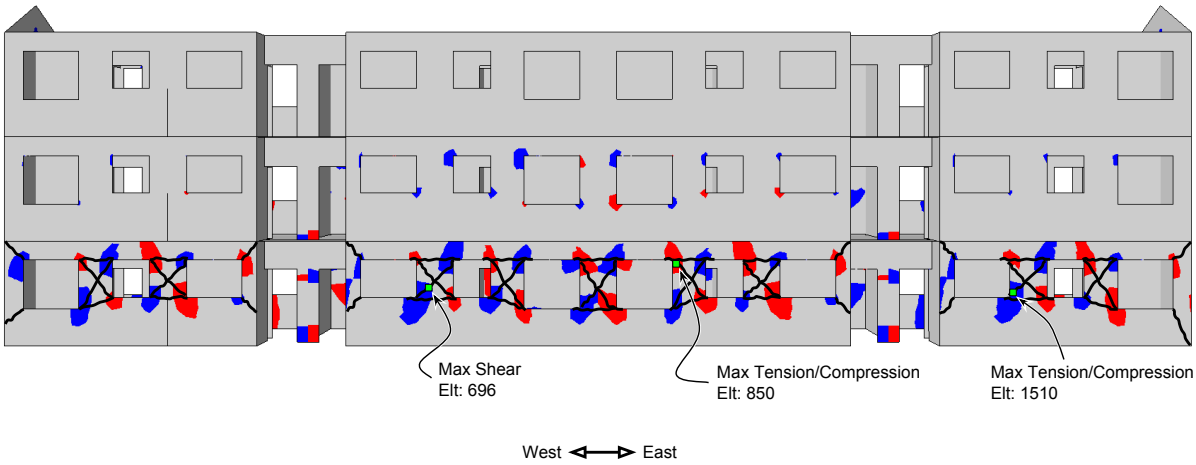

Figure 5.5: Locations of the maximum tensile, compressive and shear stresses and cracks that are likely to form in the South facing in-plane wall during excitation in the East–West direction. Tensile and compressive stresses are indicated in red and blue (depending on the direction of excitation).

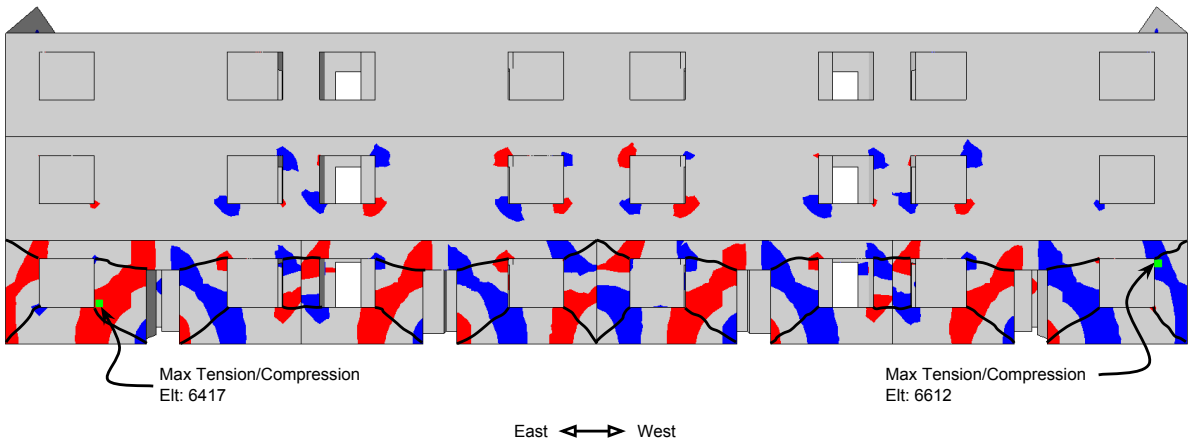

Figure 5.6: Locations of the maximum tensile and compressive stresses along with cracks that are likely to form in the North facing in-plane wall during excitation in the East–West direction. Tensile and compressive stresses are indicated in red and blue (depending on the direction of excitation).

factors (γ_m) to account for variability in the material strength and construction practice. The material partial factor is applied to the characteristic material strength properties to calculate the reduced design material properties. SANS 10164-1 specifies γ_m values of 2.9-3.5, depending on the quality of manufacturing and construction, for tensile and compressive strengths. A shear strength partial factor of 1.25 is obtained. In addition, the code allows the use of half of the compressive or tensile γ_m value when considering seismic design. Eurocode 8 suggests that $3/4\gamma_m$ be used for seismic design, while SABS 10164-1 suggests using half of the applicable γ_m value. The partial material factors add a factor of safety to a building design. For the analysis of the structure in the current project, however, the material strength data was obtained from experimental testing as discussed in Chapter 3. Retrofit of existing structures is expensive. In addition, existing structures have additional capacity, due to the use of partial factors during limit state design. It is necessary to obtain a less conservative estimation of the actual capacity of the structure, rather than providing the performance of the structure to a certain factor of safety relating to design. The use of partial factors for the seismic analysis of the URM building, will therefore not be implemented.

5.5.1 Tensile and Compressive Stress

Figure 5.7 shows the maximum tensile stress obtained during excitation of the building in the East–West direction for the various earthquakes considered.

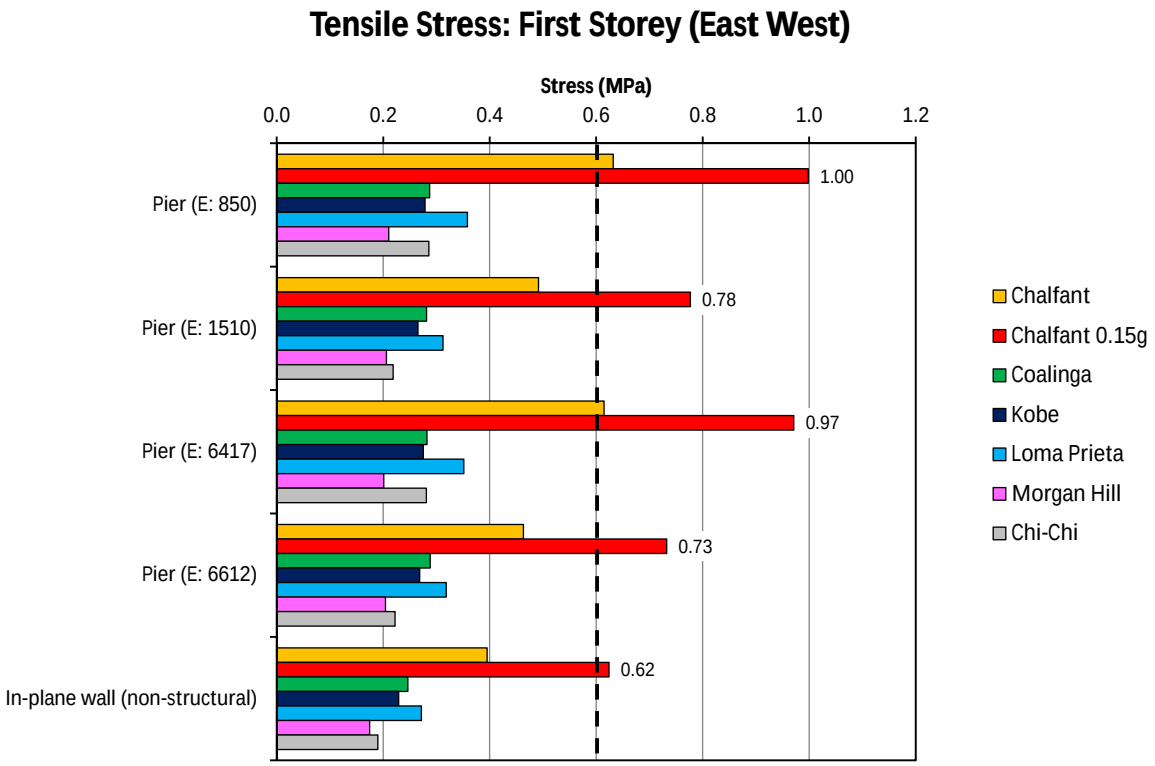

Figure 5.7: Maximum tensile stresses obtained at key locations in the first storey of the building for the various acceleration time-histories applied to the East–West model.

From Figure 5.7 it is clear that the Chalfant Valley earthquake causes the largest stresses. URM

has a maximum tensile strength of 0.6MPa, which is indicated with a dashed line in Figure 5.7. The maximum tensile strength is exceeded for two piers when excited by the 0.1g Chalfant Valley earthquake. This means that cracks will develop in these piers leading to the formation of a pier rocking mechanism. For the 0.15g Chalfant earthquake, the maximum tensile strength will be exceeded in several piers as well as non-structural walls in the bottom storey of the building.

A maximum tensile stress of 1MPa is observed in element 850, located in an in-plane structural pier. This is much larger than the maximum tensile strength of URM (0.6 MPa). This indicates a high possibility that local failure will occur in various piers in the bottom storey of the structures. Since the piers are part of the main supporting structure, partial or complete collapse of the structure could occur. Masonry does have plastic behaviour in the tensile region. Due to the brittle nature of the material, the material strength will deteriorate quickly once cracking is initiated.

The maximum compressive stresses of in-plane structural and non-structural elements are shown in Figure 5.8. The compressive stresses are similar, both in magnitude and distribution, to the

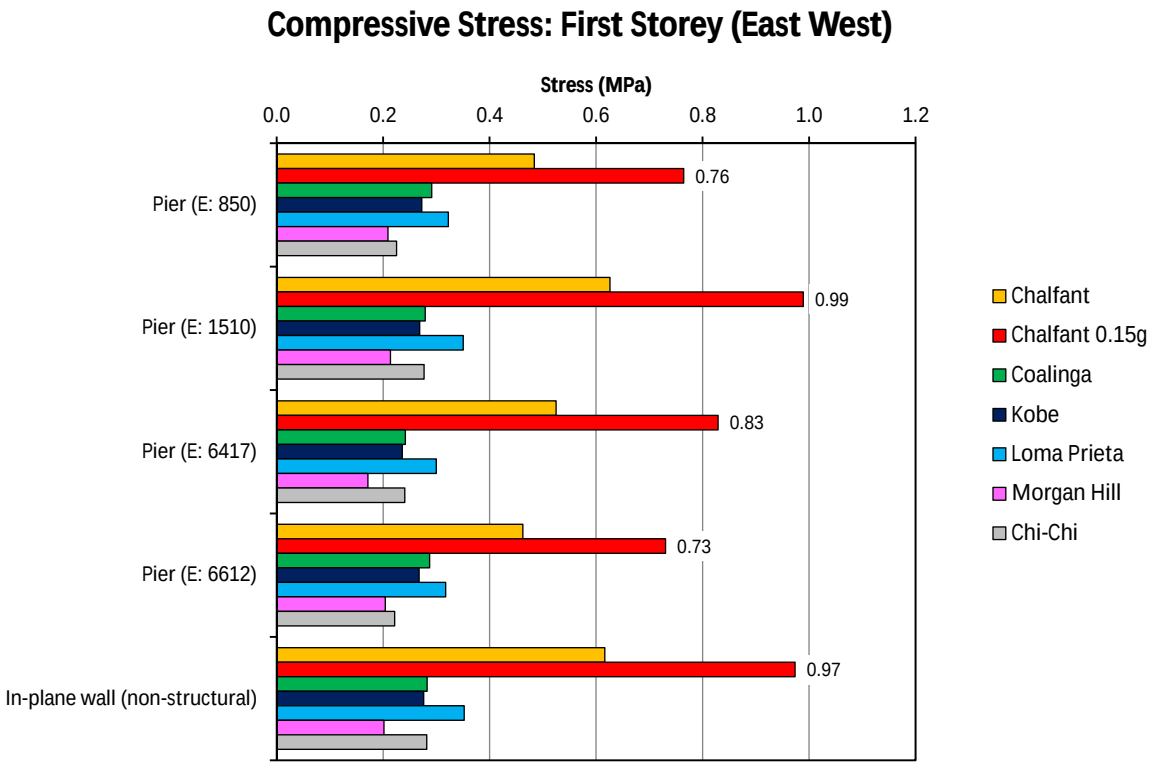

Figure 5.8: Maximum compressive stresses obtained at key locations in the first storey of the building for the various acceleration time-histories applied to the East–West model.

tensile stresses. This is due to the symmetrical layout of the structure and the oscillating nature of the applied time-histories. A maximum compressive stress of 0.99MPa is observed for the 0.15g Chalfant Valley earthquake. This will not lead to failure since it is much smaller than the maximum compressive stress (11.8MPa) of URM. This is expected since URM buildings rarely fail in compression.

5.5.2 Connections

During the analysis, connections were assumed to be sufficient to resist seismic excitation. This has to be verified. The SANS 10160-4 requirement for diaphragm-to-wall anchors in members that are not part of the main structural system stipulates that anchors should resist a force of at least $15a_g$ kN per meter wall. The design acceleration value of $a_g = 0.1$ leads to a design requirement of 1.5kN/m. For members in the main structural system, the anchorage strength of a building must be designed by providing positive anchorage in the floor-to-wall connections. The use of frictional forces between the slab and top of structural walls can not solely be relied on to transfer seismic loads. The tensile and compressive stresses in floor-to-wall connections of the first storey floor slab is presented in Figures 5.9 and 5.10 along with the stresses developed in the out-of-plane wall connection for an internal wall positioned at the top of the structure.

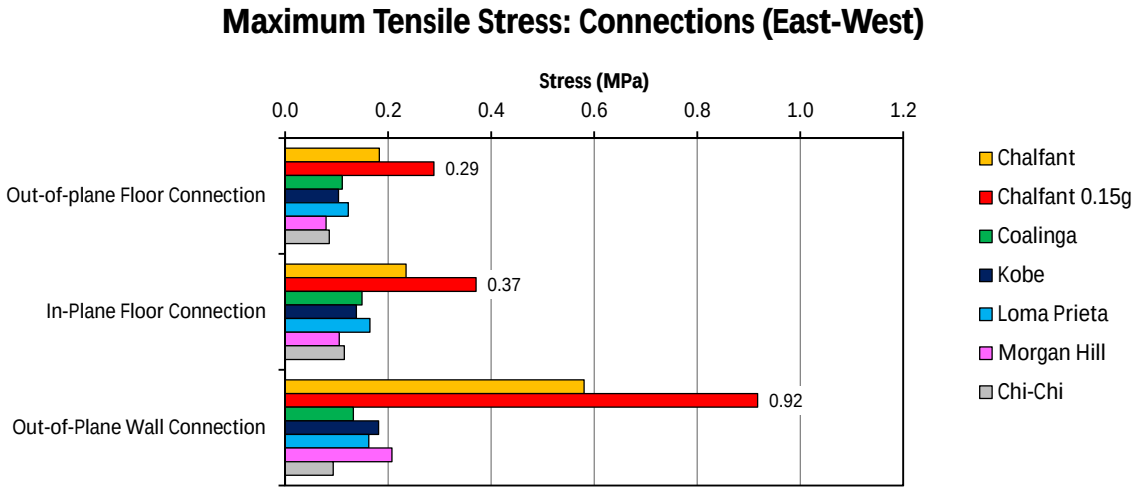

Figure 5.9: Maximum tensile stress obtained in wall-to-diaphragm as well as out-of-plane wall connections during excitation in the East–West direction.

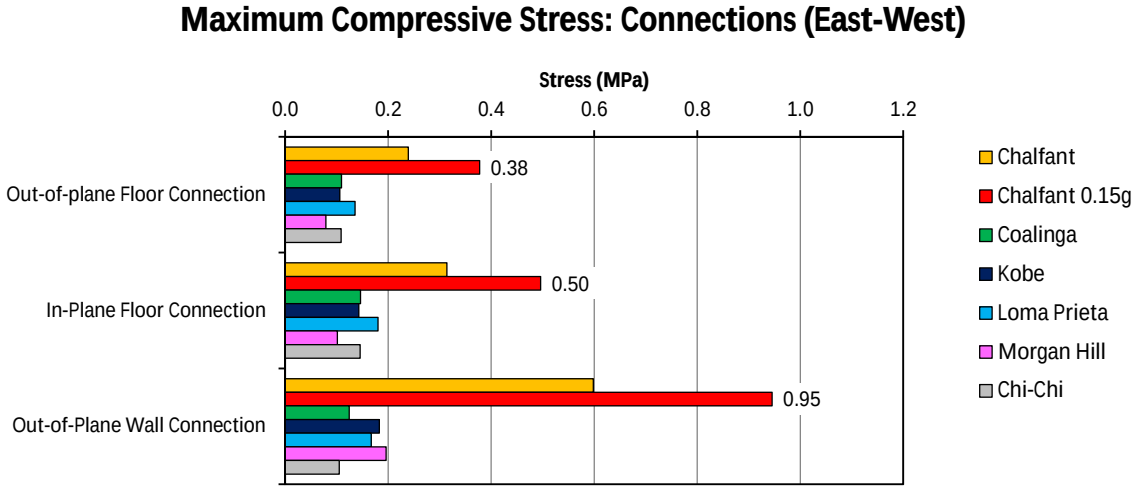

Figure 5.10: Maximum compressive stress obtained in wall-to-diaphragm as well as out-of-plane wall connections during excitation in the East–West direction.

In-plane floor-to-wall connections experienced the largest stresses with a maximum tensile stress

of 0.37MPa and maximum compressive stress of 0.5MPa observed. The larger magnitude stresses are due to the redistribution of lateral forces from out-of-plane walls to stiffer in-plane walls as well as the transfer of inertia forces, due to the mass of internal walls, through the floor diaphragm. With a slab thickness of 0.25m, the force transferred by the connections can be calculated as follows:

$0.25 \times 0.5 \times 10^6 = 125kN/m$ in compression.
$0.25 \times 0.37 \times 10^6 = 92.5kN/m$ in tension.

The calculated maximum forces are much larger than the anchorage design strength of 1.5kN/m for walls not forming part of the main structural system. The magnitude of the connection forces indicate that anchorage strength is critical. This strongly suggests that failure will occur at certain points along the in- and out-of-plane wall-to-floor connections if the structure was not specifically designed for seismic action. The specific strength of the connections should be verified, but falls outside the scope of the current project. The stresses presented in Figure 5.9 and Figure 5.10 are taken at points with maximum stress concentrations. To better assess the global behaviour of floor-to-wall connections, the average tensile and compressive stresses along an 8m wall strip are presented in Figure 5.11 and Figure 5.12.

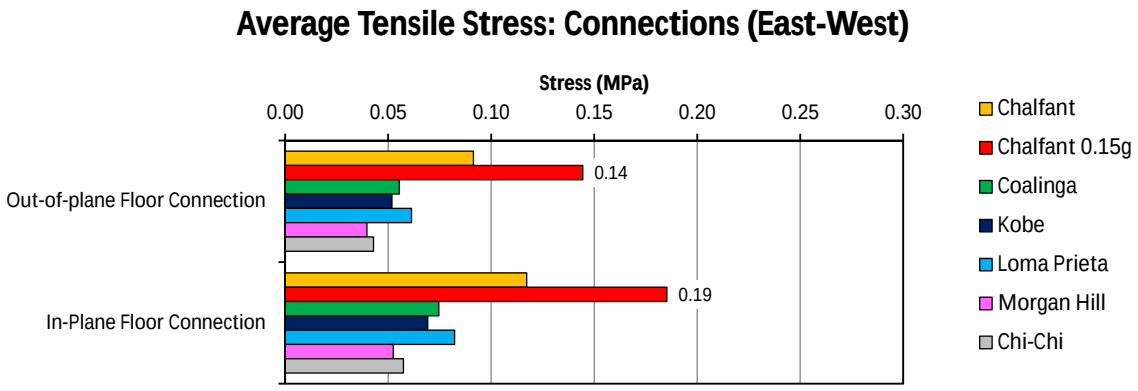

Figure 5.11: Average tensile stresses in an eight meter strip along the in- and out-of-plane wall-to-floor connections.

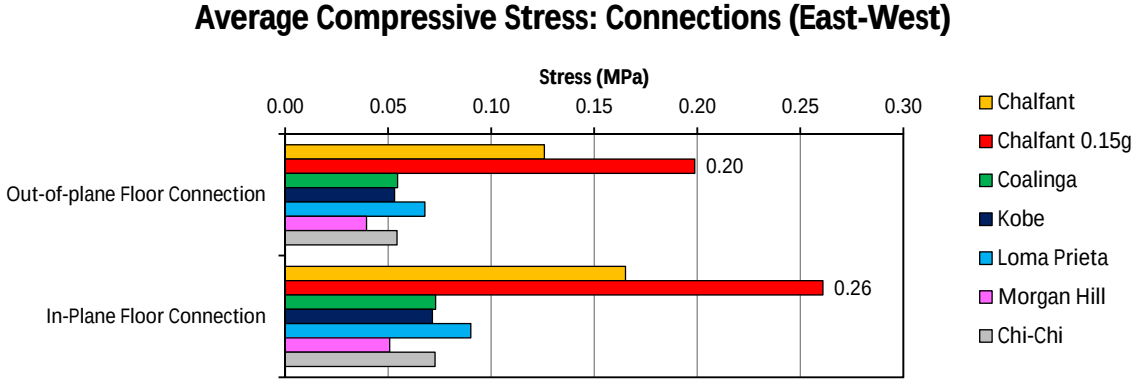

Figure 5.12: Average compressive stresses in an eight meter strip along the in- and out-of-plane wall-to-floor connections.

Figures 5.11 and 5.12 indicate that the average stress at connections along the floor slab edge is

about half of the maximum values observed at critical points. Values of 0.14MPa and 0.19MPa were recorded for the 0.15g Chalfant earthquake in tension as well as 0.2MPa and 0.26MPa in compression. When considering the average values, in-plane connections need to transfer a maximum tensile force of 47.5kN/m in tension and 65kN/m in compression. The out-of-plane wall-to-floor connections transfer a maximum tensile force of 35kN/m as well as maximum compressive force of 50kN/m. When considering the average stress at connections along the floor edges, the forces transferred by connections are still much larger than the design value of 1.5kN/m for secondary structural elements. The probability of failure of floor-to-wall connections not designed for seismic action at various locations in the building is very high when undergoing a 0.15g base excitation.

The maximum tensile stress at the vertical connections of out-of-plane internal walls is 0.92MPa. SANS 10164-1 specifies that the tensile strength for the formation of vertical cracks ranges from 0.9–1.5MPa for internal walls. The maximum tensile stress observed at the vertical connection of an internal wall, lies at the lower bound of the vertical crack strength range documented in SANS 10164-1. Failure will depend on the material properties of the specific wall. There is a moderate probability that failure could occur if weak masonry with a tensile strength at the lower bound of the values specified in SANS 10164-1 is used, since the forces that will develop are slightly larger than the cracking limit.

5.5.3 Shear

From observations of damage caused by previous earthquakes, it is evident that diagonal shear cracks in first storey piers are a common mode of failure in URM buildings (Bruneau, 1994; Tomaževič, 1999). In Section 2.5.5 it was explained that diagonal cracking in piers is as a result of principal tensile stresses forming perpendicular to the cracking plane when a pier is subjected to shear forces. This means that the maximum in-plane tensile stress will give an indication of whether the pier will fail due to diagonal shear cracks. In addition to diagonal cracks, sliding shear at the mortar bed joint could also occur. This will happen if the maximum shear stress at the base of the pier is larger than the maximum shear resistance of the bed joint. Figure 5.13 displays the maximum tensile stress at a point of diagonal shear failure as well as the maximum sliding shear stress for the different earthquakes.

The maximum tensile stress at typical diagonal crack locations is 0.52MPa which is lower than the maximum tensile resistance value of 0.6MPa. This does not mean that diagonal shear failure of piers is not possible. Figure 5.7 shows that the maximum tensile stress is exceeded in various locations possibly leading to the formation of a pier rocking mechanism. This will cause large concentrations of diagonal compression and tension forces that could result in the formation diagonal shear cracks.

In Section 2.5.5 it was shown that the sliding shear resistance of a masonry element is a function of the vertical stress in the element. The maximum shear stress of 0.55MPa, shown in Figure 5.13 exceeds the codified unloaded masonry resistance limit of 0.35MPa. This means that piers could fail if sufficient vertical compression load is not provided. By substituting the maximum shear

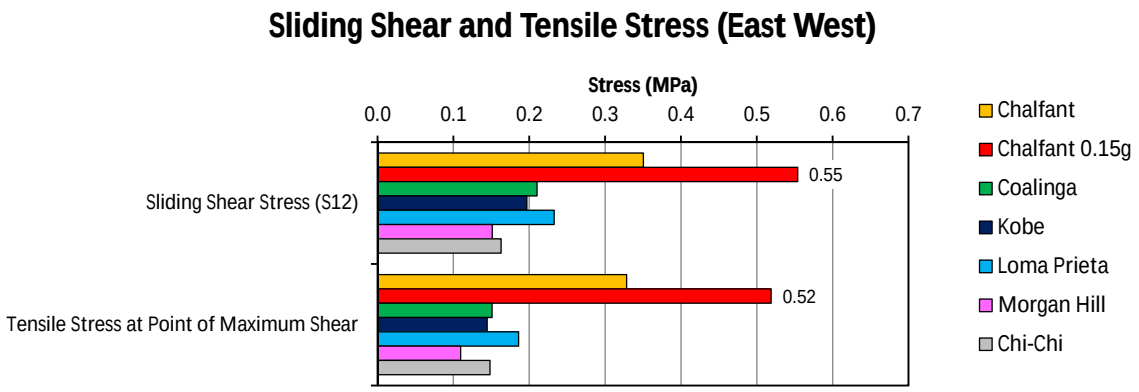

Figure 5.13: Maximum shear stress and tensile stress at locations where shear failure could occur during excitation in the East–West direction.

stress into Equation 2.8, a minimum compressive vertical stress of 0.33MPa is required to prevent sliding shear failure. This is an approximate value since the quality of the mortar joints will vary significantly throughout a structure. The formation of tensile cracks will also reduce the sliding shear resistance of the masonry piers.

If both permanent and imposed vertical loads are considered, the average vertical shear stress in first storey piers under static conditions is 0.6MPa. This is probably sufficient to prevent sliding shear failure. A critical load case occurs if the building is empty (such as after evacuation). Taking only permanent loads into account will approximately reduce the vertical load to 0.4MPa. This is very close to the 0.33MPa required to provide adequate sliding shear resistance. If horizontal cracks form in the bed joints of the masonry during the seismic excitation, the unloaded shear resistance will be reduced, leaving only the friction shear resistance to prevent sliding shear failure. During the time-history analysis, the rocking behaviour of first storey piers caused a combination of tensile and compressive stresses in the sliding shear plane. This means that during the excitation, part of the pier does not provide frictional shear resistance. With this taken into consideration, the probability of sliding shear failure is high.

5.6 Results: North–South

The results of the time-history analysis performed in the North–South direction will be discussed next. Common failure modes that were considered for the East–West direction such as diagonal cracking and sliding shear are still valid. The structural layout in the North–South direction has some important differences that will influence the building behaviour as well as critical stress locations. The locations of the maximum compressive and tensile stress concentrations are shown in Figure 5.14.

The North–South spanning structural walls do not have window openings. This means that failure of structural piers is not an option. Cracks that form due to stress concentrations at window openings will not be present in the in-plane walls. The behaviour of the solid shear walls will instead be dictated by tensile cracks and compression crushing at the heel and toe as

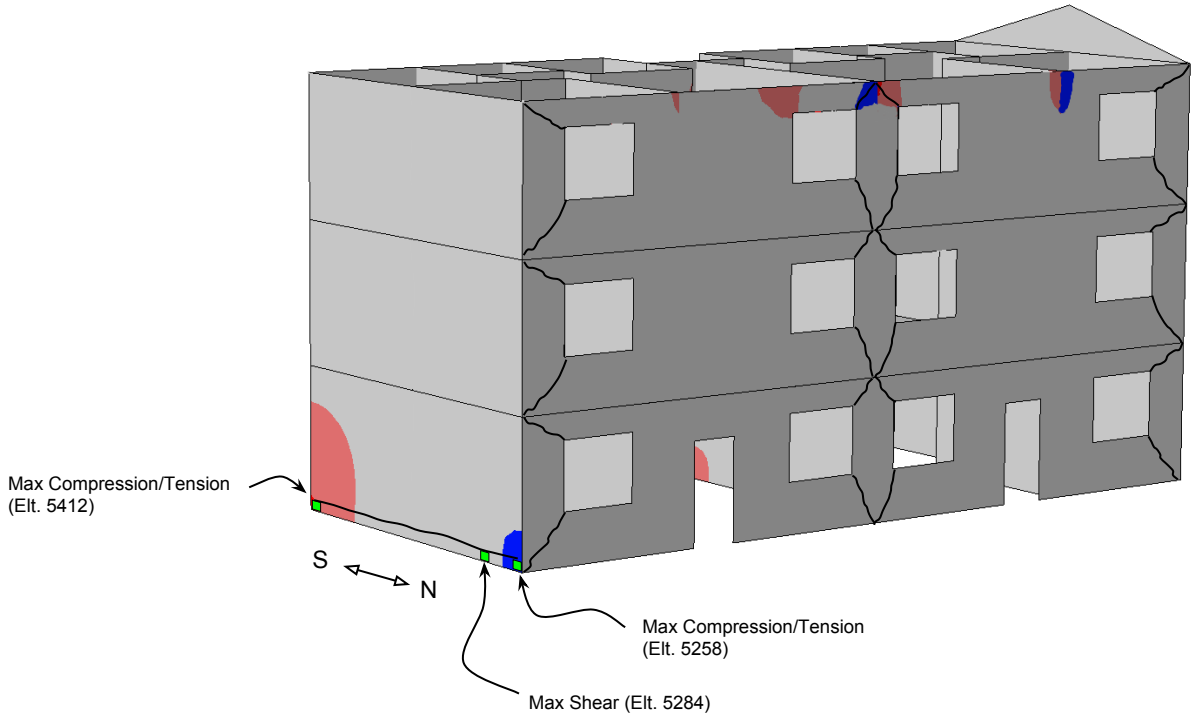

Figure 5.14: Locations of the maximum tensile, compression and shear stresses along with cracks that are likely to form in the in- and out-of-plane walls during excitation in the North–South direction. Tensile and compression stresses are indicated in red and blue (depending on the direction of excitation).

well as sliding shear failure. Cracks can be expected to form in the out-of-plane perimeter walls close to the in-plane walls since the out-of-plane walls will act as flanges with diagonal cracks developing from the openings.

5.6.1 Tensile and Compressive Stress

The largest tensile and compressive stress concentrations occur at the heel and toe of the in-plane shear walls. This is due to the base shear and moments applied to the structure as a whole resulting from the earthquake excitation. The shear walls will essentially act as cantilevers when resisting the lateral motion. Figure 5.15 and Figure 5.16 show the tensile and compressive stresses for the different earthquakes.

Figure 5.15 shows that the 0.15g Chalfant Valley earthquake will exceed the maximum tensile stress at the base of the North–South spanning in-plane shear wall. Once the maximum tensile stress is exceeded, cracks will form at the base of the wall. During the rest of the seismic excitation, the cracks will open and close and progressively extend along the wall, until the wall fails through sliding shear or loss of equilibrium (Yi, 2004). Since shear walls are the primary load path for seismic induced forces, the failure of an in-plane shear wall will typically lead to global structural collapse. The building will be able to resist the other smaller earthquakes with limited damage. The compressive stresses developed during the excitations will not reach the compressive strength of URM and will therefore not pose a significant threat to the building.

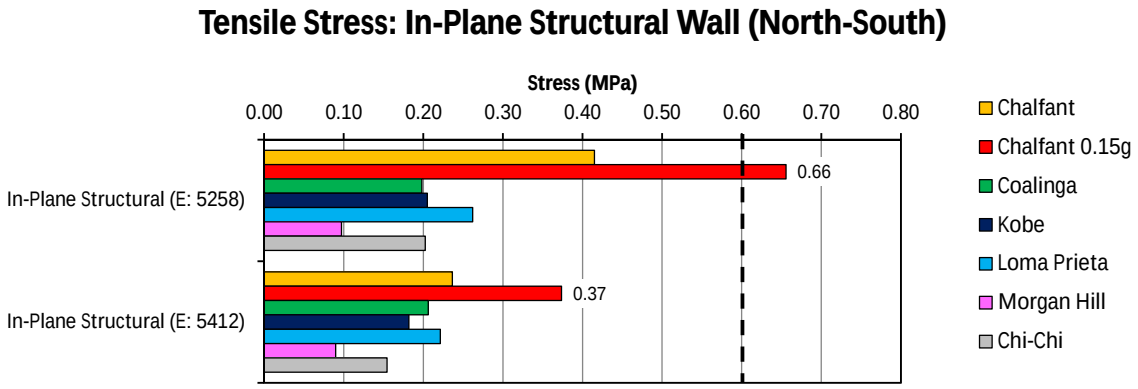

Figure 5.15: Maximum tensile stress in the in-plane structural walls during excitation in the North–South direction.

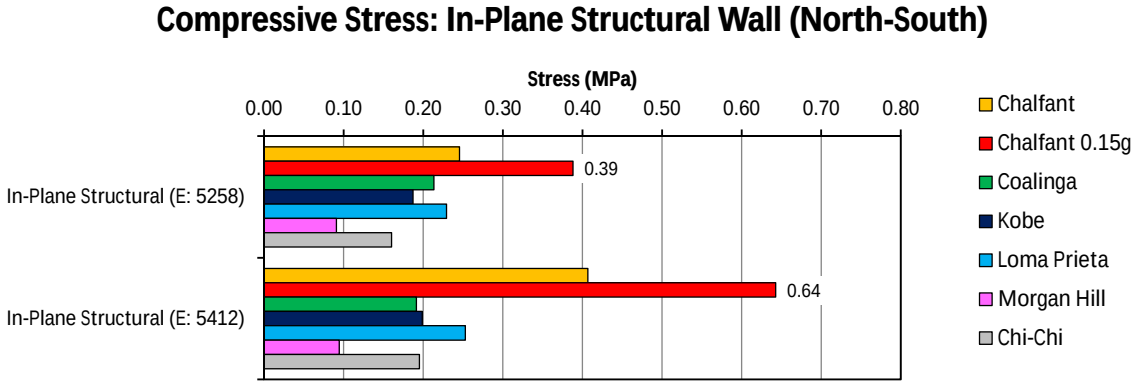

Figure 5.16: Maximum compressive stress in the in-plane structural walls during excitation in the North–South direction.

5.6.2 Connections

The stresses that develop at the floor-to-wall and out-of-plane wall connections need to be investigated. Out of plane walls will typically act as flanges to assist the in-plane walls in resisting the lateral seismic loads. The presence of window openings in the out-of-plane walls will however reduce the effective size of flanges since cracking will occur at the corners of openings and progress at an angle to the in-plane wall. Figure 5.17 and Figure 5.18 show the tensile and compressive stresses that form at the in- and out-of-plane floor-to-wall connections during the building excitation.

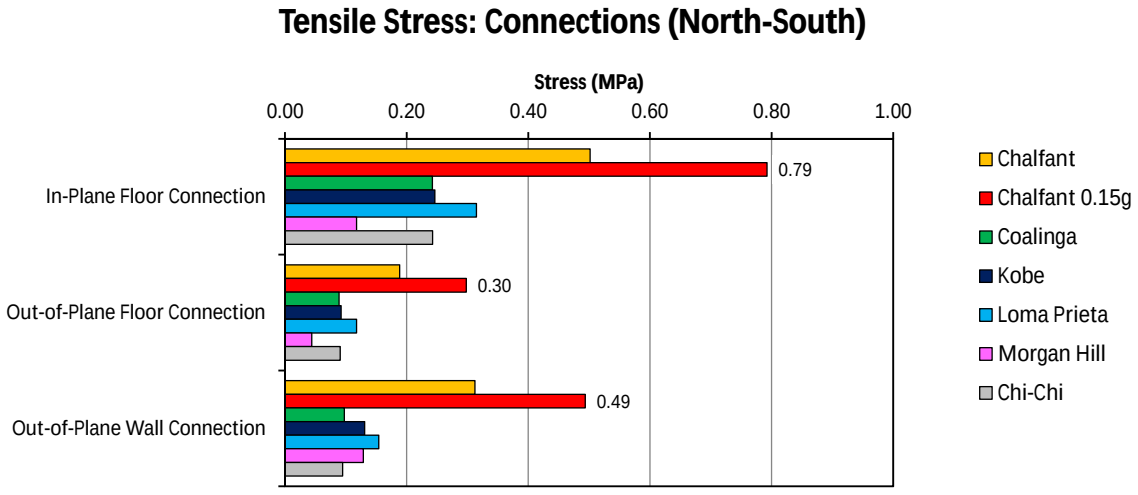

Figure 5.17: Maximum tensile stress in wall-to-floor connections at the first storey as well as out-of-plane wall connections at the top storey during excitation in the North–South direction.

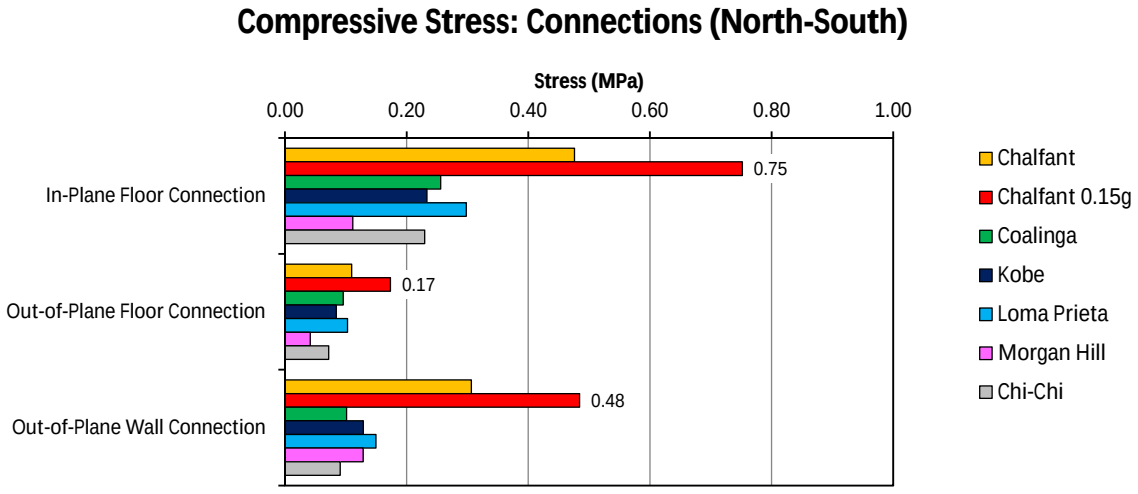

Figure 5.18: Maximum compressive stress in wall-to-floor connections at the first storey as well as out-of-plane wall connections at the top storey during excitation in the North–South direction.

The magnitude of the connection forces at the in-plane and out-of-plane floor-to-wall connections are extremely large. This suggests that failure of floor anchors is likely to occur. The connection strength of URM buildings requires further research since the connection capacity will vary

depending on the connection type (anchor rod, rebar, bolt etc) and specifics of a design for a structure. Anchorage failure will prevent the diaphragm from effectively transferring the lateral loads between in-plane shear walls and could lead to catastrophic collapse as well as damage to walls and the floor diaphragm.

5.6.3 Shear

The maximum shear stress and tensile stress at shear cracking locations are shown in Figure 5.19.

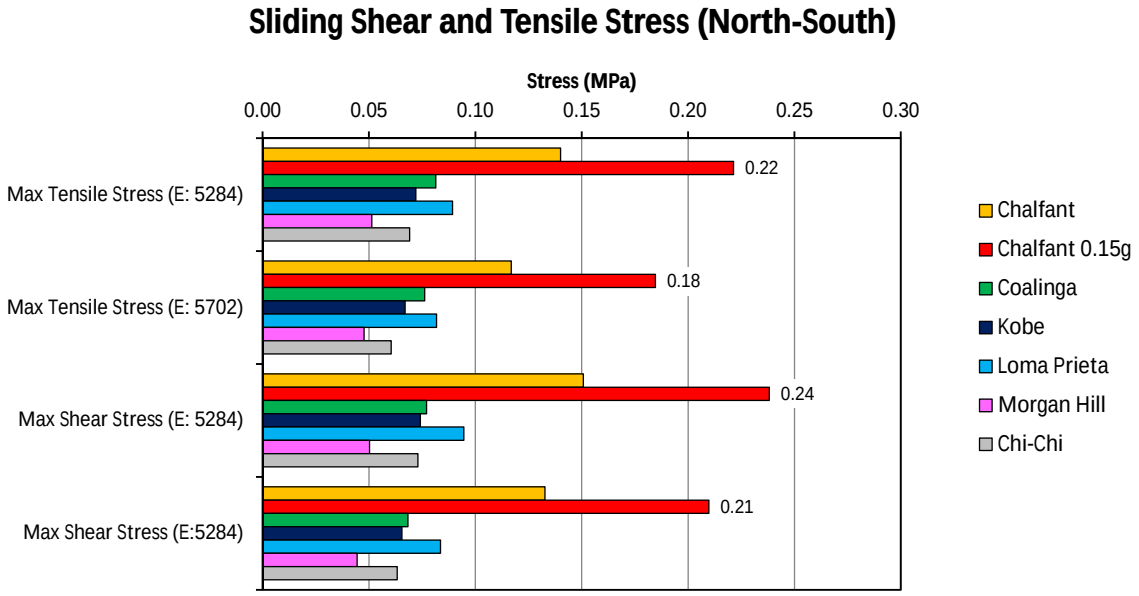

Figure 5.19: Maximum shear stress and tensile stress at key points in the in-plane structural walls for the North–South model.

The diagonal tensile stress obtained in the structural elements for the North–South direction (0.22MPa) is much smaller than the maximum tensile strength of masonry (0.6MPa). This suggests that diagonal shear cracks in in-plane structural walls are unlikely to occur. The maximum shear stress in the in-plane shear walls is smaller than the natural shear resistance of the mortar joint. This is as a result of the large cross sectional area of shear walls in the North–South direction leading to reduced shear stress. The lack of openings further improve the shear capacity of walls since the entire length of the shear walls can add lateral resistance.

5.7 Displacement Results

Displacements were measured at points along the top edge of the in-plane and out-of-plane walls. The largest displacements will occur in the top storey of the structure. Maximum displacement values are displayed in Figure 5.20 for the East–West and Figure 5.21 for the North–South direction.

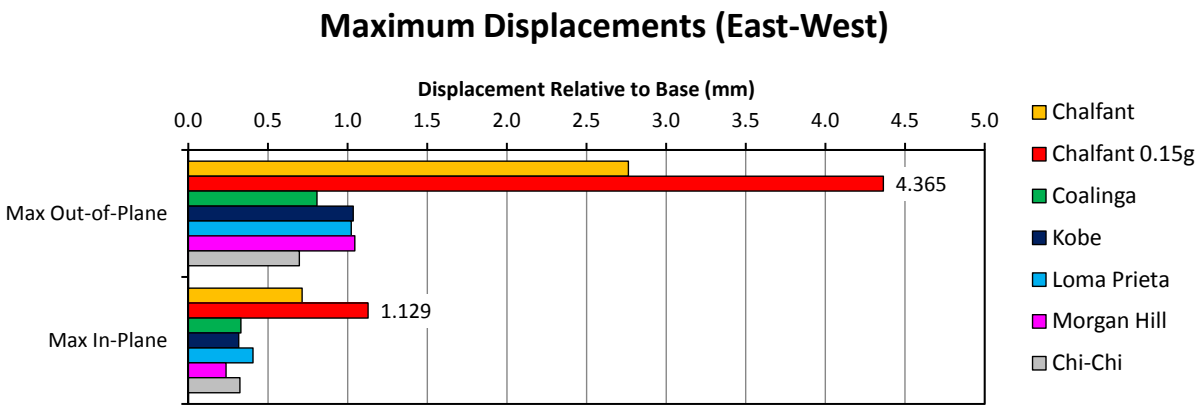

Figure 5.20: Maximum displacement of the top of the structure relative to the base for in-plane and out-of-plane walls in the East–West direction.

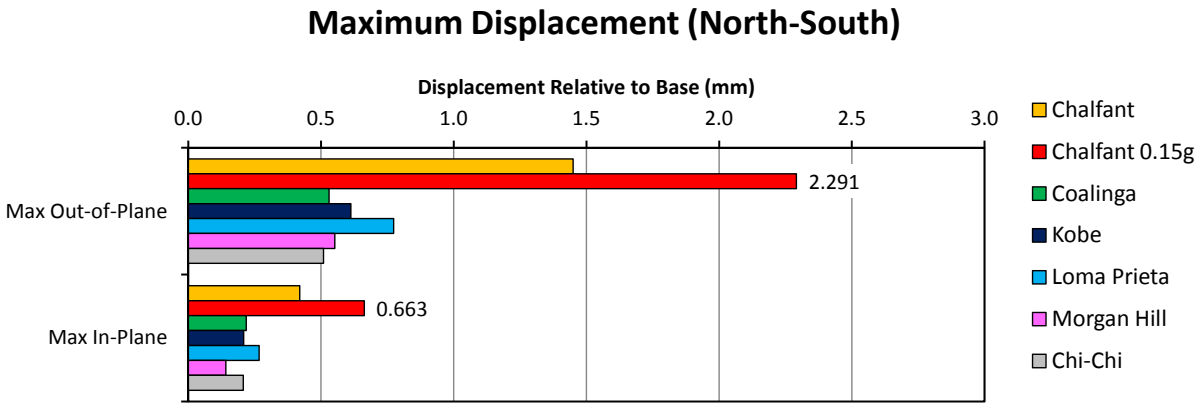

Figure 5.21: Maximum displacement of the top of the structure relative to the base for in-plane and out-of-plane walls in the North–South direction.

All displacements are measured relative to the base of the structure. The scaled 0.15g Chalfant Valley earthquake showed the largest response in both the East–West and North–South directions. The 0.1g Chalfant Valley earthquake showed displacements of almost twice the magnitude of the other earthquakes used in the study. In Figure 5.4 it is shown that the Chalfant Valley earthquake has a low period of vibration. This clearly demonstrates that low magnitude earthquakes with low peak ground displacements can have large responses if the excitation frequency approaches the natural frequency of the building. Masonry buildings are normally only a few storeys high and have large lateral stiffness. Earthquakes with high excitation frequencies (i.e. short periods) will cause increased response, even if the earthquake magnitude is less.

The maximum displacements occurred at the top of the out of plane walls with displacements of 4.4mm in the East–West direction and 2.3mm in the North–South direction. The in-plane walls showed smaller displacements due to the increased stiffness of masonry when resisting in-plane loads. A maximum displacement of 1.13mm was observed for the East–West direction and 0.66mm for the North–South direction. SANS 10160-4 places a storey drift limitation of 2.5% of the storey height on each storey of the buildings during seismic excitation. With a storey height of 3 meters, the inter-storey drift limitation will be 75mm. This is much larger than the displacements observed during excitation.

Experimental testing of one-storey single leaf masonry walls performed by Griffith et al. (2007) showed that masonry walls were able to displace half of the wall thickness before failure occurred. This amounts to a displacement of approximately 55mm for single leaf internal walls. It is clear that the displacements observed during the numerical analysis are not sufficiently large to cause failure. If the maximum tensile limit of the masonry is reached, cracking will cause increased displacements. This should be investigated during a non-linear analysis.

5.8 Discussion of Results

The building shows good resistance for earthquakes with PGA ¡ 0.1g in both the North–South and East–West directions. This is due to the length and amount of shear walls provided in both directions. The presence of window openings in the primary shear walls that lie in the East–West direction will reduce the ability of the walls to resist seismic loads. The small aspect ratios of piers that lie between adjacent window openings will give rise to the possibility of failure due to pier rocking and pier shear failure. This is very common in URM buildings and has been observed in previous earthquakes.

The ability of the floor diaphragms to transfer lateral loads between the in- and out-of-plane walls is highlighted by the analysis. Very large stresses form at the connections. If the wall-to-floor anchors fail, the diaphragm will be unable to transfer lateral loads to the load resisting shear walls. This could cause an increase in stress at certain locations since the stresses can't be redistributed between load resisting members. The importance of providing floor anchors in buildings in seismic regions is evident. The capacity of floor anchors will however depend largely on the design of individual structures and should be addressed in a future study.

The relatively small displacements at the top of the in-plane walls indicate that the structure has large stiffness, and therefore responds well to large oscillations with large vibration periods. The large stiffness of the structure is as a result of long shear walls in both orthogonal directions, low height of the structure, rigid floor diaphragm, large amount of lateral supporting walls and short distances between internal walls. These properties along with simple box shape allow the building to have a large stiffness despite the relatively small stiffness of the material (when compared to other construction materials such as reinforced concrete).

The Chalfant Valley earthquake consistently resulted in the largest stress and displacement values. This is in part due to the higher frequency of vibration (shorter periods of vibration) of the earthquake as shown in Figure 5.4. The earthquake, with a Richter magnitude of only 5.77, showed smaller peak displacement and velocity values than most of the other earthquakes. The increased vibration frequency caused the building, with a higher natural frequency due to it's large stiffness, to vibrate close to its natural frequencies. In comparison, the Chi-Chi earthquake, with much larger peak ground displacements, vibrates at lower frequencies. This will cause amplified vibrations in taller and slender structures while showing reduced responses in stiff 2 to 3-storey masonry structures.

All the perimeter walls are essentially designed to act as shear walls. This is beneficial since it increases the lateral resistance of the structure and greatly reduces the shear stresses in structural elements.

5.9 Summary

Several earthquakes were identified and used to perform a series of modal dynamic analyses on the three storey URM building. The calibrated material model discussed in Chapter 3 along with the finite element model presented in Chapter 4 were used for the analysis. Six earthquakes that can be expected to occur in the seismic active regions of the Western Cape were identified based on their magnitude and PGA values. The earthquakes showed very different acceleration, velocity and displacement profiles. This allows the response to a broad range of earthquake types to be examined. The earthquakes have Richter magnitudes ranging from 5.77–7.60 and PGA values ranging from 0.046–0.100.

Before a modal dynamic analysis can be performed, it is necessary to determine the natural frequencies and mode shapes of the structure. The first 25 modes were selected for analysis since they accounted for 90% of the modal mass of the structure in each excitation direction. The building responds primarily in the frequency range 8.9–13.4Hz. The frequencies obtained from the North–South and East–West models show good agreement with a constant stiffness model of the building. Once the relevant frequencies were identified, the acceleration time-histories were applied to the North–South and East–West models, and results recorded.

Results show that the structure has a high probability of exceeding the tensile strength of the masonry at the internal piers in the East–West direction when applying the 0.15g Chalfant Valley earthquake. In addition, the maximum tensile stress was exceeded in non-structural in-plane

walls. Although the other earthquakes did not exceed cracking limit, the 0.1g Chalfant Valley earthquake also caused cracking in several piers. This could cause the piers to form a rocking mechanism during the excitation, possibly leading to failure. The structure showed no compression failure. Stresses developed at the connections far exceeded the codified limits presented in SANS 10160-4. The probability of connection failure is very high. There is a moderate probability that vertical cracks could form at the connection between in- and out-of-plane walls at the top storey of the structure. The stresses developed are at the lower bound of SANS 10164-1 limits. This suggests that failure could occur if weak material is used. Diagonal shear stresses were within the limit for URM. Sliding shear is however likely to occur, especially after the formation of tensile cracks, since the shear stresses exceeded the unloaded shear resistance. Sliding shear will be especially critical if the building is empty since vertical compression loads are favourable to sliding shear resistance. Masonry piers will develop a combination of tension and compression stresses along the sliding shear plane during excitation. This further indicates that sliding shear could occur if the compression portion of the shear surface has insufficient vertical compression to resist shear failure.

The results show that the building performs well for most of the earthquakes except for the Chalfant Valley earthquake. The 0.15g Chalfant Valley earthquake proved most critical. The building showed poor performance with a high probability of tensile and shear cracking as well as connection failure. This suggests that although the building could possibly meet the requirements of SABS 0160 by potentially resisting a 0.1g earthquake, the building will not meet the increased design requirements implemented by SANS 10160-4 through the use of the behaviour factor. It also highlights the danger of designers using the nominal design acceleration of 0.1g and disregard the redundancy factor when implementing alternative design methods, since the capacity of the structure could be insufficient.

In the North–South direction, the maximum tensile strength was exceeded at the base of the in-plane shear walls for the 0.15g Chalfant Valley earthquake. The formation of cracks in the shear walls will likely progressively reduce the strength of the shear wall during the rest of the excitation. Similar to the results of the East–West model, the connections experienced stresses far exceeding the design strength specified in SANS 10160-4, suggesting that the probability of failure is high. Unlike the case for the East–West direction, the North–South spanning shear walls performed well in both diagonal shear and sliding shear resistance. This can be attributed to the lack of openings in the North–South spanning shear walls.

The building performed better in the North–South direction than in the East–West direction. It is a result of the increased amount of shear walls present in the North–South direction. A lack of openings also increase the cross sectional area to provide additional shear resistance. Other factors such as the formation of stress concentrations at openings and pier rocking mechanisms are also avoided. The building did however show that cracking at the heel/toe of the in-plane shear walls is likely for the 0.15g Chalfant Valley earthquake. This is due in part to the reduced aspect ratio in the North–South direction leading to increased moments about the base of the structure. In Section 4.3 it was shown that the building does not meet the requirement that $L < 4B$. This further illustrates the importance of basic conceptual design guidelines especially

when designing a building using a non-ductile material such as URM.

The linear analysis shows possible failure of structural and non-structural elements due to cracking. URM does however show post cracking strength. The results obtained during the modal dynamic analysis will be verified by performing additional analyses in Chapter 6. A sensitivity analysis will be performed to assess the impact that variable parameters have on the building response. Finally a non-linear implicit dynamic analysis will be performed to assess the post-cracking behaviour. This will verify whether the material has sufficient ductility to resist the earthquakes even if cracking of certain elements has occurred.

Chapter 6

Implicit Non-Linear Analysis and Result Verification

6.1 Introduction

The modal dynamic analysis performed in Chapter 5 provides an efficient approach to analysing dynamic problems within the linear range. It allows for many different input parameters to be studied and compared without requiring large amounts of computational power or time. Results obtained from a modal dynamic analysis will be accurate if sufficient modes are used to capture the dynamic behaviour of the building and if the building responds primarily in lower modes. It is good practice to perform alternative analyses to validate results and ensure that assumptions are realistic.

In order to take non-linear material properties into account, a non-linear dynamic analysis must be performed. This can be achieved by performing an implicit dynamic analysis. It is much more time consuming and requires more computational power. The results obtained from the implicit analysis will however allow the post cracking behaviour of URM to be studied. This is necessary to verify whether the material possesses sufficient post cracking resistance to resist an earthquake that exceeded the elastic capacity during the modal dynamic analysis, discussed in Chapter 5.

The URM building model that was analysed using a modal dynamic analysis in Chapter 5 will be simplified as a mass-spring multi-degree-of-freedom (MDOF) system and analysed to confirm whether the displacement results presented in Section 5.7 are accurate. A sensitivity analysis will be performed to study the effect that varying parameters have on the model's response. This is necessary since a FE model is a simplification of a real world problem that is subject to various uncertainties and external influences. The behaviour factor, discussed in Section 2.4.4, can be used to account for the non-linear capacity of URM when performing an elastic analysis. The use of the behaviour factor will be discussed in Section 6.3.1. The effect that different damping values have on the results will be discussed in Section 6.3.2.

Finally an implicit dynamic analysis will be performed using a critical earthquake identified

in Chapter 5, which will take the plastic behaviour of URM into account. Previous analyses indicated that the probability of failure of certain structural elements due to tensile cracking is high. Behaviour of the structure in the inelastic range will determine whether the building has sufficient ductility to improve the seismic performance.

6.2 Analysis of an equivalent MDOF System

A simple method to verify the results of the 3D modal dynamic analysis presented in Section 5.4, would be to model the building as a mass-spring system. The stiffness of the horizontal load resistance system is represented as springs and the mass of the different storeys are simplified as lumped masses. The response of the mass-spring system should be of the same order as that of a full 3D model. This will neglect displacements of individual elements such as the out-of-plane walls. However, the displacement of the main stiffness elements should be approximately the same as the full 3D model. A basic MDOF mass-spring simplification of the building is shown in Figure 6.1.

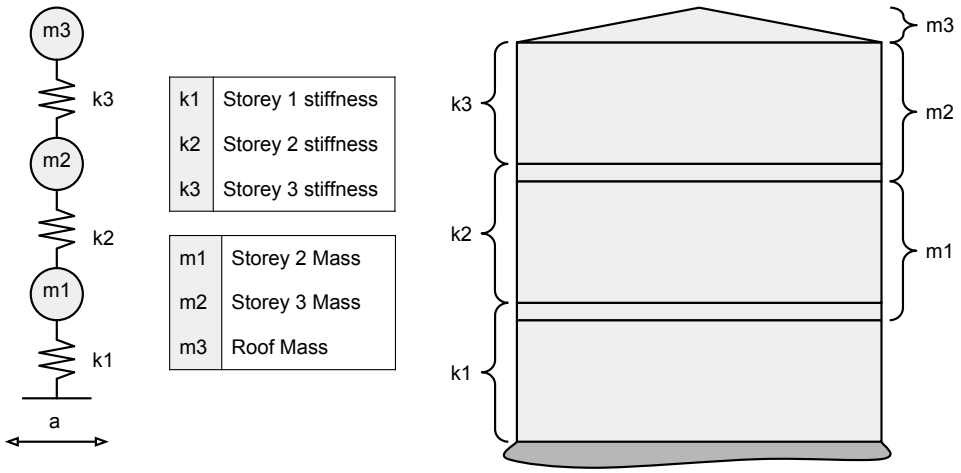

Figure 6.1: MDOF mass-spring simplification of the building.

The three spring stiffness values represent the lateral stiffness of the walls on each floor. This is determined by modelling a single storey, including the in- and out-of-plane walls and floor slab. Boundary conditions at the bottom of the storey are specified to match the way in which the storeys are tied together in the 3D model (i.e. either pin or fix connections). A unit horizontal displacement is applied to the top of the storey while the bottom is pinned. The total reaction force caused by the unit displacement will give the stiffness of the storey. The mass of each storey can easily be calculated if the dimensions and mass densities are known. Storey masses are added as lumped masses to the spring elements for m_1 and m_2. The mass of the roof is added as lumped mass, m_3, to the top of the spring system.

Mode shapes of the system are determined after which an acceleration time-history is applied to the base of the mass-spring model. Modal damping is applied to all modes by specifying a damping ratio of 0.1 as used in Chapter 5. The Chalfant Valley time-history, described in Section 5.2, is applied to the base of the model using a modal dynamic analysis. Displacements

at the top of the mass-spring system relative to the bottom along with the displacement history of the model analysed in Chapter 5 are shown in Figures 6.2 and 6.3 for the East–West and North–South directions respectively.

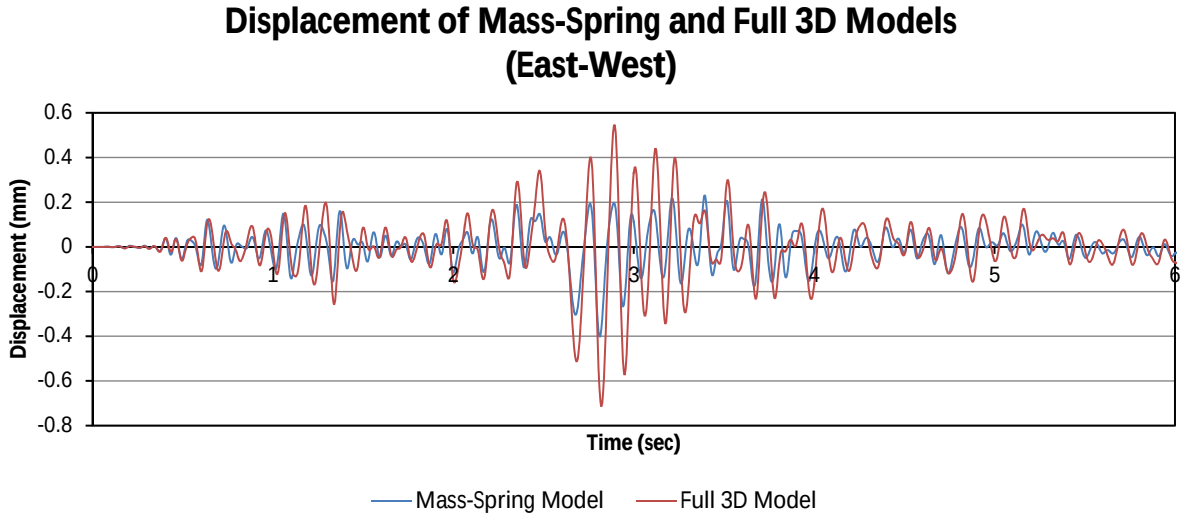

Figure 6.2: Displacement histories of the Chalfant Valley earthquake for the East–West direction of the mass-spring system and the top of an in-plane shear wall analysed in Chapter 5.

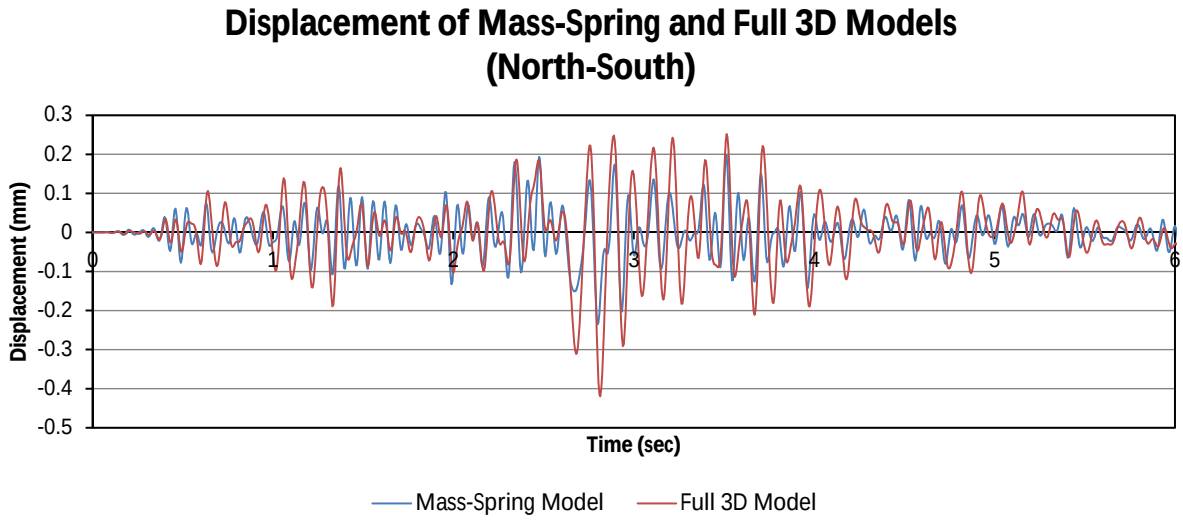

Figure 6.3: Displacement histories of the Chalfant Valley earthquake for the North–South direction of the mass-spring system and the top of an in-plane shear wall analysed in Chapter 5.

Displacement results show that the mass-spring system reached lower displacements than obtained during the modal analysis. This is due to the large simplification of the mass-spring system and an inability to represent the behaviour of separate structural elements during the seismic excitation. The distribution of the building mass can be improved by assigning a portion of the first storey mass to the value used for m_1 during the analysis. The majority of the first storey mass is distributed in the in-fill walls without a connection to the overhead slab and should have little effect on the displacement at the top of the structure. Portions of the structural wall mass in the first storey must however be included in m_1 to obtain better results. The increased mass will provide increased displacements at the top of the structure. The mass-

spring analysis results confirm to some extent that the modal dynamic analysis results obtained in Chapter 5 are plausible and that the modelling techniques are sound, however, improving the mass distribution will allow the exact displacements recorded for the 3D model to be obtained. The current mass-spring model is unable to accurately represent the peak displacement results of in-plane walls and does not model the behaviour of out-of-plane walls.

6.3 Sensitivity Analysis of the 3D Model

Chapters 2 to 5 give a good indication of the uncertainties relating to the analysis and seismic behaviour of URM buildings. Past earthquakes give an idea of possible failure modes and critical structural elements. A number of earthquakes were used in Chapter 5 to analyse the structure. This allows the building response to be determined for different dynamic excitation parameters such as frequency of excitation, PGA, earthquake magnitude and acceleration profiles. In addition, the building was analysed in the two main orthogonal directions since the building has different stiffnesses and aspect ratios in the different directions. The Chalfant Valley earthquake showed the largest response. It is now necessary to consider the effects that other important parameters that have not yet been considered, could have on the model. By considering a number of parameters, the building is analysed in a general case as a representative URM structure in the Cape Town area, rather than limiting the analysis to a single structure.

6.3.1 Behaviour Factor

As previously discussed in Section 2.4.4, SANS 10160-4 suggests the use of a behaviour factor to account for the non-linear behaviour of materials. This is applied to the design response spectra to reduce the response of the structure to seismic excitation thereby reducing the design base shear force. In addition to reducing the seismic loads acting on the structure, the behaviour factor is applied to the elastic displacement of the structure to calculate an increased inelastic displacement value. This simulates the expected non-linear behaviour of materials as was shown in Figure 2.7.

The behaviour factor for URM is 1.5. Since the design PGA value is directly related to the magnitude of the design base acceleration, the effect of the behaviour factor can be accounted for by reducing the PGA. A maximum response was obtained for the 0.15g Chalfant Valley earthquake time-history. Reducing the magnitude of acceleration by a factor of 1.5 will lead to a 0.1g PGA. Results in Section 5.5 indicate that the maximum elastic tensile stress of the structure is exceeded for a 0.1g excitation. This suggests insufficient ductility to resist the 0.15g Chalfant Valley earthquake.

SANS 10160-4 stipulates that the elastic displacement of the structure should be increased by a factor of $0.7q$, where q is the behaviour factor, to determine the inelastic displacement when checking inter-storey drift. This will not have a large effect on the maximum displacement of URM since the behaviour factor has a value of 1.5, resulting in a 5% increase in displacement.

6.3.2 Damping

Different damping ratios can be applied to URM buildings depending on the level of damage that the building has developed. In Section 3.3.1 a damping ratio of 0.1 was assumed for URM buildings when using a viscous damping model. This relates to URM in its cracked state. A modal dynamic analysis was performed using a reduced damping value of 0.05 as typically specified for URM buildings in their undamaged state in order to verify the damping ratio of 0.1. The Chalfant Valley earthquake acceleration history with a PGA of 0.1g was applied to the structure. A comparison between the displacement results for damping ratios of 0.1 and 0.05 is presented in Figures 6.4 and 6.5 in the East–West direction for in-plane and out-of-plane walls respectively.

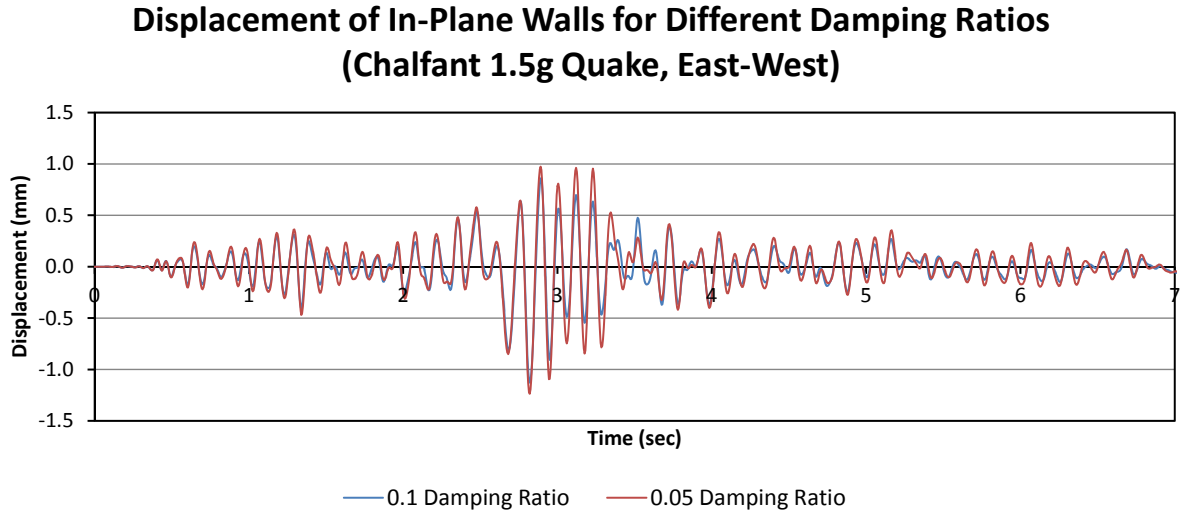

Figure 6.4: Displacement of in-plane shear walls for different damping ratios (East–West).

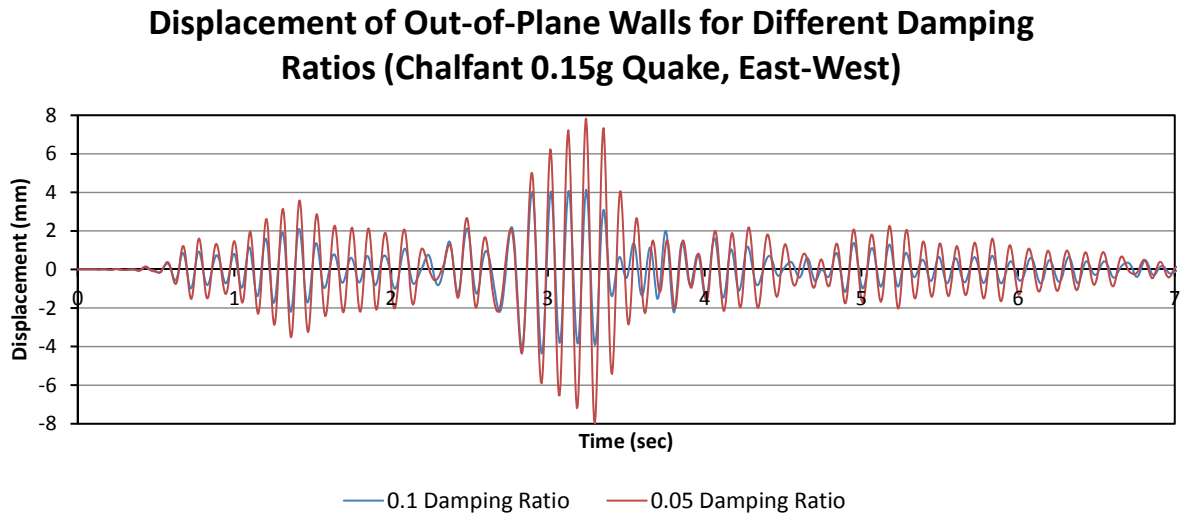

Figure 6.5: Displacement of out-of-plane walls for different damping ratios (East–West).

Results indicate that the maximum displacement response of in-plane walls in the East–West direction is influenced noticeably when reducing the damping ratio. The magnitude of the

displacements is sufficiently small that the increased displacement should not cause failure. This does indicate however that a noticeable increase in stresses could result from reducing damping as discussed later in this section. In general, reducing damping has a larger effect on out-of-plane wall behaviour due to the reduced stiffness and aspect ratio. The out-of-plane walls and specifically internal walls will undergo larger oscillation with increased velocity leading to increased damping. For lower damping values, the oscillating walls will retain more energy between oscillations allowing the movement to be amplified by the building acceleration. Once the building acceleration decreases, it will take longer for movement to damp out. Results indicate that damping is an important parameter to consider for non-structural and other less-stiff elements with regard to displacement. Displacement results for damping ratios of 0.05 and 0.1 is shown in Figures 6.6 and 6.7 for the North–South direction.

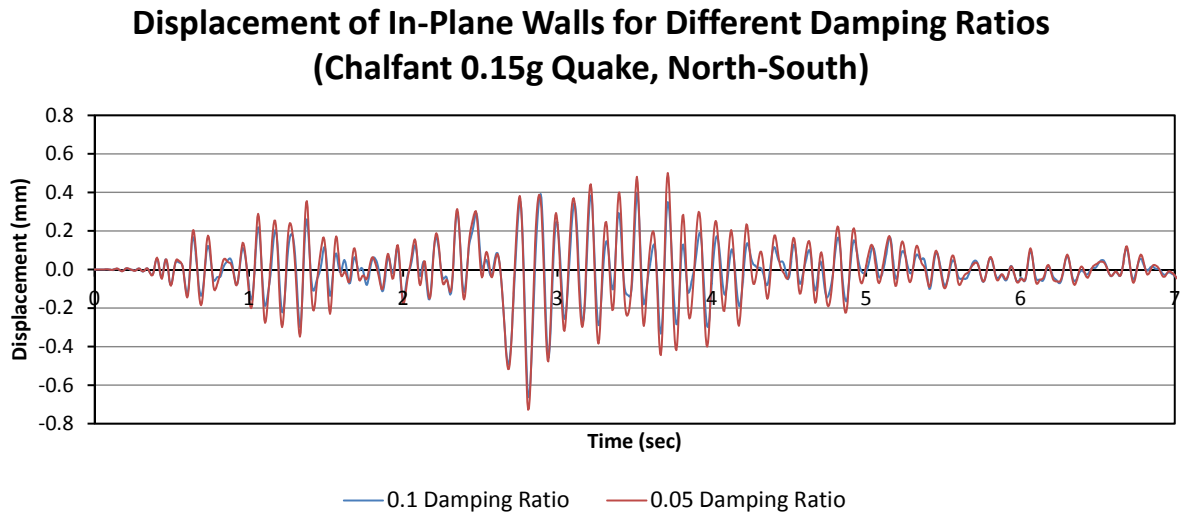

Figure 6.6: Displacement of in-plane shear walls for different damping ratios (North–South).

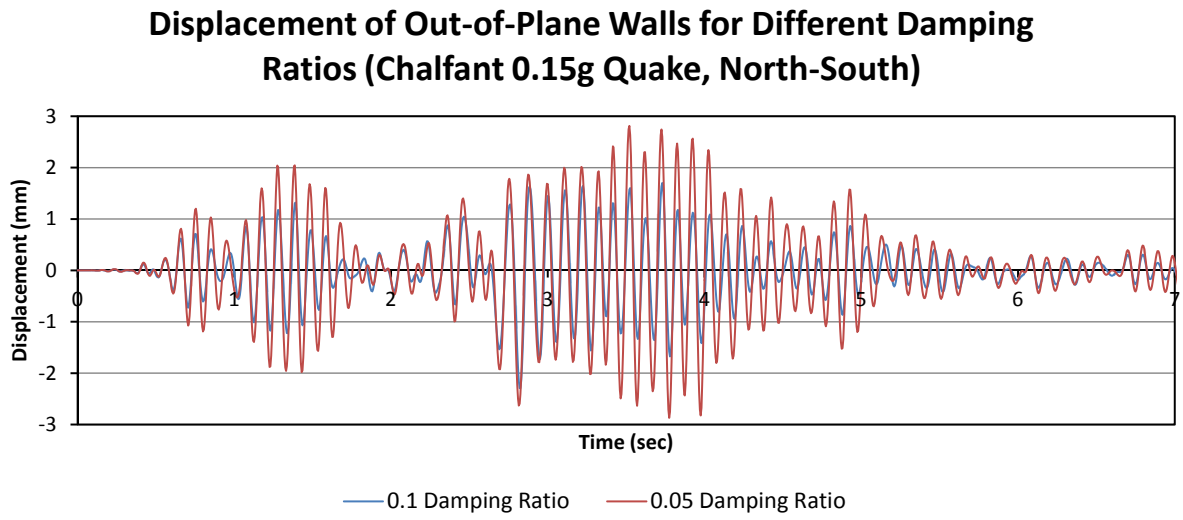

Figure 6.7: Displacement of out-of-plane walls for different damping ratios (North–South).

The results in the North–South direction is similar to results obtained in the East–West direction. In-plane walls are affected less by the damping values than out-of-plane walls, suggesting that

damping will have a larger effect on the response of less stiff elements when displacement is considered. Several critical in-plane elements were identified during the initial modal dynamic analyses in Chapter 5. Although in-plane walls were not affected severely by reducing damping, it is also necessary to consider the possible increased stresses that can develop due to a reduced damping ratio. The maximum tensile stress in these elements for damping ratios of 0.1 and 0.05 is shown in Table 6.1

Table 6.1: Maximum tensile stresses for critical elements with damping ratios of 0.05 and 0.1.

	East–West Stress (MPa)		**North–South Stress (MPa)**	
Element	**E: 850**	**E: 1510**	**E: 5258**	**E: 5412**
Damping 0.1	0.998	0.777	0.656	0.374
Damping 0.05	1.096	0.896	0.723	0.479
% difference	10%	15%	10%	28%

Reducing the damping ratio from 0.1 to 0.05 increased stresses between 10% and 15% for the East–West direction and between 10% and 28% for the North–South direction. This indicates that a reduced damping ratio has a significant effect on stress results. The damping ratio of 0.05 should therefore be implemented for the undamaged elastic analysis. If stresses exceed the cracking limit of the material, a larger damping ratio can be assumed. During the modal dynamic analysis performed in Chapter 5, stresses in both the East–West and North–South directions exceeded the tensile limit of the material indicating that the probability of cracking is high. This confirms the choice of a higher damping ratio since damping will increase once cracking has occurred.

6.4 Non-linear Implicit Analysis

The modal dynamic analysis performed in Chapter 5 was able to predict whether cracking will occur and how the structure is likely to fail. It did not however take the post cracking capacity of URM into account. A non-linear material model will be able to accurately predict the behaviour of the structure in both the elastic and inelastic range. Results should match the elastic analysis until the point that the maximum tensile or compressive stress is reached. Thereafter the behaviour will depend on the non-linear behaviour of the material. Failure will occur once the ultimate strain value is reached. Since masonry has a very large compressive strength compared to tensile strength, it is expected that tensile cracking will dominate the inelastic analysis. An implicit dynamic analysis was performed to study the non-linear behaviour of the structure in the East–West direction. It is much more computationally intensive than the modal dynamic analysis. It was therefore decided to perform the analysis using the 0.15g Chalfant Valley earthquake in the East–West direction, since this was the most critical case.

Initially an elastic implicit dynamic analysis was performed with the elastic material properties for in- and out-of-plane walls used in Chapter 5. The factored 0.15g Chalfant earthquake time-history was applied to the base of the structure in the East–West direction. For the modal dynamic analysis, damping was specified using a viscous damping model with a damping ratio of 0.1. Damping for the implicit analysis is specified using a Rayleigh damping model as dis-

cussed in Section 3.3.1. Values for α and β are determined iteratively until the results of the implicit dynamic analysis match that of the modal dynamic analysis. The results will match the viscous damping values exactly for the two dominant lateral displacement modes. As shown in Section 5.3, modes 1 and 4 are the dominant lateral excitation modes. Damping for the other modes will be governed by the Rayleigh model. Modes 1 and 4 occur at frequencies of 8.8Hz and 8.95Hz. The dominant torsional mode, mode 10, has a frequency of 9.61Hz. The small difference in frequencies of the dominant modes will ensure that the damping for higher modes are not dramatically affected by the Rayleigh model. It was determined that values of $\alpha = 6$ and $\beta = 0.0025$ provide a good representation of the viscous damping model.

Plastic material properties are included in the model using the damaged concrete plasticity model in ABAQUS. Calibration of the model is explained in Section 3.2.3. To improve analysis time, a critical 6 second segment of the earthquake is used for analysis. Results are verified at the same elements as used in the modal dynamic analysis.

A critical element (element 850, shown in Figure 5.5) located in a pier on the first storey of an in-plane shear wall is studied for failure. The element developed the maximum tensile stress concentration during the modal dynamic analysis in Section 5.5.1. Since yielding and therefore cracking of the element occurred during the excitation, the tensile stress is no longer an indication of failure since the stress in the material will not exceed the maximum tensile stress. Elastic, inelastic and total strain results of the element is shown in Figure 6.8.

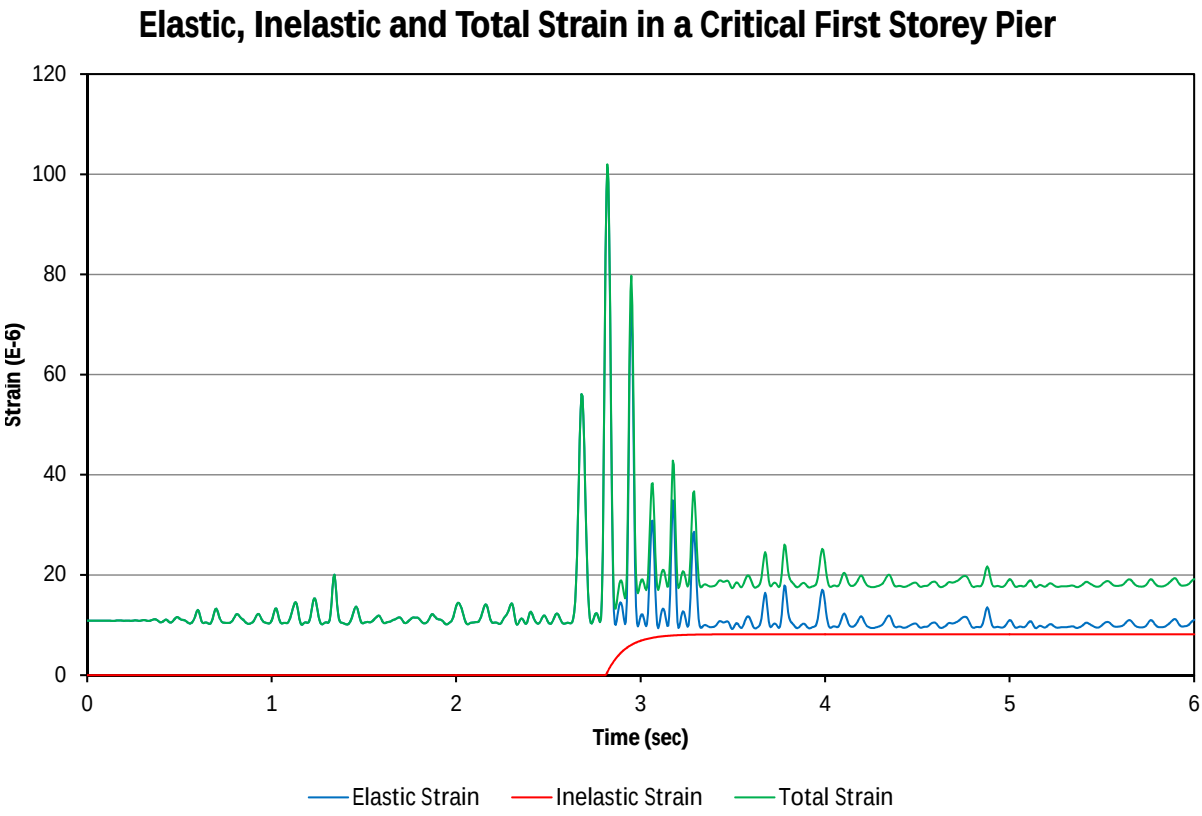

Figure 6.8: Elastic, inelastic and total strain in a critical pier located on the first floor in-plane shear wall.

The results show that the model remains elastic until a peak strain value is reached at 2.8 seconds. Once the yield strain of the material is exceeded, plastic strain will increase. At 2.8 seconds, increasing plastic strain values are recorded until the strain stabilises at a value of 8.15μ. This is also reflected by the resulting offset between the elastic and total strain graphs. Cracking has therefore occurred leading to permanent deformation and strength reduction. The plastic strain must be compared to the plastic material model of the URM building to evaluate the extent of the damage. Tomaževič (1999) suggests that material damage should be limited to a point where 80% of the maximum strength is available in order to prevent unreasonable damage to the building. This occurs at a plastic strain of 20μ. This means that 41% of the plastic strain capacity of the material is used to resist the 0.15g Chalfant earthquake.

From the results it can be deduced that an earthquake with several acceleration peaks exceeding the elastic limit of the material has a high probability of producing sufficient plastic strain so that an excessive reduction in strength will lead to failure. The Chalfant 0.15g earthquake however, has a few large accelerations that is unable to cause failure. The building shows some reserve capacity in the plastic range. From the inelastic strain results, it is clear that the reserve capacity of a building can easily be exceeded at peak accelerations once cracks develop. This means that the certainty to which the plastic capacity of the material can be relied on to resist earthquakes is questionable. The unpredictability of earthquakes increases the probability that failure can occur since several acceleration peaks of sufficient size can progressively reduce the material strength until failure occurs.

6.5 Summary

In order to verify results obtained from a modal dynamic analysis in Chapter 5, the building was simplified as a simple mass-spring system. The stiffness of the spring elements represent the lateral stiffness of each storey. Storey and roof masses were lumped at storey level and included in the model. Separate models were created for the North–South and East–West directions and analysed by applying an acceleration time-history to the model bases. Displacements obtained from the mass-spring model were smaller than that of the full 3D model. This can be attributed to the way in which the building mass was lumped in the mass-spring model. The simplification of the building mass distribution for the mass-spring model must be improved if accurate displacement results are to be obtained. Displacement profile and magnitudes were however comparable (apart from the smaller observed peak values), therefore confirming that the modal dynamic results are indeed plausible.

A sensitivity analysis was performed to explore the effect that damping and the use of a behaviour factor has on the 3D building model. The use of the behaviour factor was discussed by considering the 0.15g Chalfant earthquake. The factor will essentially reduce the magnitude of the PGA to 0.1g. The maximum tensile strength of certain structural elements is however still exceeded for the reduced PGA value as shown in Chapter 5. This suggests that the building is at risk of failure even if non-linear behaviour is accounted for through the use of the behaviour factor.

The effect of damping was studied to confirm whether a choice of a damping ratio of 0.1 as used in the modal dynamic analysis can be justified. Two damping ratios were studied relating to damaged (damping ratio of 0.1) and undamaged (damping ratio of 0.05) URM as suggested by literature in Chapter 3. The analysis showed that damping has a significant effect on the tensile stresses developed in critical in-plane elements. An increase of between 10% and 28% was observed when the reduced damping ratio was used. This confirms that a damping ratio for undamaged URM of 0.05 should be used for initial linear dynamic analyses to determine if cracking occurs. Once cracking has been identified, an increased damping ratio can be specified to account for the effects of cracking. For this study, stresses developed when assuming a damping ratio of 0.05 were large enough to initiate cracking. The use of a damaged material damping ratio of 0.1 in Chapter 3 can therefore be justified since damage to structural elements will likely occur. Where displacement is concerned, damping had little effect on in-plane walls. Out of plane walls showed significant increases in peak displacements when lower damping ratio's were specified. It is therefore necessary to apply a smaller damping ratio when displacement is a critical parameter especially when studying out-of-plane walls and other less stiff elements. In this study, displacement was negligible to the performance of the building.

Finally an implicit dynamic analysis was performed. Initially elastic material properties were specified. This allowed the Rayleigh damping parameters to be calibrated using dynamic displacement results obtained in Chapter 3. A non-linear material model was applied to the implicit model after which the building was analysed in the East–West direction by applying a PGA time-history of the 0.15g Chalfant Valley earthquake. Plastic strain values obtained in critical structural elements suggest that cracking in these elements occurred. Maximum plastic strains obtained indicate that 41% of the plastic strain capacity of the material was used. It was assumed that failure of a structure occurs when material strength is degraded to 80% of the maximum tensile strength. Whether a building can safely resist an earthquake under reduced material strength will depend on the specific building and properties of materials used and requires further research.

Chapter 7

Conclusion and Recommendations

7.1 Conclusions

In this study, a typical 3 storey URM structure, located in underprivileged areas in the southern parts of the Western Cape, was identified and analysed to determine if it would be able to resist a moderate size earthquake. There are many complexities regarding the material behaviour of URM due to the non-homogeneous anisotropic properties of the material. A material model was calibrated in Chapter 3 with different stiffnesses assigned to the in- and out-of-plane masonry walls to model the varied stiffness that URM has when excited in the in- and out-of-plane directions. Both the elastic and plastic material properties of URM were assigned in order to define the pre- and post-cracking behaviour of the structure.

The basic layout of the building was discussed in Chapter 4. Structural cavity walls located at the perimeter of the building along with several double leaf internal walls provide the primary vertical and horizontal load resisting system. Concrete slabs at floor level act as horizontal diaphragms to transfer horizontal loads from out of plane walls to the in-plane shear walls. The floor system also plays a role in redistributing the lateral loads from less stiff and damaged elements to other undamaged elements with larger stiffnesses.

Two FE models were created in ABAQUS to model the behaviour of the building when excited from the East–West and the North–South directions. For each model, stiffnesses calibrated for in- and out-of-plane behaviour obtained in Chapter 3 were applied to the in- and out-of-plane walls. Connections were specified as being either pinned, fixed or free depending on the capacity of the connection to transfer forces. For analysis purposes, a combination factor of $1G_k + 1Q_k$ is assumed (where G_k – the characteristic permanent load and Q_k – imposed load) as per the requirements of SANS 10160-4. A combination factor of 0.3 was used to reduce the live load that is applied to the floor slabs.

The building was analysed with respect to the basic layout and design requirements presented in SANS 10160-4. The building adhered to most of the requirements and showed good distribution of structural walls as well as a symmetrical layout. Many lateral internal walls are provided at short distances. This is highly beneficial since they provide invaluable lateral support to the out

of plane walls. The reason for the good structural layout is not necessarily a result of seismic code specifications. It is rather an indirect effect resulting from the simplicity of medium to low cost residential buildings. Simple box structures are easy to design and construct. They are very effective at carrying vertical loads. Due to the small size of the rooms within the apartments, many internal partition walls aid the load bearing walls by providing lateral support. The small size of the apartments mean that long spans are avoided. Other unfavourable features such as soft storeys and discontinuities along the height of the structure are uncommon in residential URM structures located in underprivileged areas. The building did however have a large number of openings in the North and South facing perimeter walls. This can be problematic since these are the only structural walls that act as shear walls in the East–West direction. A perforated shear wall will have reduced lateral capacity. Stress concentrations normally form at the corners of openings leading to diagonal cracking. The presence of piers of small aspect ratio between the window openings could lead to a pier rocking failure mode that results in the failure of one or more piers or the loss of equilibrium leading to collapse. Most URM buildings of this type are expected to perform well with regard to the basic design requirements.

Several earthquakes were selected in Chapter 5 based on the seismic hazard properties of the Western Cape. The PGA's ranged from 0.055g to 0.1g. The earthquake with the largest PGA, the Chalfant Valley earthquake, was scaled to 0.15g to perform an additional analysis. The nominal design acceleration presented in SABS 0160 is 0.1g. SANS 10160-4 requires the use of the redundancy factor, a factor that increases the design acceleration to a maximum of 0.15g. The selection of earthquakes allows the performance of the structure to the different design accelerations to be confirmed. If designers disregarded the redundancy factor, a design acceleration of 0.1g would be used. This scenario is also treated by the choice of earthquakes. A frequency analysis determined that the first 25 modes sufficiently represented the dynamic behaviour of the structure. It includes 90% of the participating mass with all modes that have a participation of more than 5% included. Natural frequencies for the lateral East–West, North–South and Torsional modes ranged from 8.8 to 13.4Hz. A high natural frequency is expected for an URM structure with high stiffness and low height. The structure responded primarily in its first modes in each of the two orthogonal directions of excitation. This behaviour forms a fundamental part of the assumptions made in SANS 10160-4 when using the lateral static force method to design URM structures.

A modal dynamic analysis was performed by applying the selected earthquake time-histories to the two ABAQUS models. The unique properties of the different earthquakes were reflected in the results that showed large variation for the different earthquakes. Earthquakes with higher frequencies of excitations, such as the Chalfant Valley earthquake showed markedly higher responses than the other similarly sized earthquakes. The Chi-Chi earthquake, with very large peak displacements, showed comparatively smaller response. This shows that earthquakes of moderate size can cause increased responses in URM structures if a high frequency of excitation is maintained.

The building response exceeded the maximum tensile strength of masonry, taken as $0.6MPa$, at all the selected piers in the East–West direction when considering the 0.15g Chalfant Valley

earthquake. This suggests a high probability of a pier rocking mechanism developing. Although a pier rocking mechanism could be stable under cyclic loading, the mechanism has a large potential of becoming unstable, leading to failure. Stresses in the North–South shear walls showed that cracking is likely to occur at the heel or toe of the shear walls. This suggests that the North–South response is affected by flexural behaviour due to the aspect ratio of the building and shear walls. Failure will depend on the excitation experienced after cracking is first initiated since the weakened cracking plane will cause tensile forces to concentrate at the newly formed crack, causing the crack to extend along the wall. This not only reduces the moment resistance capacity of the wall further, but also affects the shear resistance, especially when considering sliding shear.

In the North–South direction, the extent of the cracking is unlikely to cause failure for the selected earthquakes due to the amount of shear walls provided. The East–West direction is considered critical when regarding tensile and compressive cracks. The building performed well for excitation under the other earthquakes with failure unlikely to occur. This can be attributed to the basic symmetric structural layout leading to an effective structural system.

The 0.1g Chalfant Valley earthquake showed increased response leading to cracking of piers in the East–West direction. This has a moderate probability of leading to localized failure. Localised collapse has a high probability of leading to global collapse. The presence of a large amount of openings in the East–West structural walls is blamed for the poor performance of the structure in the East–West direction.

For both the East–West and North–South directions, large stresses developed in the connections for all the earthquakes. This is of concern since the floor-to-wall connections are an essential part of the structural system when considering seismic response. The capacity of different connections was not included in the analysis since it will depend on the design of a particular building, and can vary greatly. Results show that the stresses will lead to large forces that need to be transferred by the connections. The forces are much larger than the suggested 1.5kN/m capacity specified in SANS 10160-4 for structural elements that are not part of the main structural system. This suggests that large scale anchorage failure could occur in secondary structural and non-structural elements. This could result in collapse of out-of-plane walls and floor diaphragms. In addition, the rigidity of the structure will be compromised. This will greatly reduce the ability of the structure to act as a unit to effectively resist lateral loads. The friction developed between the floor slab and supporting walls could add additional resistance at the floor-to-wall connections. Many designers choose to add a movement joint between the slab and the structural wall it is resting on to accomodate temperature movement. If a positive connection between the slab and supporting walls are not provided, the connections will be unable to transfer lateral loads. Detailed connection behaviour is outside the scope of the current study.

In addition to tensile cracking, sliding shear was identified as a likely failure mode for in-plane piers in the East–West direction. This is as a result of the low shear resistance of URM. The presence of existing tensile cracks will further reduce the shear capacity of the piers. There is a moderate possibility of diagonal shear occurring if diagonal forces increase due to the rocking of piers. The building performed well in the North–South direction due to the amount of

uninterrupted shear walls. Results show that displacements are within limits.

The linear modal analysis suggested that the probability of failure of the structure in the East–West direction was high due to tensile cracking, shear sliding and connection failure. The North–South performance was significantly better. Tensile cracking can still be a problem as well as connection failure.

Results from a mass-spring simplification of the model provided reduced displacements at the top of the building, when compared to the in-plane wall displacement of the modal analysis. The procedure of lumping the building mass at floor levels did not accurately model the mass distribution of the 3D model, and should be improved. Including a larger portion of the first floor mass and increasing the portion of mass assigned to the top of the structure should increase the deflections obtained during analysis and increase the accuracy of the results. The mass-spring analysis results confirm to some extent that the modal dynamic analysis results are plausible and that the modelling techniques are sound, however improved results must be obtained if the modal dynamic results are to be matched with good accuracy.

A sensitivity analysis performed on the critical East–West model in Chapter 6 considered the impact that the use of a behaviour factor and reduced damping will have on the analysis results. Applying the behaviour factor will reduce the design acceleration from 0.15g to an effective acceleration of 0.1g. The analysis showed that failure is still likely to occur for the 0.15g Chalfant Earthquake if the 0.15g PGA value is reduced to 0.1g by applying the behaviour factor, suggesting that URM buildings will have a risk of collapse during 0.15g earthquakes.

Reducing the damping will lead to significant increases in the stresses developed in the in-plane walls. This further confirms the modal analysis results suggesting that cracking of structural elements is likely to occur. Once cracking has commenced, the increased damping ratio will be applicable. A reduced damping ratio should be used initially when performing future analyses. Once cracking has been confirmed, the damping ratio can be adjusted accordingly. For this project however, the increased damping ratio is acceptable since cracking of structural elements occurred.

An implicit dynamic analysis was performed to determine the response of the building to the 0.15g earthquake when taking the non-linear properties of masonry into account. Results revealed cracking of the in-plane piers occurred. Failure is expected to occur when the masonry strength is reduced to 80% of the undamaged strength. Failure through tensile cracking did not occur. The building relied heavily on the plastic capacity of the material. This is problematic since URM is a brittle material with little post-cracking capacity. An earthquake with several peak accelerations has a high probability of exceeding the limited plastic capacity of the material, causing failure to occur.

Linear results showed a high probability that the structure will fail in the East–West direction for the 0.15g as well as 0.1g excitations. The amount of window openings in the in-plane shear walls greatly reduce the seismic resisting capacity. The North–South direction showed better performance due to the lack of windows in the in-plane shear walls. The non-linear analysis showed that the building was able to resist the 0.15g earthquake. Due to the high uncertainty

of material strength of URM in South Africa, it is not clear to what degree the plastic capacity of URM can be relied on for seismic resistance. If a structure resists an earthquake, the damage could lead to an unusable structure. There is a need to determine the amount of damage that is regarded as acceptable for South African conditions. Ductility plays an important role in seismic resistance. It will increase the post cracking behaviour of the structure. This should be considered when specifying construction materials. Construction quality should be closely monitored since it can have adverse effects on the strength of URM buildings.

It is concluded that a typical URM building has a high probability of failing during a 0.15g earthquake excitation or to be damaged to an extent where the structure is unsafe for use. This magnitude earthquake can be expected to occur in the southern parts of the Western Cape. The good conceptual layout of the buildings will improve the performance to an extent were damage could be limited for so that catastrophic collapse does not occur. This will however rely heavily on the ability of floor anchorage to transfer seismic loads between structural elements.

7.2 Recommendations for Future Studies

There are various recommendations for further research that were found during this study, namely:

- There is a great need to quantify the construction quality in South Africa and the effect that it has on material performance.
- Testing of in-situ materials of existing URM structures is necessary to determine the material strength of older URM structures.
- Experimental research is required to expand on current material cracking numerical models. Input parameters are available to analyse concrete. Input parameters need to be determined for different URM types to allow these models to be used for analysis.
- A large scale analysis of the current buildings of Cape Town and its surrounding areas must be undertaken to determine the distribution of different structure types. This can be used along with studies such as this one to evaluate the ability of local structures to resist earthquakes on a broad scale.
- This study showed that connections and floor anchorage were likely to fail during seismic events. Further research is required to assess the current connections found in existing URM buildings.
- Damping has a large effect on the response of a structure. Damping must be experimentally determined for different levels of damage of URM structures.
- Additional research is required to determine the plastic behaviour of local materials.
- Further research is needed to quantify the extent of damage that a building can reasonably be expected to sustain during a seismic event and to what level this damage is to be limited for South African residential buildings.

References

Alipour, A., & Zareian, F. (2008). Study of rayleigh damping in structures; uncertainties and treatments. In *Proceedings of the 14th world conference on earthquake engineering.* Beijing, China.

AS/NZS 1170.1. (2002). *Structural design actions — Permanent, imposed and other actions.* Sydney, Australia and Wellington, New Zealand.

Atkinson, R., Amadei, B., Saeb, S., & Sture, S. (1989). Response of masonry bed joints in direct shear. *Journal of Structural Engineering*, *115*(9), 2276–2296.

Bakhteri, J., Makhtar, A. M., & Sambasivam, S. (2004). Finite element modelling of structural clay brick masonry subjected to axial compression. *Jurnal Teknologi B*, *41*(B), 57–68.

Ballio, G., Calvi, M., & Magenes, G. (1993). Experimental and numerical investigation on a brick masonry building prototype. *Reports*, *1*, 2–0.

Bosiljkov, V. Z., Totoev, Y. Z., & Nichols, J. M. (2005). Shear modulus and stiffness of brickwork masonry: An experimental perspective. *Structural Engineering and Mechanics*, *20*(1), 21–44.

Bothara, J. K., Dhakal, R. P., & Mander, J. B. (2010). Seismic performance of an unreinforced masonry building: an experimental investigation. *Earthquake Engineering & Structural Dynamics*, *39*(1), 45–68.

Bruneau, M. (1994). State-of-the-art report on seismic performance of unreinforced masonry buildings. *Journal of Structural Engineering*, *120*(1), 230–251.

Calderini, C., Cattari, S., & Lagomarsino, S. (2009). In plane seismic response of unreinforced masonry walls: comparison between detailed and equivalent frame models. In *2nd international conference on computational methods in structural dynamics & earthquake engineering* (pp. 22–24). Rhodes, Greece.

Calvi, G. M., & Magenes, G. (1991). Experimental evaluation of seismic strength of old masonry structures. *Brick and Block Masonry*, *1*, 490–497.

Clay Brick Association South Africa. (2002). *Clay masonry technical guide.* Clay Brick Association.

Davies, N., & Kijko, A. (2003). Seismic risk assessment: with an application to the South African insurance industry. *S. Afr. Actuarial J*, *3*, 1–28.

de Felice, G., & Giannini, R. (2001). Out-of-plane seismic resistance of masonry walls. *Journal of earthquake engineering*, *5*(02), 253–271.

Dhanasekar, M., & Haider, W. (2008). Explicit finite element analysis of lightly reinforced masonry shear walls. *Computers & structures*, *86*(1), 15–26.

Dhanasekar, M., Kleeman, P. W., & Page, A. W. (1985). Biaxial stress-strain relations for brick masonry. *Journal of Structural Engineering*, *111*, 1085.

Doherty, K., Griffith, M. C., Lam, N., & Wilson, J. (2002). Displacement-based seismic analysis for out-of-plane bending of unreinforced masonry walls. *Earthquake engineering & structural dynamics*, *31*(4), 833–850.

Drysdale, R. G., & Hamid, A. A. (1979). Behavior of concrete block masonry under axial compression. *ACI Journal Proceedings*, *76*.

Dunaiski, P. E., Retief, J. V., & Goliger, A. (2007). *Proposed new South African loading code SANS 10160* (Tech. Rep.). Institute for Structural Engineering, University of Stellenbosch and Built Environment, CSIR.

Eurocode 8 EN 1998-1. (2004). *Design of structures for earthquake resistance–part 1: General rules, seismic actions, and rules for buildings.* European Committee for Standardization.

Ewing, B. D., & Kowalsky, M. J. (2004). Compressive behavior of unconfined and confined clay brick masonry. *Journal of Structural Engineering*, *130*(4), 650–661.

Genna, F., Di Pasqua, M., Veroli, M., & Ronca, P. (1998). Numerical analysis of old masonry buildings: a comparison among constitutive models. *Engineering structures*, *20*(1), 37–53.

Ghobarah, A., & El Mandooh Galal, K. (2004). Out-of-plane strengthening of unreinforced masonry walls with openings. *Journal of Composites for Construction*, *8*(4), 298–305.

Griffith, M. C., Lam, N. T. K., Wilson, J. L., & Doherty, K. (2004). Experimental investigation of unreinforced brick masonry walls in flexure. *Journal of Structural Engineering*, *130*(3), 423–432.

Griffith, M. C., Vaculik, J., Lam, N. T.-K., Wilson, J., & Lumantarna, E. (2007). Cyclic testing of unreinforced masonry walls in two-way bending. *Earthquake Engineering & Structural Dynamics*, *36*(6), 801–821.

Hendry, A. W. (1973). The lateral strength of unreinforced brickwork. *The Structural Engineer*, *51*(2), 43–50.

Ip, F. (1999). *Compressive strength and modulus of elasticity of masonry prisms* (PhD thesis). Carleton University.

Kaushik, H. B., Rai, D. C., & Jain, S. K. (2007). Stress-strain characteristics of clay brick masonry under uniaxial compression. *Journal of materials in Civil Engineering*, *19*(9), 728–739.

Kijko, A., Retief, S. J. P., & Graham, G. (2002). Seismic hazard and risk assessment for Tulbagh, South Africa: Part i–assessment of seismic hazard. *Natural Hazards*, *26*(2), 175–201.

Lane, J. W., Watermeyer, R. B., & De Villiers, P. D. (1991). Masonry materials and design for movement. *SAICE lecture course, Structural Division, Johannesburg, South Africa.*.

Lawrence, S. J. (1983). *Behaviour of brick masonry walls under lateral loading* (Unpublished doctoral dissertation). The University of New South Wales.

Lee, J., & Fenves, G. L. (1998). Plastic-damage model for cyclic loading of concrete structures. *Journal of engineering mechanics*, *124*(8), 892–900.

Linzer, L. M., Bejaichund, M., Cichowicz, A., Durrheim, R. J., Goldbach, O. D., Kataka, M. O., ... others (2007). Recent research in seismology in South Africa. *South African Journal of Science*, *103*(9-10), 419–426.

Lotfi, H., & Shing, P. (1991). An appraisal of smeared crack models for masonry shear wall analysis. *Computers & structures*, *41*(3), 413–425.

Lourenço, P. (1996). Computational strategies for masonry structures.

Lubliner, J., Oliver, J., Oller, S., & Oñate, E. (1989). A plastic-damage model for concrete. *International Journal of Solids and Structures*, *25*(3), 299–326.

McNary, W. S., & Abrams, D. P. (1985). Mechanics of masonry in compression. *Journal of Structural Engineering*, *111*(4), 857–870.

Pacific Earthquake Engineering Research Center. (2013, January). *Peer ground motion database.* Retrieved from `http://peer.berkeley.edu/products/strong_ground_motion_db.html`

Page, A. (1995). The shear capacity of membrane type damp-proof courses in masonry. *Transactions of the Institution of Engineers, Australia. Civil engineering*, *37*(1), 29–39.

Page, A. W. (1996). Unreinforced masonry structures-an Australian overview. *Bulletin-New Zealand national society for earthquake engineering*, *29*, 242–255.

Priestley, M., Calvi, G., & Kowalsky, M. (2007). *Direct displacement-based seismic design of structures.*

Romano, A. (2006). *Modelling, analysis and testing of masonry structures* (PhD thesis). Università dgli Studi di Napoli Federico II.

SABS 0160. (1989). *South African national standard. Code of practice: General procedures and loadings to be adopted in the design of buildings.* Pretoria: South African Bureau of Standards.

SANS 10160-2. (2009). *Basis of structural design and actions for buildings and industrial structures — Part 2: Self-weight and imposed loads.* Pretoria: South African Bureau of Standards.

SANS 10160-4. (2009). *Basis of structural design and actions for buildings and industrial structures — Part 4: Seismic actions and general requirements for buildings.* Pretoria: South African Bureau of Standards.

SANS 10164-1. (1980). *The structural use of masonry — Part 1: Unreinforced masonry walling.* Pretoria: South African Bureau of Standards.

Saradj, F. M. (2007). Earthquake intensity, damage, and conservation of unreinforced masonry buildings. *Architectural Science Review*, *50*(2), 130–140.

Simsir, C. C., Aschheim, M. A., & Abrams, D. P. (2004). Out-of-plane dynamic response of unreinforced masonry bearing walls attached to flexible diaphragms. In *Proceedings of the 13th world conference on earthquake engineering* (pp. 1–4). Vancouver, BC.

Simulia Corp, D. S. (2010). *Abaqus theory manual 6.12.* Providence, Rhode Island, USA.

Singh, M., Kijko, A., & Durrheim, R. (2009). Seismotectonic models for south africa: synthesis of geoscientific information, problems, and the way forward. *Seismological Research Letters*, *80*(1), 71–80.

South African Council for Geosciences. (2013, January). *Historical earthquakes in south africa.* Retrieved from `http://www.geoscience.org.za/index.php?option=com_content&view=article&id=1612`

Stockl, S., Beckhaus, K., & Fritsche, T. H. (1998). Influence of test method on the results of

deformation measurements on uniaxially loaded mortar specimens. *Masonry international*, *12*(1), 32–38.

Syrmakezis, C., Chronopoulos, M., Sophocleous, A., & Asteris, P. (1995). Structural analysis methodology for historical buildings. In *Proceedings of the fourth international conference on structural studies of historical buildings* (Vol. 95, pp. 373–382). STREMA.

Tarbuck, E. J., & Lutgens, F. K. (2008). *Earth: An introduction to physical geology* (Ninth ed.). Pearson Prentice Hall.

Tomaževič, M. (1999). *Earthquake-resistant design of masonry buildings* (Vol. I). London: Imperial College Press.

Tomaževič, M., Bosiljkov, V., & Weiss, P. (2004, August). Structural behaviour factor for masonry structures. In *13th world conference on earthquake engineering.* Vancouver, B.C., Canada.

Truong Hong, L., & Laefer, D. F. (2008). Micro vs. macro models for predicting building damage due to underground movements.

UBC. (1997). Unform building code. international conference of building officials [Computer software manual]. Witthier, California.

USGS. (2012, November). *Earthquake facts and statistics.* Retrieved from `http://earthquake.usgs.gov/earthquakes/eqarchives/year/eqstats.php`

USGS. (2012, May). *Seismicity of the Earth 1900–2010, Eastern Margin of the Australia Plate.* Retrieved from `http://earthquake.usgs.gov/earthquakes/world/seismicity_maps/`

Vaculik, J. (2012). *Unreinforced masonry walls subjected to out-of-plane seismic actions.* (Unpublished doctoral dissertation). The University of Adelaide School of Civil, Environmental and Mining Engineering.

Vaculik, J., & Griffith, M. (2007). Shaketable tests on masonry walls in two-way bending. In *Australian earthquake engineering society conf. 2007.* Wollongong, NSW.

Wium, J. A. (2010). Background to draft SANS 10160 (2009): Part 4 — seismic loading. *Journal of the South African Institute of Civil Engineering*, *52*(1), 20–27.

Wium, J. A., & van Zijl, G. P. A. G. (2005). *The South African loading code: Revision of provisions for seismic loading* (Tech. Rep.). Department of Civil Engineering, University of Stellenbosch.

Yi, T. (2004). *Experimental investigation and numerical simulation of an unreinforced masonry structure with flexible diaphragms* (Unpublished doctoral dissertation). Georgia Institute of Technology.

Yi, T., Moon, F. L., Leon, R. T., & Kahn, L. F. (2006). Analyses of a two-story unreinforced masonry building. *Journal of structural engineering*, *132*(5), 653–662.

Zucchini, A., & Lourenço, P. B. (2007). Mechanics of masonry in compression: results from a homogenisation approach. *Computers & structures*, *85*(3), 193–204.

Appendix A

Earthquake Data

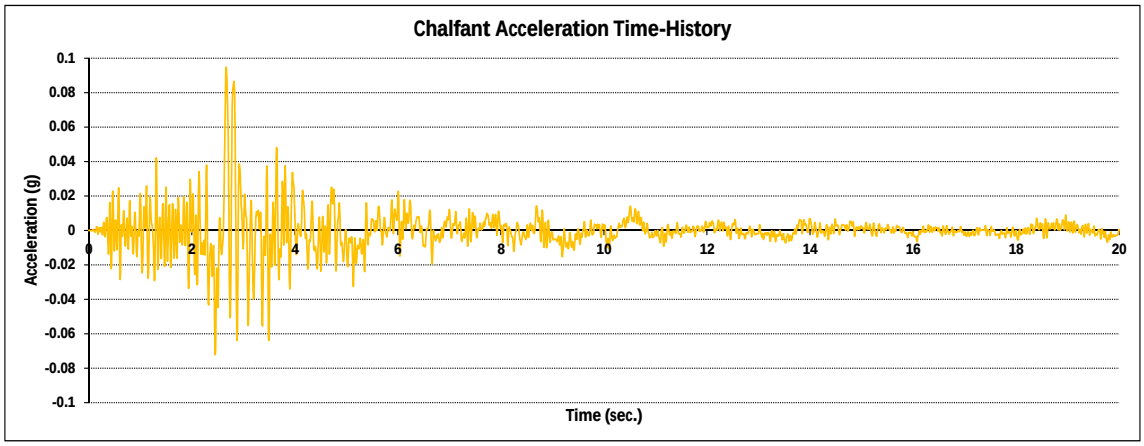

Figure A.1: Acceleration time-history of the Chalfant Valley (1986) earthquake used for analysis.

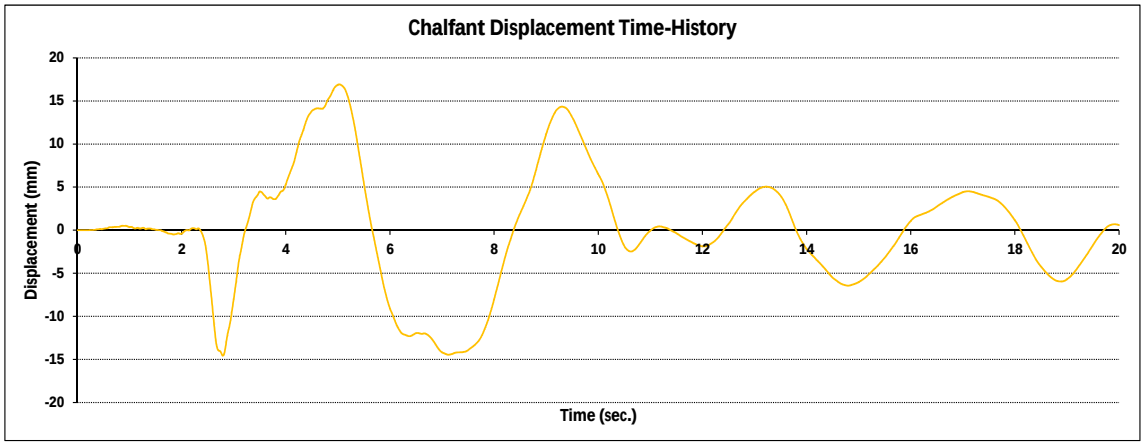

Figure A.2: Displacement time-history of the Chalfant Valley (1986) earthquake used for analysis obtained through integration of the acceleration time-history.

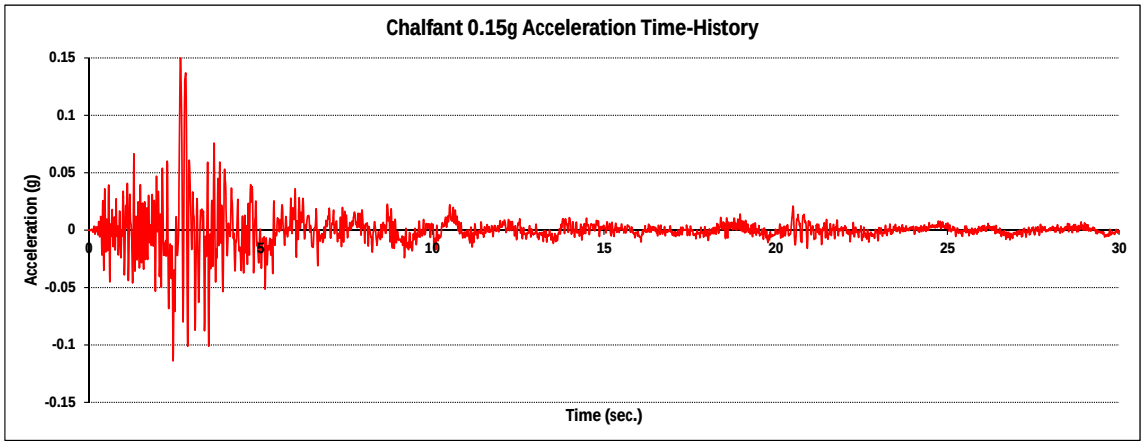

Figure A.3: Acceleration time-history of the Chalfant Valley (1986) earthquake scaled to 0.15g, used for analysis.

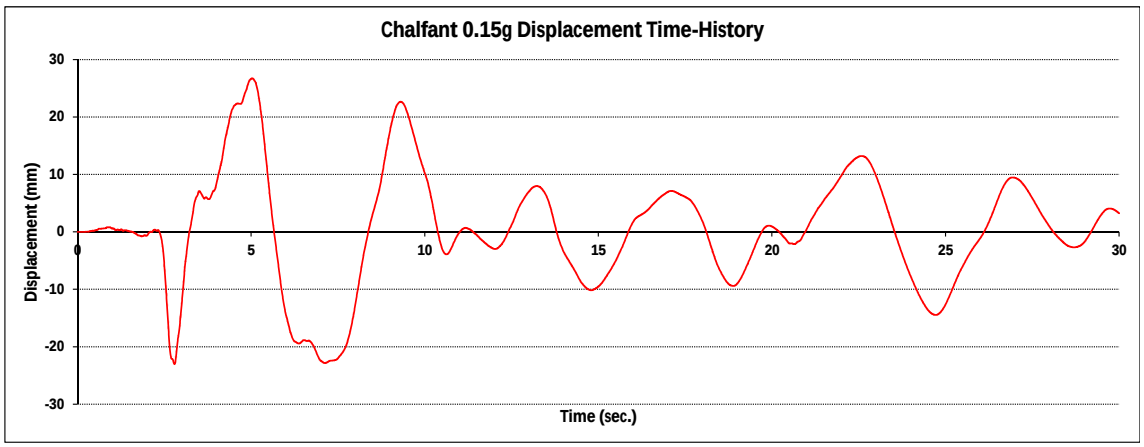

Figure A.4: Displacement time-history of the Chalfant Valley (1986) earthquake scaled to 0.15g, used for analysis. Obtained through integration of the acceleration time-history.

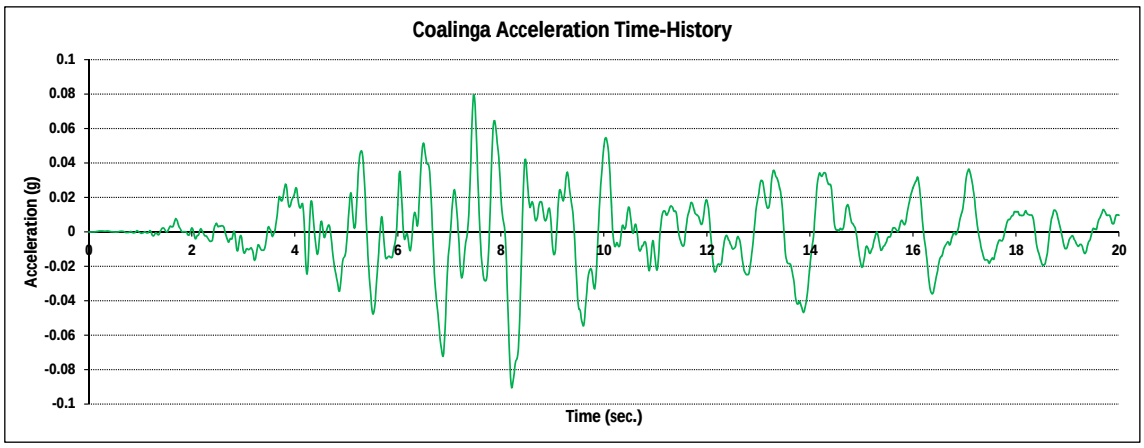

Figure A.5: Acceleration time-history of the Coalinga (1983) earthquake used for analysis.

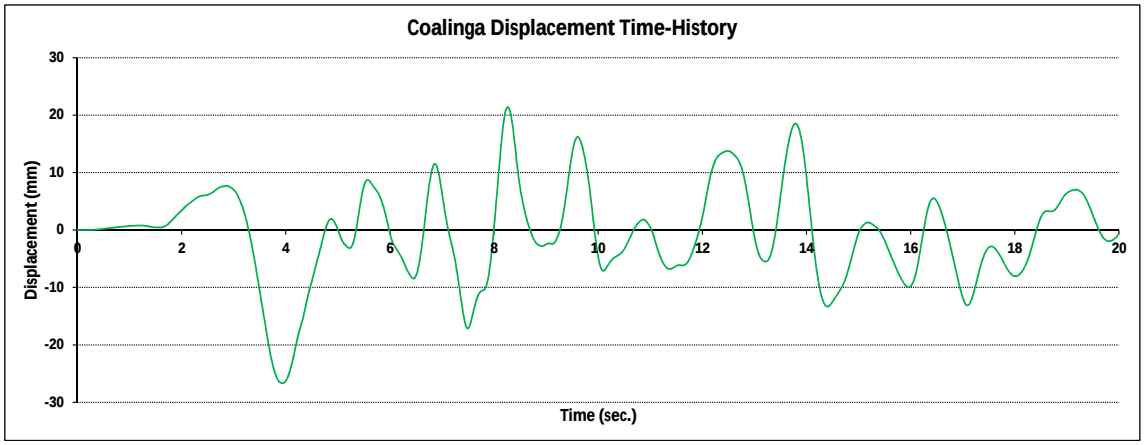

Figure A.6: Displacement time-history of the Coalinga (1983) earthquake used for analysis obtained through integration of the acceleration time-history.

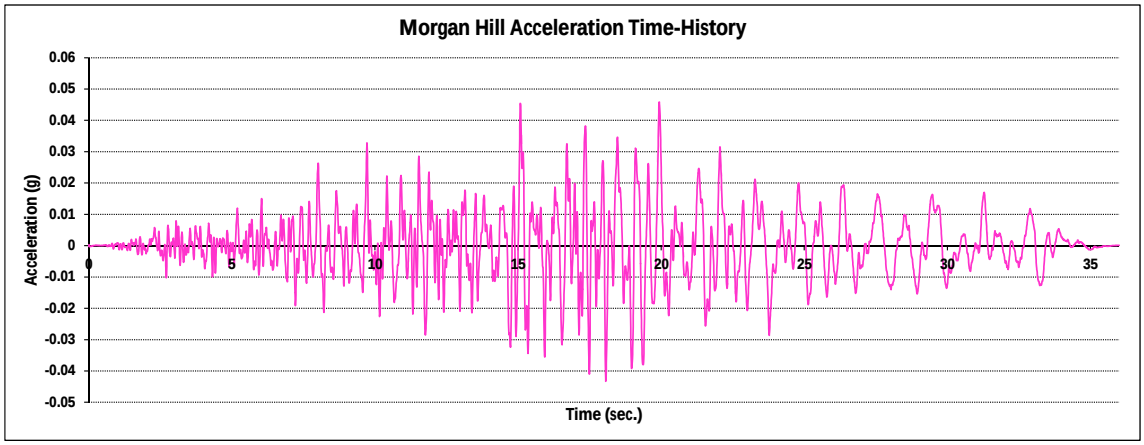

Figure A.7: Acceleration time-history of the Morgan Hill (1984) earthquake used for analysis.

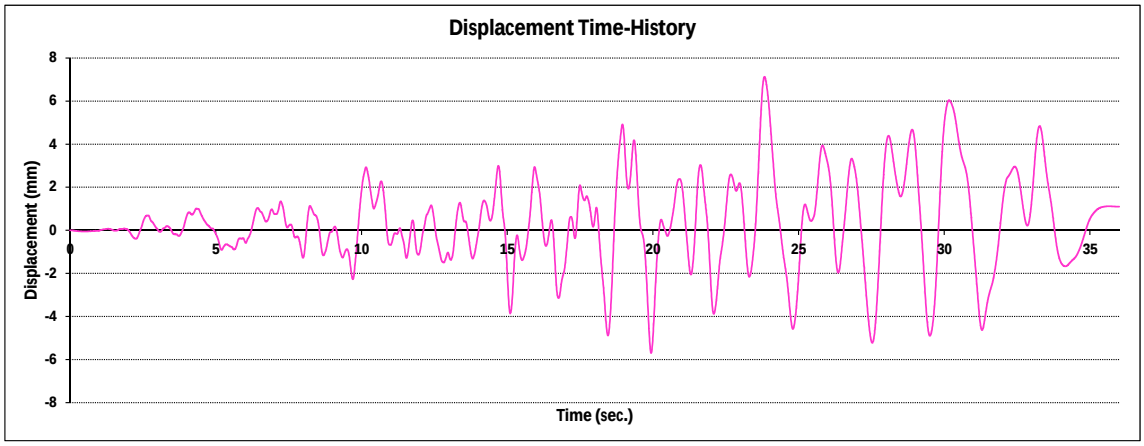

Figure A.8: Displacement time-history of the Morgan Hill (1984) earthquake used for analysis obtained through integration of the acceleration time-history.

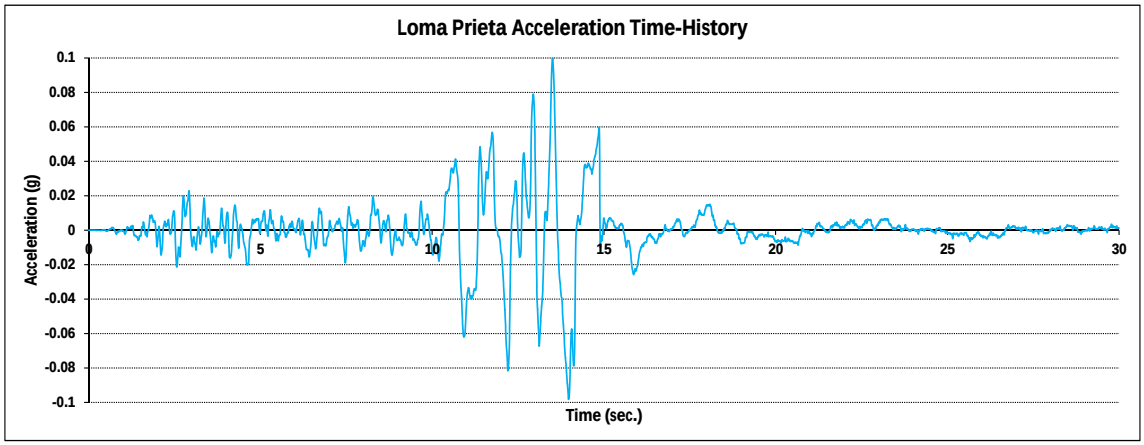

Figure A.9: Acceleration time-history of the Loma Prieta (1989) earthquake used for analysis.

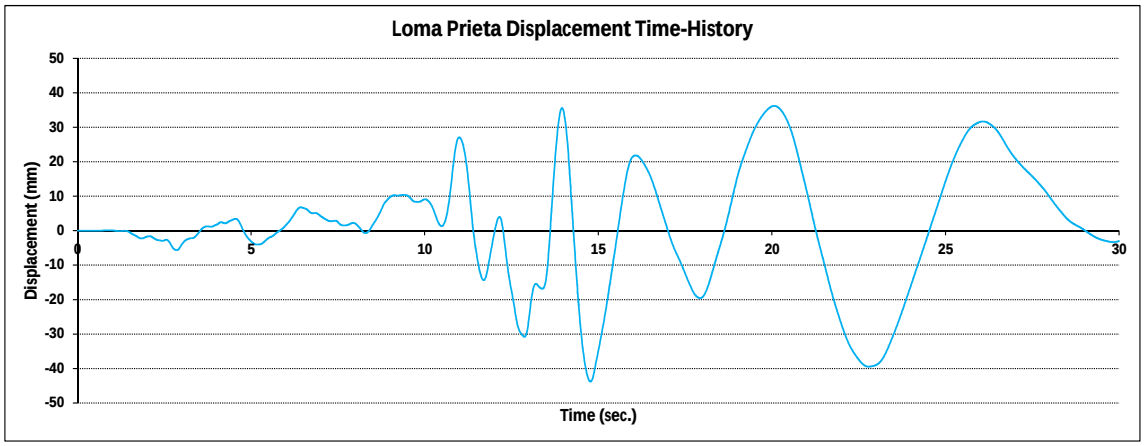

Figure A.10: Displacement time-history of the Loma Prieta (1989) earthquake used for analysis obtained through integration of the acceleration time-history.

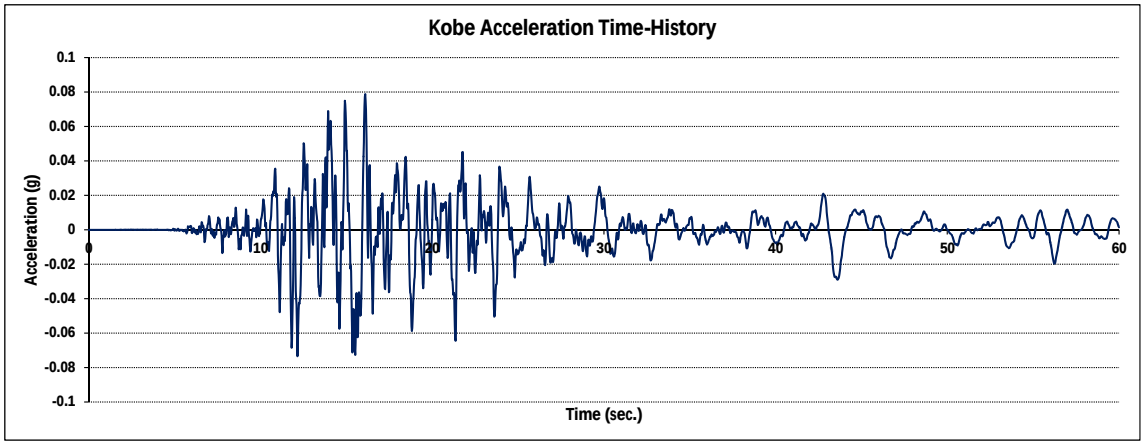

Figure A.11: Acceleration time-history of the Kobe (1995) earthquake used for analysis.

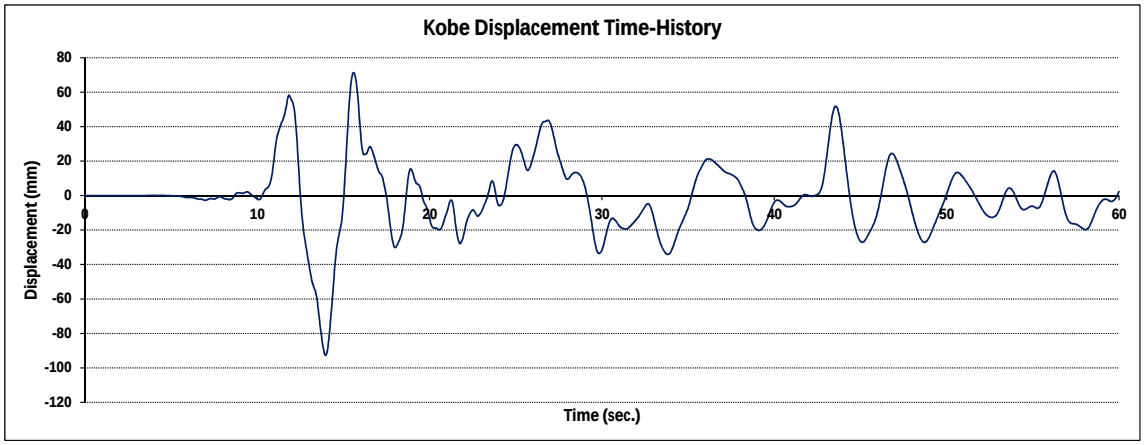

Figure A.12: Displacement time-history of the Kobe (1995) earthquake used for analysis obtained through integration of the acceleration time-history.

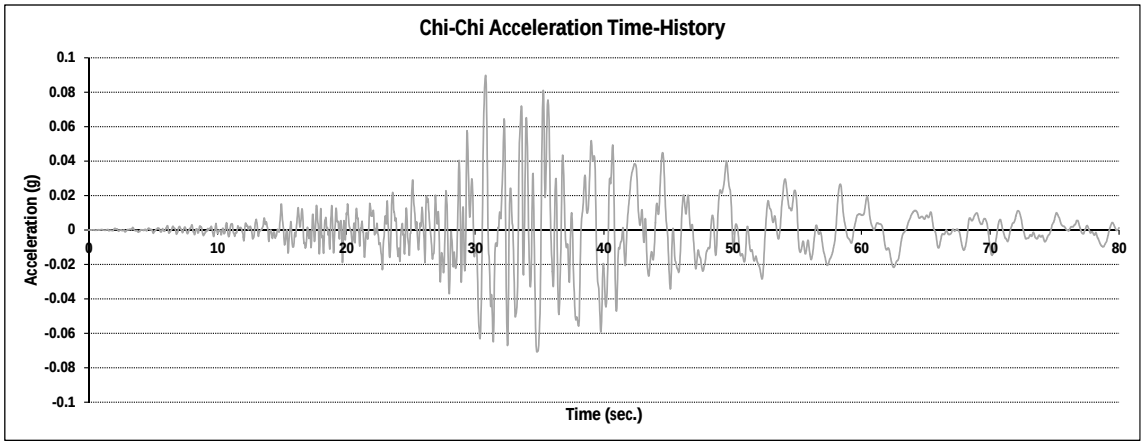

Figure A.13: Acceleration time-history of the Chi-Chi (1999) earthquake used for analysis.

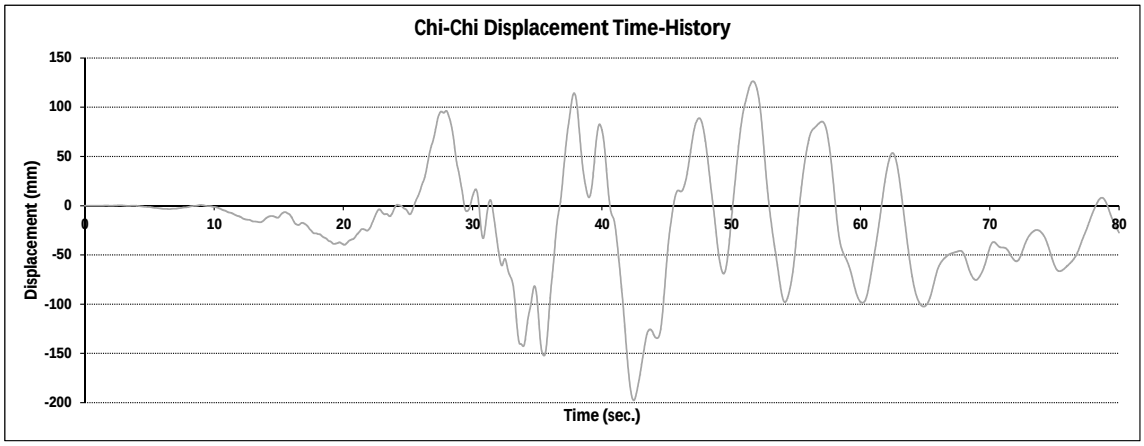

Figure A.14: Displacement time-history of the Chi-Chi (1999) earthquake used for analysis obtained through integration of the acceleration time-history.